STUDIES OF TARTARIC ACID MODIFIED NICKEL SUPPORTED CATALYSTS
FOR ENANTIOSELECTIVE HYDROGENATION REACTIONS

by

MARCO ANTONIO LÓPEZ MARTÍNEZ

A thesis submitted to
The University of Birmingham
for the degree of
DOCTOR OF PHILOSOPHY

School of Chemistry
College of Engineering and
Physical Sciences
The University of Birmingham
November 2010

UNIVERSITY OF BIRMINGHAM

University of Birmingham Research Archive

e-theses repository

ABSTRACT

This thesis investigates the catalytic properties of tartaric acid-nickel supported catalysts, obtained from hydrotalcite-like compound precursors, in the enantioselective hydrogenation of methyl acetoacetate to methyl 3-hydroxybutyrate. Variables of reaction during modification such as pH and tartaric acid concentration, as well as Ni particle size above a minimum threshold of ca. 20 nm, proved not to have a major effect on enantioselectivity. However, the nature of the cations constituting the catalyst support was found to influence the enantioselectivity observed. Specifically, when iron or chromium were constituents of the supporting oxide matrix, enantioselectivities were found to be much higher. For systems containing nickel, magnesium (or zinc) and aluminium as the cations present in the parent hydrotalcite phase, when a series of materials of the same composition obtained from different synthetic methods, the urea hydrolysis method leads to catalysts with enantiodifferentiation ability, whereas materials prepared by the coprecipitation method does not.

Also, this thesis researches the use of different types of ordered mesoporous silicas as supports of tartaric-acid nickel in the aforementioned reaction. Even though the techniques of metal deposition explored did not allow incorporation of Ni in the internal surface of the materials, it was found that the morphology of the support plays an important role in enantioselectivity. In addition, for a given material, the incorporation of Ni via solid state reaction resulted in a catalyst with improved catalytic properties compared to one prepared by wet impregnation techniques.

DEDICATION

To my parents: Antonio López Díaz and Martha Martínez Bernal

To my sibs: Martha Ericka, Arturo, Juan Pablo, Guadalupe del Carmen and

Guadalupe de los Lagos

To my nieces and nephews: Maria Fernanda, Natalia, Ian Ulises, Daniel and Naresh

ACKNOWLEDGEMENTS

CONTENTS

CHAPTER 2. TECHNIQUES

CHAPTER 3. HLCs AS PRECURSORS OF SUPPORTED TA-Ni CATALYSTS

CHAPTER 4. OMS AS SUPPORTS OF TA-Ni CATALYSTS

ABBREVIATIONS

AAS	Atomic Absorption Spectroscopy
e.e.	Enantiomeric Excess
CTAB	N-Hexadecyltrimethylammonium Bromide
DTA	Differential Thermal Analysis
D-TA	D-(+)-Tartaric Acid
GC	Gas Chromatography
HLCs	Hydrotalcite-Like Compounds
HPLC	High Liquid Pressure Chromatography
L-TA	L-(+)-Tartaric Acid
MAA	Methyl Acetoacetate
MCM-41	Mobil Composition of Matter No. 41
MCM-48	Mobil Composition of Matter No. 48
MHB(R)	Methyl (R)-3-Hydroxybutyrate
MHB(S)	Methyl (S)-3-Hydroxybutyrate
MS	Mass Spectrometry
Na-TA-Ni	Sodium-Tartaric Acid-Nickel
Ni ACAC	Nickel Acetylacetonate

Ni-Ci	Nickel Citrate
OMS	Ordered Mesoporous Silicas
o.y.	Optical Yield
RaNi	Raney Nickel
RaNi-Al	Raney Nickel Aluminum
SBA-2	Santa Barbara No. 2
TA	Tartaric Acid
TA-NaBr-Ni	Tartaric Acid-Sodium Bromide-Nickel
TA-NaBr-RaNi	Tartaric Acid-Sodium Bromide-Raney Nickel
TA-Ni	Tartaric Acid-Nickel
TA-RaNi	Tartaric Acid-Raney Nickel
TEOS	Tetra Ethyl Ortosilicate
TGA	Thermogravimetric Analysis
TG-DTA	Thermogravimetric and Differential Thermal Analysis
XRD	X-Ray Diffraction

CHAPTER 1. INTRODUCTION

1.1 Importance of Catalysis

Catalysis is essential in life as most of the chemical reactions that take place in our organisms are carried out by natural catalysts, best known as enzymes. On the other hand, our life style is ruled by catalysis as most of the products we consumed such as chemicals, combustibles, polymers, pharmaceuticals, food and drinks, amongst others, have been produced using at least a catalyst at some stage of their manufacture. As the global economy is based on catalytic technologies there is great interest in the further study/development of catalytic systems. Moreover, catalysis is a viable alternative in the control of the generation of pollutants, handling and disposal of hazardous materials, etc.

Even though Berzelius coined the term catalysis during his studies in 1835,[1] Döbereiner had already worked on the use of platinum as a catalyst in 1823.[2] However, there are even older examples of catalytic processes. In 1781, acids were used to catalyse the conversion of starch into sugar.[3] In 1746 in Birmingham, England, nitric oxide was used as a catalyst in the lead chamber process for oxidation of sulphur oxide to give sulphur trioxide in the manufacture of sulphuric acid.[4] Before the sixteenth century ether was made by distilling spirits in the presence of sulphuric acid. There is archaeological evidence that the use of yeast for fermenting starch during brewery was used in Ancient Egypt since around the 6th millennium BC.

1.2 Definition of Catalysis/Catalyst

Catalysis is the phenomenon that takes place in a chemical process when a catalyst is used. A catalyst is defined as the substance (or mixture of substances) that changes the rate which a chemical reaction occurs without modifying the chemical equilibrium and that remains unchanged after reaction. The catalyst lowers the energy of activation, stabilises intermediates and provides an alternative reaction pathway. The reduction of the difference in energy between starting material and transition state increases the number of molecules/molecular collisions with the energy needed to reach the kinetic barrier in order to complete the transition. This effect is best seen in the potential energy diagram of the Figure 1.2.1.
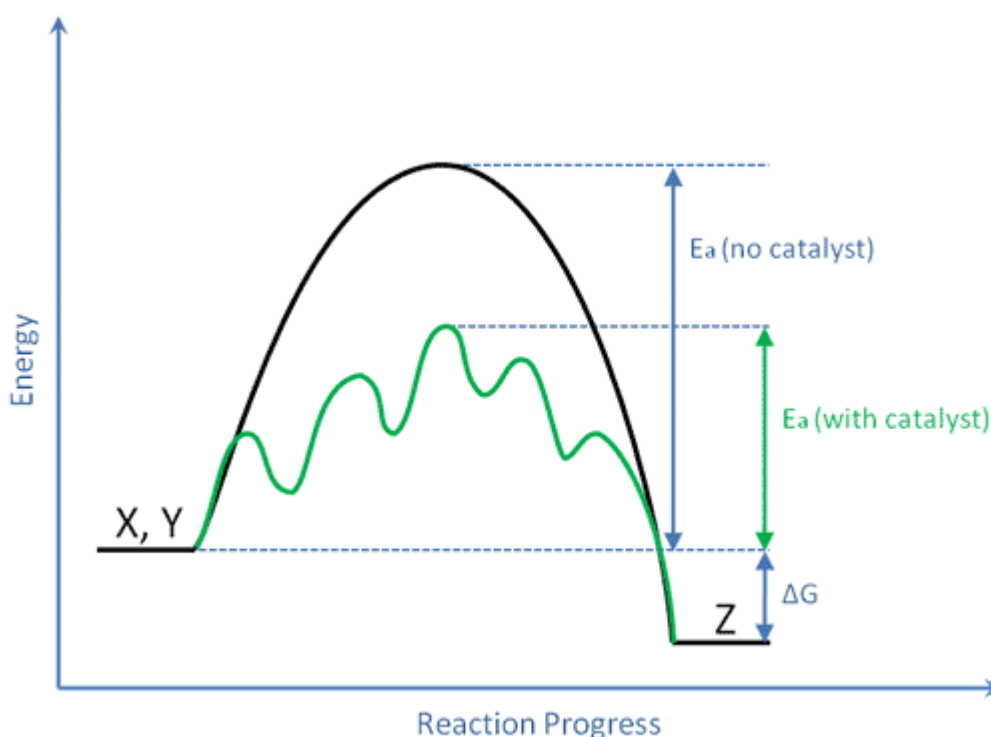
Figure 1.2.1: Potential energy diagram showing the effect of a catalyst in a hypothetical exothermic reaction. X and Y represent the reactants and Z represents the product.

1.3 Properties of a Catalyst

The selection of a catalyst is based mainly on parameters such as catalytic activity and selectivity, as well as the stability of those two during catalytic performance, but costs and availability of raw materials for its manufacture are factors to take into account along with the others. The right balance of all of these standards would allow the best suitable catalyst for a given process.

1.3.1 Catalytic Activity

Catalytic activity can be defined as the amount of reactant that is transformed into product by the catalyst, at given conditions of reaction. It can be described in terms of rate (moles of product per volume unit or mass of catalyst per time unit), in terms of activity per active site (turn over number, TON) or turn over per unit time (turn over frequency, TOF); or simply as a conversion (moles of transformed reactant per moles of initial reactant).

1.3.2 Selectivity

Selectivity can be defined as the amount of desired product obtained with respect to the total amount of transformed reactant. Therefore, it can be described as moles of desired product per moles of converted reactant. A catalyst is considered more selective if it gives rise more desired product.

1.4 Types of Catalysis

Catalytic systems are classified in two main categories:

1. Homogeneous catalysis, where catalyst and reactant(s) are in one phase, and

2. Heterogeneous catalysis, where the catalyst is insoluble in the reaction medium.

Biocatalysts deals with enzymes and microorganisms and is always considered another type of catalysis. However, strictly speaking, it falls in either of the two other categories.

1.4.1 Homogeneous Catalysis

In this category, catalysts are acids, bases, salts, soluble enzymes or organometallic compounds. The catalyst is dissolved in a solvent which can also be a reactant. The catalyst is distributed homogeneously in the system. This makes the reaction rate uniform in the whole system. As all of the molecules participate in the catalytic process, this kind of system often shows high selectivities. In addition, it is possible to control the temperature in highly exothermic reactions. Some of the most important industrial catalytic processes that use organometallic complexes include: polymerization, addition and oxidation of olefins; to obtain polyethylene, polybutadiene and polypropylene oxide, respectively. Another application of organometallic complexes is in processes such as hydrogenation of $C=C$,[5-11] $C=N$,[11, 12] $C=O$[12-14] bonds; as well as isomerisation, epoxidation, cyclopropanation, addition

and sulfoxidation for the production of fine chemicals.[15-19] Examples of these are shown in Figure 1.4.1.1.

$$Ru(OOCCF_3)_2 / binap$$
$$20°C, 100 \text{ bar}$$
ee 97%
ton 50'000; tof 500h[-1].

Ir / josiphos4
50°C, 80 bar
ee 80%
ton 2'000'000; tof 400'000h[-1]

$$Rh(binap)_2^+$$
100°C
ee 97%
ton 400'000 (recycled, 2% loss); tof 440h[-1]
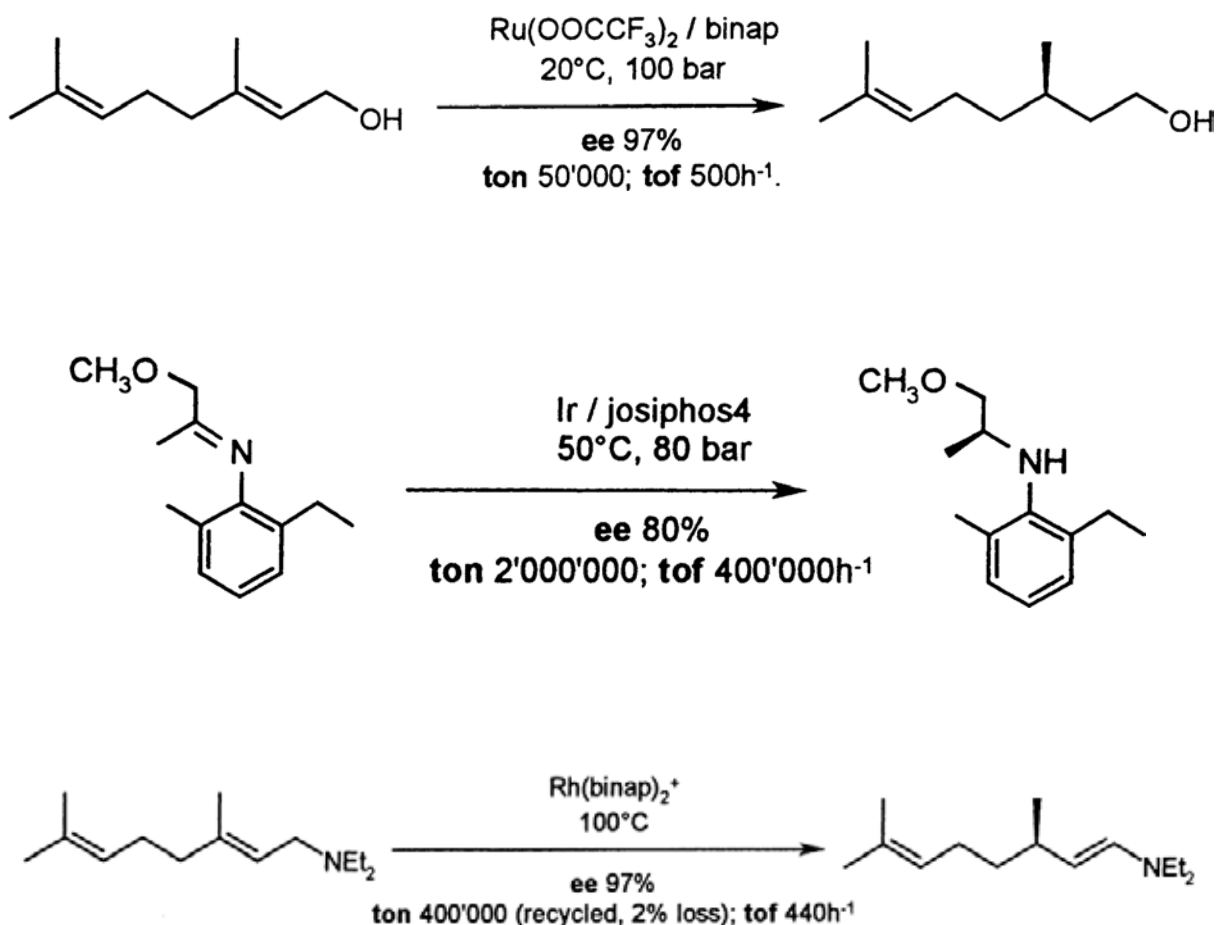
Figure 1.4.1.1: Examples of industrial homogeneous catalytic processes for the production of fine chemicals.[14]

A drawback of homogeneous catalysts is the high costs and availability of chiral ligands and metal precursors. Moreover, ligand synthesis, high catalyst loading, isolation of products, recovery and recycling of noble metals, as well as severe problems of corrosion of reactors and tubing when acids are used, are critical issues to be solved.

1.4.2 Heterogeneous Catalysis

Most heterogeneous catalysts are inorganic solids that act on substrates in a liquid or gaseous reaction mixture. Thus, this system presents two phases and a contact surface. Reaction takes place in the interphase. The general steps of the catalytic process are:

   i. diffusion of reactants towards the catalyst

   ii. adsorption of reactants on the catalyst

   iii. reaction on surface

   iv. desorption of product from surface

   v. diffusion of products away from the catalyst

Heterogeneous catalysts are heavily used in industry, specifically in oil refining and petrochemistry, in processes such as hydrodesulphurisation (HDS), hydrodenitrogenation (HDN), fluid catalytic cracking (FCC), hydrocracking, hydrogenation, dehydrogenation, oxidation and isomerisation.

According to the key properties responsible for their catalytic behaviour, heterogeneous catalysts can be classified in the following subcategories:

1. Oxidation-reduction

2. Acid-base

3. Bifunctional

1.4.2.1 Oxidation-Reduction Catalysts

The best known catalyst of this category is the three-way catalytic converter, commonly used in motor vehicle exhaust systems. Its task is to reduce the toxic emissions from an internal combustion engine, according to the following mechanisms:

i. Reduction of nitrogen oxide to nitrogen and oxygen:

$$2NO_x \rightarrow xO_2 + N_2$$
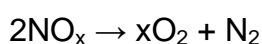
ii. Oxidation of carbon monoxide to carbon dioxide:

$$2CO + O \rightarrow 2CO_2$$
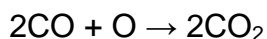
iii. Oxidation of unburned hydrocarbons to CO_2 and water:

$$C_xH_{2x+2} + [(3x+1)/2]O_2 \rightarrow xCO_2 + (x+1)H_2O$$
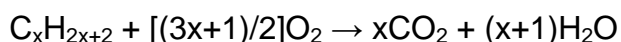
The active metals are platinum, palladium and rhodium, which are supported on a ceramic honeycomb washcoated with alumina or silica.

1.4.2.2 Acid-Base Catalysts

These catalysts present acidic and basic sites. According to Brönsted, an acid is a substance which donates a proton, whereas a base accepts it. On the other hand, Lewis acids are those which accept a pair of electrons and Lewis bases those which donate them. Examples of this subcategory are stoichiometric metal oxides such as MgO, Al_2O_3, CsO, BaO, etc.

1.4.2.3 Bifunctional Catalysts

These materials present a combination of the properties of the last two categories: oxidation-reduction and acid-base. Both support and supported phase activate different steps in the chemical reaction, following different catalytic schemes. It is evident that the materials used as supports can present catalytic activity themselves. The main industrial application of this type of catalysts is on catalytic reforming, which is a process to convert petroleum refinery naphthas with low-octane ratings into reformates or high-octane liquid products, which are components of high-octane gasoline (petrol). Examples of bifunctional catalysts are platinum or rhenium supported on either silica or silica-alumina.

A drawback of solid catalysts though is that they may be deactivated or destroyed by secondary processes during reaction. However, due to their easy recovery, handling and re-use, along with the growing interest/restrictions for environmental friendly technologies, these catalysts are a viable alternative to current stoichiometric catalysts. Current research on heterogeneous catalysts is focused on the optimisation of existent catalysts, developing of new ones, understanding mechanisms of reaction and deactivation of active phases, amongst others.

1.4.3 Components of a Heterogeneous Catalyst

A heterogeneous catalyst is a very complex material. Its main components are:

1. Active phase
2. Support
3. Promoter

1.4.3.1 Active Phase

The active phase is responsible for the activity of the catalyst. This phase can be constituted of one or more chemical species. The active phase can be expensive and/or very sensitive to the conditions of reaction. Therefore, it is often dispersed/stabilised in a support.

1.4.3.2 Support

The catalytic support is the matrix where the active phase is deposited. The material support is usually a solid with high surface area which provides thermal and mechanical stability to the active phase. Very often, the support is just not a phase on which to disperse the catalyst but also, under certain conditions, it acts as an active phase itself. In some other cases, it influences the structure of the active phase. The morphology of the support, and more concretely, its porosity, is another important factor to consider when reactions are dependent on size and shape of reactant

molecules. Examples of catalytic supports are metal oxides and their mixtures, amorphous silicas, activated carbons, etc.

1.4.3.3 Promoter

Small amounts of this element/compound in the catalyst can modify activity/selectivity of the active phase and/or improve the mechanical properties of the support.

1.5 Enantioselective Catalysis

A key word in organic synthesis is selectivity, which is necessary to obtain a high yield of a desired product. Even though there are a large number of selective organic reactions available, there is still an area where organic chemists are struggling, and that is when chirality is involved.

Chirality is of extremely high importance in nature due to the manner in which the human body interacts differently with different enantiomers. The use of even parts per million of the wrong enantiomer can have detrimental consequences when it is applied for physiological consumption. The most remarkable example of the intake of the wrong isomer took place in the 60's, when the drug thalidomide was administered to pregnant women leading to birth defects. Therefore, the synthesis of bioactive molecules used as pharmaceuticals, vitamins, agrochemicals, fragrances and flavours, amongst others, has to be in enantiomerically pure form.

Synthetically, there are many ways to prepare optically active molecules, e.g. separation of enantiomers via classical resolution, the chiral pool approach, use of enzymatic and microbial transformations, and enantioselective catalysis. In the catalytic approach, the most successful examples are those related to homogeneous systems. Their research led to a Nobel Prize in 2001.[20]

1.5.1 Enantioselective Catalysts

A successful approach for the creation of heterogeneous enantioselective catalysts for hydrogenation reactions is to adsorb an enantiomerically pure chiral compound from solution onto an achiral metal surface.[21-67]

Research carried on heterogeneous enantioselective catalytic systems, have proved that not every chiral molecule is suitable to interact with a given metal (and vice versa), and that the resulting system modifier-metal is substrate specific.[21-28, 63-65] At the end of the 70's, the most successful chirally modified metal catalysts were obtained: α-amino acids or α-hydroxy acids adsorbed on Ni,[28-34] and cinchonidine alkaloids adsorbed onto Pt.[63-65] The resulting Ni based catalysts are suitable for C=O hydrogenations of 1,3-β-diketones, 2-alkanones, β-ketosulfones and β-ketoesters,[28-34, 36-38, 40, 41, 44, 45, 47, 51-54] whereas the resulting Pt based catalysts are suitable for the hydrogenation of α-ketoesters.[63-65]

Tartaric acid (TA) adsorbed onto Ni leads to the highest enantiodifferentation (discrimination between two enantiomers) in the hydrogenation of the simplest β-ketoester: methyl acetoacetate (MAA).[60] This reaction is important because its

product, methyl 3-hydroxybutyrate (MHB), is a useful precursor in the manufacture of β-lactams (Figure 1.5.1). Its further manipulation leads to pharmaceuticals.
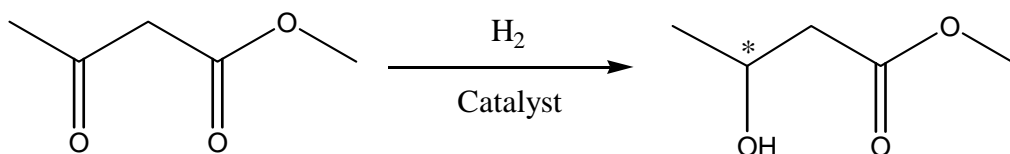
Figure 1.5.1: Enantioselective hydrogenation of MAA to MHB.

On the other hand, the synthesis of the BINAP ligand in 1980[68] led to the development of a vast number of metal-ligand catalysts for the production of various speciality chemicals[69] (Figure 1.5.2). In particular, Ru^{II}-BINAP species are highly selective in the hydrogenation of carbonyl compounds.[70-72]

binap   Ar = Ph
tolbinap Ar = p-Tol

binol
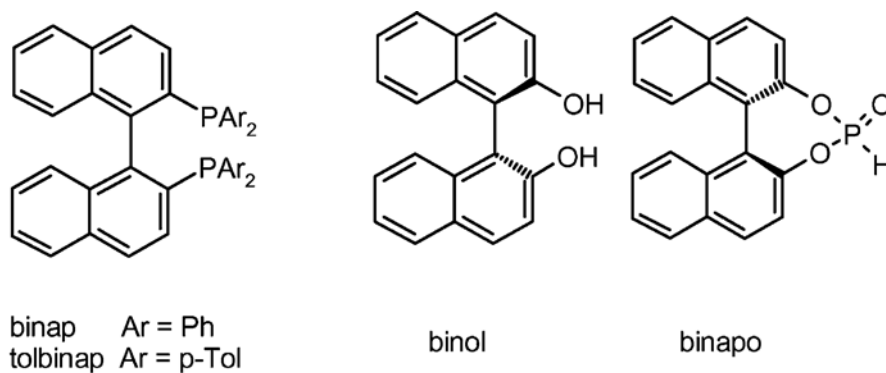
binapo

Figure 1.5.2: Metal-ligands of the BINAP family.

josiphos1 R = Ph R' = cy-Hex
josiphos2 R = Ph R' = t-Bu
josiphos3 R = Ph R' = 2-Naph
josiphos4 R = Ph R' = 3,5-Xyl
josiphos5 R = Ar R' = t-Bu
Ar = 3,5-Me-4-OMe-Ph

HCd   R = H   R' = Et
quinine   R = OMe   R' = Vin
DHQ   R = OMe   R' = Et

salen
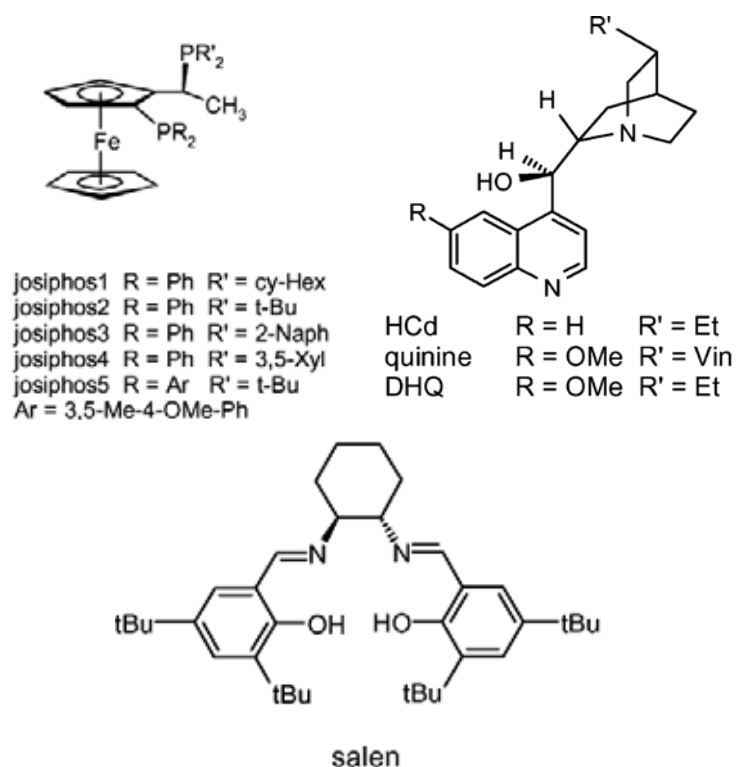
Figure 1.5.3: Structures of other popular ligands.

Figure 1.5.3 shows some other structures of ligands used in catalytic systems.

For obvious reasons there is much interest in immobilising these complexes into carriers.[73-76] The method of carrier preparation consists mostly in the organo-functionalisation of the inner surfaces of ordered mesoporous silicas (OMS) (see Chapter 4 for further details on OMS) by postsynthetic grafting methods, followed by covalent tethering. It is in these conditioned cavities where the complexes with catalytic activity are immobilised. Despite the success of this method, the use of expensive ligands and the long process of support and catalyst preparation makes still desirable to opt for easiest techniques such as the chiral modification of metal surfaces. Therefore, it is of particular interest to investigate further the TA-Ni system.

1.6 TA-Ni Catalyst

RaNi has been the most used source of Ni for the development of TA-Ni catalysts for the hydrogenation of MAA.[28, 32, 38, 40, 47, 51, 55, 56, 61, 66, 67, 77-90] From the vast amount of work done over this catalytic system, it has been learnt that replacing L-TA by its opposite enantiomer reverses the enantioselectivity of the catalytic process[32, 38] and that the enantiodifferentiation ability of the catalyst is affected by parameters such as pH,[28, 32, 66] pH adjusting reagent,[56] solvent,[89] temperature,[28, 66] time and use of co-modifiers[66] during modification; and for reaction variables such as pressure, temperature, solvent type, substrate ratio and substrate concentration, during catalysis.[82]

1.7 TA-Ni Supported Catalyst

During the early stage of the studies on RaNi as precursor of TA-Ni, a bimetallic catalyst of Ni-Pd supported on Kieselguhr showed comparable enantioselectivity in the hydrogenation of MAA to that showed by TA-RaNi catalyst.[91] This fact opened a new aim in this exciting field due to the perspective that a modified Ni catalyst would be promising with the aid of additional effects of a support. Most of the work done over supported Ni has been carried out using silica as the carrier.[92-109] Other supports such as Kieselguhr,[66] zirconia,[66] aluminas,[66, 110, 111] titania,[66, 111] zeolites,[111-114] and ceria[115] have been studied as well.

The most remarkable attribute of all of these studies is that enantioselectivity has proved to be affected by the nature of the Ni source and the nature of the material

used as support under the same parameters of modification and catalytic test. Ni particle size[77, 93, 95, 98, 102, 104, 108, 111] and support porosity[96] are particularly important factors in the design of enantioselective metal supported catalysts.

Moreover, most of the methods of preparation of supported catalysts lead to irreproducible reaction rates and optical yields. Detailed work on supported systems has shown that the enantioselective properties of the catalyst are still affected by reaction parameters during the modification step,[109] and as a consequence, enantioselectivity is not just considered to be very sensitive to modification parameters during the modification procedure, as in the case of unsupported systems, but to many synthetic factors during catalyst design as well.

1.8 Understanding the Nature of TA-Ni and its Influence in the Hydrogenation of MAA

Despite the effort made to understand the reaction on the catalyst, the fact is that the actual source of enantiodifferentiation and the nature of the asymmetric hydrogenation site are not well understood.

As the enantioselective performance of the catalyst is linked directly to the presence of chiral modifiers, the local nature of the chiral molecule at the surface is central to understand the chiral influence it exerts on the reaction.

From all the experimental data obtained through years, there have been many audacious attempts to try to elucidate the mechanism of the enantioselective hydrogenation of MAA over chirally modified Ni. Izumi[67] proposed a model for TA-Ni

in which TA is adsorbed as a chelate, while Tai[116] proposed that TA is adsorbed on the catalyst surface as sodium tartrate. As mentioned before, substrate specificity is one characteristic of enantioselective catalysts, and for the enantioselective hydrogenation of MAA the most suitable catalyst is Ni modified with either α-aminocarboxylic or α-hydroxycarboxylic acids. Two facts are true in these systems:

i.   replacing the modifier by its antipode reverses the enantioselectivity of the process, and

ii. amino and hydroxy acids of identical configuration, used as modifiers, display the opposite sign of enantioselectivity.[51]

Groenewegen et al. [92] studied the adsorbed complexes of amino acids, hydroxy acids and MAA on supported Ni by means of IR spectroscopy. From their results, they showed that the complexes of MAA and amino acids chemisorbed on supported Ni by sublimation were absorbed in the form of metal chelates. Those structures remained the same when they were coadsorbed on the same surface. In contrast, hydroxy acids were adsorbed on Ni as carboxylates. In this composition, the hydrogen of the carboxyl group is available for bonding to another adjacent molecule. The differences between the structures of chemisorbed amino acid and hydroxy acid onto Ni could explain the difference in reactivity when they are used as modifiers. Then, according to these researchers, a hydrogen bond between the OH of the adsorbed hydroxy acid and the oxygen atom of the methoxy group of the adsorbed MAA would be formed. However, the evidence that the IR spectra of α-aminocarboxylic acids adsorbed on Ni is indistinguishable to that of the amino acid-Ni coordination compounds, and the findings that Ni modified with amino acids

showed comparable enantioselectivities to Ni modified with amino acid-Ni complexes led to further research on Ni modified with TA-Ni complexes.[117] The results obtained suggest that the formation of TA-Ni or Na-TA-Ni complexes is essential for enantioselectivity. This idea is supported by the observation that Ni modification is carried out with TA solutions which pH is adjusted using NaOH, where TA has exchanged two protons for Na ions. Therefore, the authors propose that Na-TA-Ni in conjunction with Ni metal are responsible for enantioselectivity. In this sense, Ni metal would:

i. serve as a chemical reagent for the formation of Na-TA-Ni when the modification is carried out either with TA or Na-TA, i.e. the modification is a corrosive process in which Ni atoms would be pulled out from the Ni lattice and complexed by TA molecules,

ii. act as carrier of Na-TA-Ni complex, and

iii. dissociate hydrogen molecules. One of the Ni atoms of the adsorbed complex would be the site on which the hydrogenation of MAA takes place.

Based on the arguments of Thomson and Webb,[118] Hoek *et al.*[117] claimed that the hydrogen for this active site is obtained from the complex and then the stoichiometry of the complex is re-established by transfer of hydrogen chemisorbed in the Ni metal to the complex. This concept would explain why both Ni (the one present in the complex and the metallic one) are required for the enantioselective hydrogenation. When Cu was used for preparing the tartrate complexes instead of Ni, enantiodifferentiation was not observed.

The idea claimed by Groenewegen et al.[92] that in the absence of metallic Ni hydrogenation does not take place was rejected by Keane et al.[106] who analysed the solutions left after modification, and found species with catalytic activity and enantiodifferentiation ability leached out during modification. They claim that the product of hydrogenation of one of their catalysts had a high concentration of Ni and by just adding fresh ketone to the product of reaction containing MAA, MHB and the solvent, by repeating the catalytic step they could raise the %mol conversion of MHB.

According to Osawa et al.,[119] TA is adsorbed on the catalyst surface as a nickel sodium tartrate. One of the hydroxyl groups of TA is close to the catalyst surface, and the second hydroxyl group is away from the surface. MAA is adsorbed through two hydrogen bonds between the two hydroxyl groups of TA and two carbonyl groups of MAA. The carbonyl group of MAA to be hydrogenated is fixed at site 1 (Figure 1.8.1).
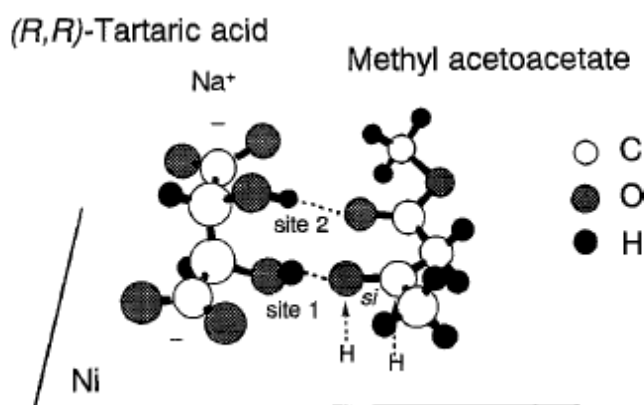
Figure 1.8.1: Mode of enantiodifferentiation over TA-RaNi catalyst for the hydrogenation of MAA (Taken from reference[119]).

However, given that the complexity of a real catalytic system makes it almost impossible to elucidate the local nature of the chiral molecule at the surface, there have been studies on a mimic of a catalytic system by adsorbing pure enantiomers of chiral molecules on defined single crystal metal surfaces.[120-136]

The first example is the adsorption of (R,R)-TA on Cu(110).[120, 122] The molecule shows dynamic adsorption behaviour highly sensitive to coverage and temperature. As these parameters are varied, the adsorbed molecules change between the monotartrate, bitartrate or dimer forms (Figure 1.8.2), the three forms in which TA molecules can exist. Moreover, these studies revealed the ability for molecules to self-organise on the surface leading to nanostructures with different crystalline architectures which exhibit various hierarchies of chiral expression (Figure 1.8.3).[120-122]
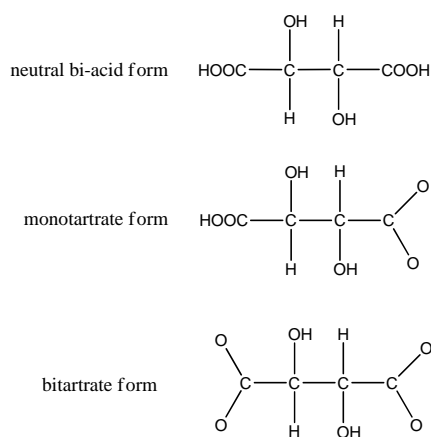
Figure 1.8.2: Three different forms in which TA can exist.

In the first expression of chirality, the chiral centres of the molecule are preserved upon adsorption for all the various forms that it adopts. In the second level of chiral expression, the molecule is bonded to Cu via the two carboxylate groups. This

adsorption geometry facilitates intramolecular hydrogen-bonding between the OH groups at the chiral centres and the oxygens of the carboxylic group, leading to an asymmetric distortion in the molecule, which is enantiomeric-specific (the (R,R) enantiomer distorts one way and the (S,S) distorts in the mirror configuration). The next level of chiral expression arises from the organisation of individual adsorbates at the surface. Rows of three bitartrate molecules are formed on the surface. These rows go forward to self-assemble into long chains. Neither chain coincides with a mirror symmetry direction of the underlying surface. This macroscopic surface organisation is therefore chiral. Furthermore, switching adsorbate flips the organisational chirality. In the final level of chiral expression, adsorption stress leads to the creation of vacant, chiral nanochannels. Each longer trimer chain is separated from the adjacent trimer chain by a vacant channel. These nanochannels are also directed along a non-symmetric direction and create therefore chiral spaces on Cu (Figure 1.8.3).
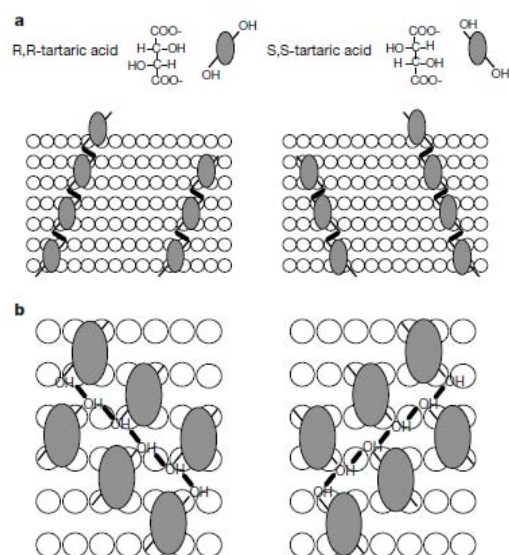
Figure 1.8.3: Spatial alignment and intermolecular hydrogen-bonding interactions of the α-hydroxy groups on the two enantiomers of TA. Left column, (R,R)-TA; right column, (S,S)-TA. The short, thick lines show extended hydrogen-bonding interactions: in a, these interactions dictate the direction of long chain growth; in b, they `weave together' the three molecular chains (Taken from reference[121]).

According to those results, it was concluded that the nanochannels provide a confined environment within which reacting molecules can dock in preferential orientations forcing hydrogenation to occur at one reactant face only. Therefore, the active site for these systems is described by groups of modifiers acting cooperatively to confer enantioselectivity to the reactive metal sites.

Studies over (R,R)-TA on Ni(110) shows that the chiral adsorbate changes dynamically as temperature and coverage change as in the case of Cu(110)[123] (Figure 1.8.4). A major difference between both systems is in the organisation of the bitartrate species. In contrast to the two dimensional arrays observed in the tartaric acid on Cu(110) system, only one dimension chains occur on Ni(110). Moreover, detailed studies have shown that adsorption leads to a highly strained bitartrate-Ni_4 complex at the surface where a strong asymmetric distortion of the bitartrate molecule is created, and a reorganisation of the bonding Ni atoms into chiral arrangements takes place simultaneously.[130, 132] The Ni atoms are pulled away from their symmetric positions and distorted to give an oblique unit mesh where all mirror planes are locally destroyed (Figure 1.8.5). Finally, calculations on polar charge distributions of the bitartrate-Ni_4 complex show that the transmission of chirality from the adsorbate to the solid is not just restricted to a geometrical reorganisation but to a direct electronic communication between the chiral centres of the acid and its bonding groups (O-Ni), leading to a chiral distribution of bondlengths.

	Bitartrate	Monotartrate	
300 K			Multilayer
270 K & 170 K	Monotartrate		Bi-Acid Form
90 K	Physisorbed Bi-acid Molecules (COOH-CHOH-CHOH-COOH)		

Increasing Coverage   └ Saturation ML
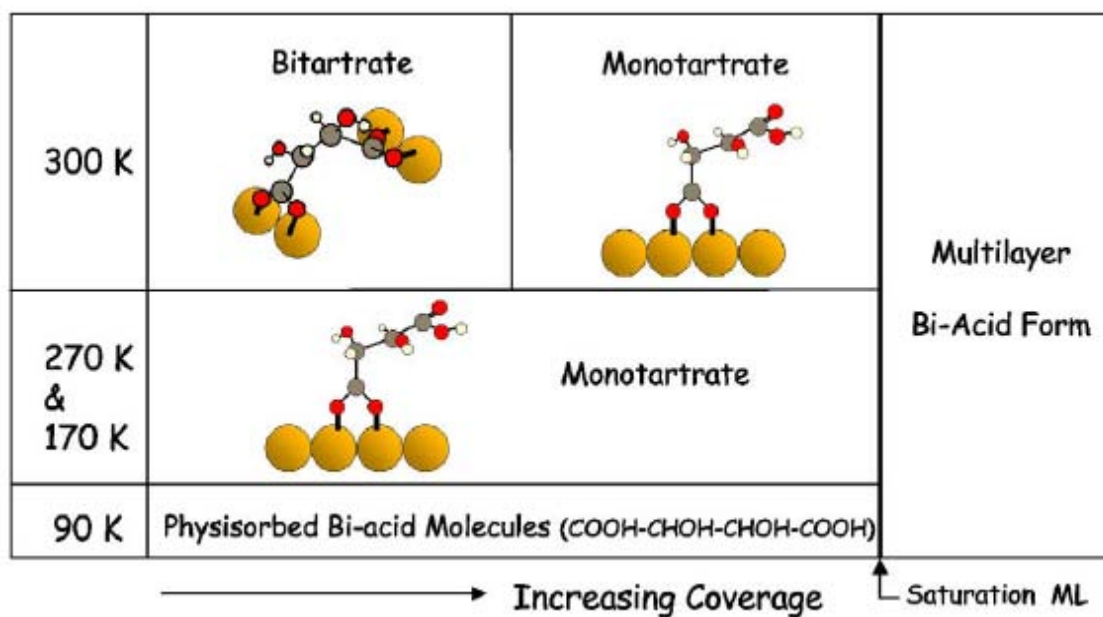
Figure 1.8.4: Adsorption phase diagram showing the chemical nature adopted by (*R*,*R*)-TA molecules on the Ni(110) surface as a function of temperature and coverage (taken from reference [132]).
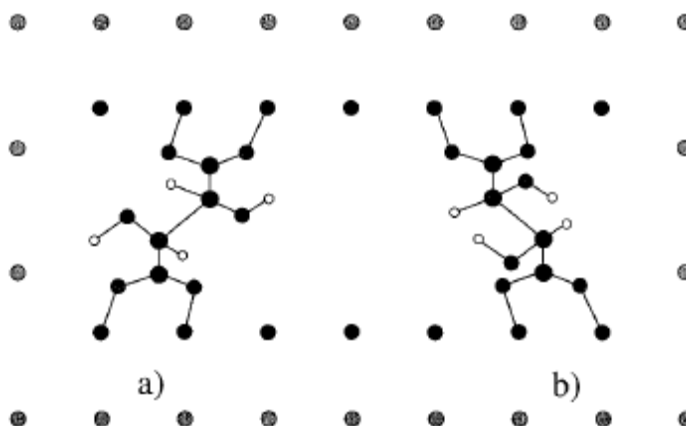
Figure 1.8.5: Depiction of the relaxed bitartrate-Ni$_4$ species adsorbed in twin mirror chiral footprints at the Ni(110) surface (Taken from reference[123]).

The studies of more significance in catalysis are those made over Ni(111) because Ni is the most active metal and the (111) surface is the most thermodynamically stable face on Ni nanoparticles.[125] In contrast to the studies done over Cu(110) where channels between ordered domains of tartrate molecules have

been seen, the ordering of the chiral modifiers result in an ordered array of vacancies on the surface. These vacancies may provide a chiral adsorption site for the reactant to dock into it (Figure 1.8.6). Although the size of the vacancy in the ordered array could accommodate the smallest β-ketoester, MAA, there is no evidence that this happens.[124]

As the chiral modification is carried out in aqueous solutions, studies over oxidised Ni(111) surfaces have been carried out.[134] The interaction of tartrate with pre-oxidised Ni particles may facilitate etching of Ni from the surface. According to the authors, this fact could reveal chiral arrangements of Ni responsible for the enantioselectivity during catalysis.
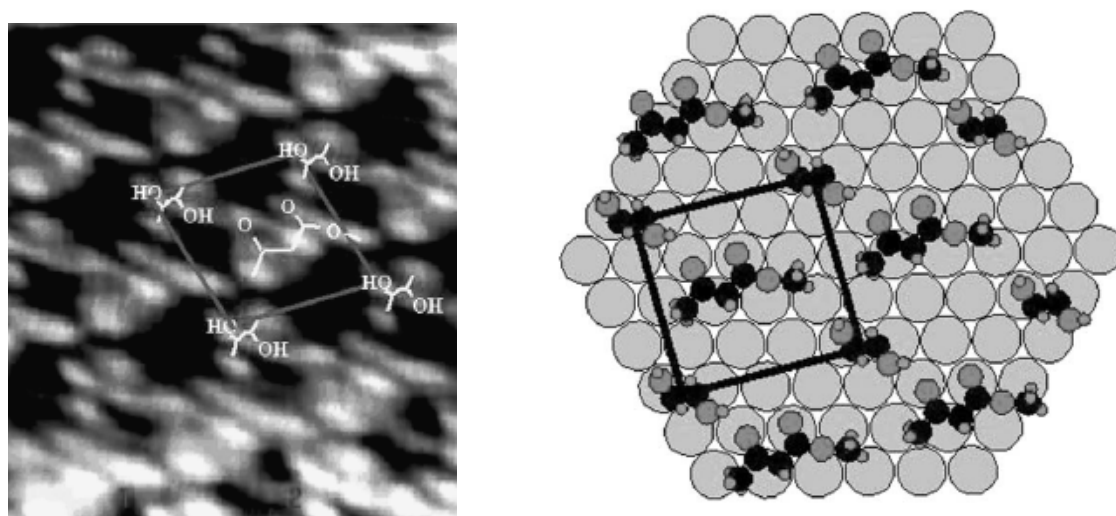
Figure 1.8.6: Left: STM image of MAA onto a Ni(111) surface modified by a low coverage of (R,R)-TA N.B. just one unit cell is represented for clarity. Right: schematic diagrams showing possible model structures for the two ordered structures created by MAA adsorption onto (R,R)-TA modified Ni(111). N.B. for clarity only the hydroxy groups of the tartrate species are shown. (Taken from reference[124]).

All of these admirable attempts to understand the active site in TA-Ni catalysts for the hydrogenation of MAA have given another dimension to the subject matter. Nevertheless, the truth is that we do not have an absolute understanding of the catalytic phenomena which would help to rationalise the design of better catalysts.

Despite the fact that TA-RaNi has been claimed to show an almost perfect enantiodifferentiation in the reaction of interest,[60] still research is carried on this system. Some of the novel approaches consist of the use of ultrasound during modification,[77-79] and the use of chiral solvents[89] and Na acetate[90] during catalysis.

Due to its potential industrial application, there is a special interest in further researching TA-Ni. The facts that TA-Ni can be prepared from different Ni sources,[59] that Ni activated through thermal processes gives comparable results to Ni activated from solution,[66] synergic effects between support and metal can enhance the catalytic properties of the solid,[111] and that previous studies on supported Ni have produced ambiguous results because of the lack of a method to obtain materials with controlled Ni particle size, all of them have led us to look for alternative methods for designing reproducible catalysts.

We are proposing the use of hydrotalcite-like compounds, HLCs, as precursors of supported Ni. The use of these precursors allows better control of Ni particle size and greater flexibility in the nature of the catalyst support. In our contribution to this exciting field, we are exploring as well the use of OMS to support Ni as an alternative to amorphous silicas. Their regular porous systems could play an important role in the performance of the active phase.

1.9 AIMS

- To synthesise HLCs containing Ni and a wide range of other cations (i.e. Mg, Zn, Fe, Al, Cr) and their mixtures using hydrolysis urea and coprecipitation methods

- To fully characterise the materials obtained by XRD and TG-DTA

- To develop supported Ni on mixed oxides through thermal treatments on HLCs

- To synthesise OMS of MCM-41, MCM-48 and SBA-2 types

- To characterise the materials obtained by low angle XRD and nitrogen physisorption

- To incorporate Ni into OMS by liquid and solid state reactions

- To chirally modify Ni supported on mixed oxides obtained from HLCs and on OMS with TA and to optimise the variables affecting e.e. during chiral modification (i.e. pH, time, solvent, temperature, etc.)

- To research the catalytic properties of all of the materials in the hydrogenation of MAA

- To analyse the postmodifier solutions by HPLC and AAS to determine the extent of TA adsorbed onto and Ni leached from the solids

Chapter 2 describes the techniques used in these studies. Chapter 3 investigates the use of HLCs as precursors of supported Ni to design enantioselective catalysts. The use of OMS as supports of TA-Ni catalysts is explored in Chapter 4. Finally, Conclusions and Future Work Direction are presented in Chapter 5.

CHAPTER 2. TECHNIQUES

2.1 XRD

2.1.1 Principles

2.1.1.1 Generation of X-Rays

X-rays are a form of electromagnetic radiation with wavelengths in the range of 0.01 and 10 nm, which are located in between γ-rays and the ultraviolet rays in the electromagnetic spectrum, and were discovered by Wilhelm Röntgen in 1895.

X-rays are usually generated in the laboratory using X-ray tubes. There are two types of tubes: sealed tube and rotating anode tube. The sealed tube consists of a cathode coupled with an anode. Both components are placed inside a metal/glass or a metal/ceramic container sealed under high-vacuum (Fig. 2.1.1.1.1).
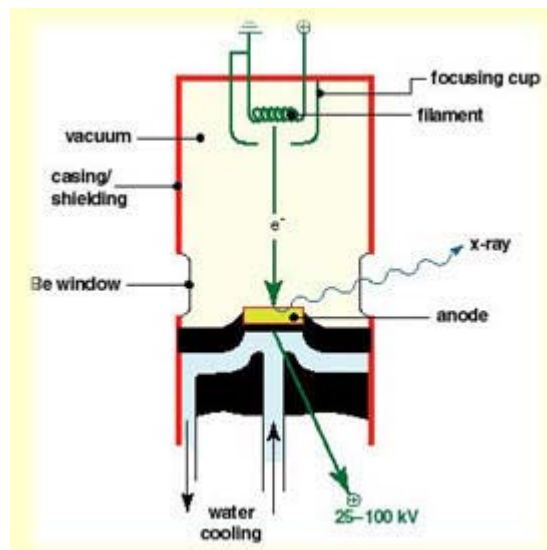
Fig. 2.1.1.1.1: Diagram of a typical sealed X-ray tube.

The generation of X-rays occurs by the collisions of accelerated electrons provided by the cathode (which is usually a heated tungsten filament) with a water-cooled metal target (commonly Cr, Fe, Cu, Mo and Ag). The electron beam is accelerated towards the anode, by a potential difference of ~30 kV maintained between the cathode and the anode. This generates a current of 10-50 mA in the tube. About 1% of the energy generated is emitted/radiated perpendicular to the path of the electron beam as X-rays which exit the tube through beryllium windows. The rest of the energy is released as heat. Therefore the anode must be continuously cooled with chilled water to avoid target meltdown.[137]

The low thermal efficiency of the sealed X-ray tube can be substantially improved by using a rotating anode X-ray source. In this design, a massive disk-shaped anode is continuously rotated at a high speed while being cooled by a stream of chilled water. Both anode mass and anode rotation improves the X-ray tube input power.

The X-ray spectra generated in the X-ray tube usually have two components, a broad continuous spectrum of wavelengths known as white radiation and a number of fixed, or monochromatic wavelengths (Fig. 2.1.1.1.2). The continuous part of the spectrum is generated by electrons decelerating rapidly, or stopped by the collision and some of their lost energy is converted in electromagnetic radiation. White radiation, also known as *bremsstrahlung* (German for "braking radiation"), is generally highly undesirable in X-ray diffraction analysis applications.

On the other hand, the monochromatic X-rays result from the transitions of upper level electrons in the atom core to vacant lower energy levels, from which an electron was rejected by the impact with an electron accelerated in the X-ray tube. The energy

differences between various energy levels in an atom are element-specific and therefore, each chemical element emits X-rays with a constant, characteristic distribution of wavelengths that appear due to excitations of core electrons by high energy electrons bombarding the target. For Cu the $2p \rightarrow 1s$, called $K\alpha$, has a wave length of 1.5418 Å and the $3p \rightarrow 1s$ transition, $K\beta$, 1.3922 Å. The $K\alpha$ radiation is used in diffraction experiments. In fact, the $K\alpha$ radiation is a doublet, $K\alpha_1$ = 1.54051Å and $K\alpha_2$ = 1.54433 Å, because the transition has a slightly different energy for the two possible spin states of the $2p$ electron that makes the transition, relative to the spin of the vacant $1s$ orbital. In some X-ray experiments, diffraction by the $K\alpha_1$ and $K\alpha_2$ radiations is not resolved and a single line or spot is observed instead of a doublet (e.g. in powder diffractometry at low angle). In other experiments, separate diffraction peaks may be observed. However, this can be overcome by removing the weaker $K\alpha_2$.[138]
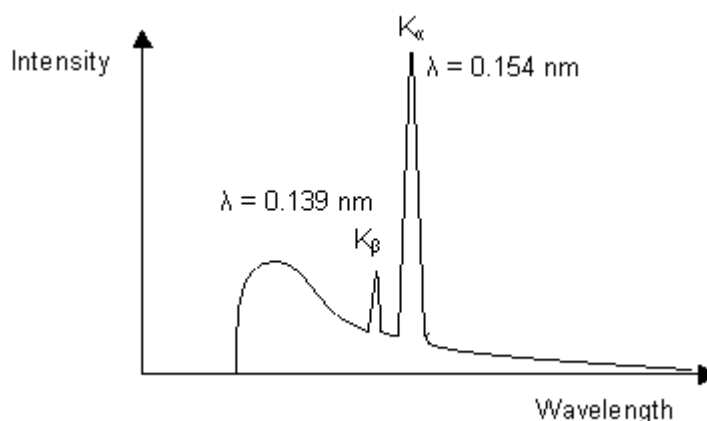
Fig. 2.1.1.1.2: X-ray emission spectrum of Cu.

For most diffraction experiments, a monochromatic beam of X-rays is desired and not a continuous spectrum. In the spectrum of X-rays emitted by Cu, the *Kα* line(s) is the most intense and it is desired to filter out all other wavelengths, leaving the *Kα* for diffraction experiments. For Cu radiation, a sheet of Ni foil is a very effective filter. The energy required to ionize 1*s* electrons of Ni corresponds to a wavelength of 1.488 Å, which lies between the values of the *Kα* and *Kβ* lines of the Cu spectrum. Cu *Kβ* radiation, therefore, has sufficient energy to ionize 1*s* electrons of Ni whereas Cu *Kα* does not. Ni foil is effective in absorbing the Cu *Kβ* radiation and most of the white radiation, leaving a monochromatic, reasonably clean beam of *Kα* radiation. The atomic number of the element in the filter generally is one or two less than that of the target material.

Monochromatised X-rays are generally colimated to a single direction before they are directed to the material to be studied. This is needed in order to improve the quality of the powder diffraction pattern. Collimation can be achieved by placing a slit between the X-ray source and the sample.

X-rays are used to obtain the diffraction pattern because their wavelength λ is typically the same order of magnitude (1-100 Å) as the spacing *d* between planes in a crystal. The phenomenon of X-ray diffraction is described by the Bragg's law.

2.1.1.2 Bragg's Law

Bragg proposed a model to describe the X-ray diffraction phenomenon. This model makes use of a set of evenly spaced sheets running through a crystal, usually

passing through the centres of the atoms of the crystal lattice. The orientation of a particular set of sheets is identified by its three Miller indices (h, k, l). Incoming X-rays are scattered specularly (mirror-like) from each plane (Figure 2.1.1.2.1). From the former assumption, X-ray scattered from adjacent planes will combine constructively (constructive interference) when the angle θ between the plane and the X-ray results in a path length difference that is an integer multiple n of the X-ray length λ.
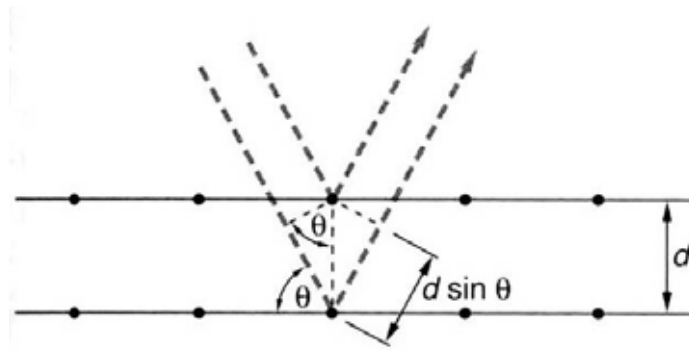
Figure 2.1.1.2.1: Schematic representation of the Bragg's law.

The assumptions described above and represented in Figure 2.1.1.2.1 are summarised in the following equation:

$$2d\sin\theta = n\lambda$$

The intense spot arising from constructive interference is known as reflection. A reflection is said to be indexed when its Miller indices (or, more correctly, its

reciprocal lattice vector components) have been identified from the known wavelength and the scattering angle 2θ. Such indexing gives the unit cell parameters, the lengths and angles of the unit cell, and the space group. Moreover, once the angle θ corresponding to a reflection has been determined, *d* may be calculated.

2.1.2 Powder XRD

Powder XRD is an analytical technique mainly used to identify a sample of a solid substance by comparison of the positions of the diffraction lines and their intensities with a large data bank. This technique is also used to assess sample purity and to determine unit cell dimensions.

The initial idea of Max von Laue that a crystal might not be suitable orientated to act as a diffraction grating for a single wavelength, but whatever its orientation, the Bragg law would be satisfied for at least one of the wavelengths if a range of wavelengths was used, was further studied by Peter Debye and Paul Scherrer. In their approach, they used monochromatic radiation and a powdered sample instead. The use of a powder sample guaranteed that at least some of the crystallites were orientated so as to satisfy the Bragg condition for each set of planes (*hkl*).[139]

The diffracted beams lie on a cone around the incident beam of half-angle 2θ (Figure 2.1.2.1). Similarly, other crystallites are orientated with different planes satisfying the Bragg's law. They give rise to a cone of diffracted intensity with a different half-angle. In principle, each set of (*hkl*) planes gives rise to a diffraction

cone, because some of the randomly orientated crystallites will have the correct angle to diffract the incident beam.
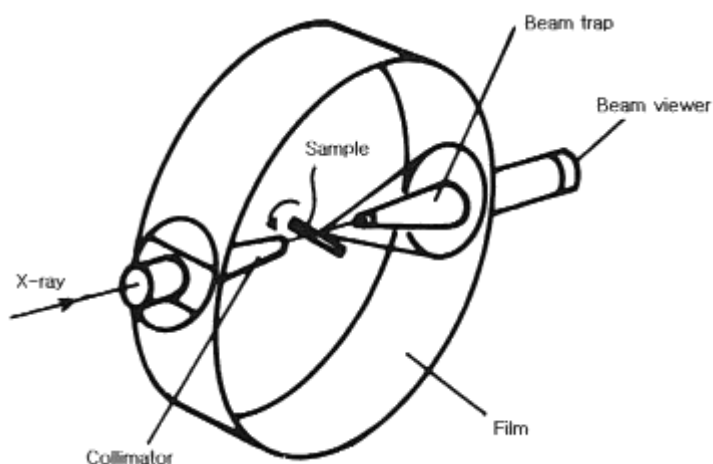
Figure 2.1.2.1: Debye-Scherrer camera

2.1.3 Instrumentation

X-ray difractometers consist of three basic elements: X-ray tube, sample holder and X-ray detector. As the sample and detector are rotated, the intensity of the reflected X-rays is recorded. When the geometry of the incident X-rays impinging the sample satisfies the Bragg equation, constructive interference occurs and a peak in intensity occurs. A detector records and processes this X-ray signal and converts the signal to a count rate which is then output, generating the diffraction pattern.

X-ray diffractometers can be operated in both transmission and reflection configurations. In both cases, the sample preparation consists of placing the powder in a disc container and its surface carefully flattened. In the transmission configuration (known also as theta-theta configuration), the sample is still while the

X-ray tube and the detector are rotated around it. The angle formed between the tube and the detector is 2theta. In the reflection configuration, the disc is put on one axis of the diffractometer and tilted by an angle θ while a detector (scintillation counter) rotates around it on an arm at twice this angle. This configuration is known as Bragg-Brentano or theta-2theta configuration.

2.2 TG-DTA

2.2.1 TGA

Thermogravimetric analysis (TGA) is a technique used to determine changes in weight with respect to changes in temperature. This method provides information such as the temperature at which the degradation of a material occurs, the amount of inorganic and organic components in materials, as well as moisture content, amongst others.

The equipment consists of a high precision balance with a pan to load the sample. The pan is generally platinum. The pan is placed in a small electric heated oven containing a thermocouple (Fig. 2.2.1.1). Analysis consists of increasing the temperature gradually and plotting weight percentage against temperature. Before analysis, the system is purged with an inert gas in order to avoid oxidation or other undesired reactions. Another apparatus can be installed at the outlet of the equipment in order to analyse the composition of species released from the materials, i.e. mass spectrometer, gas chromatograph, IR spectrophotometer, etc.
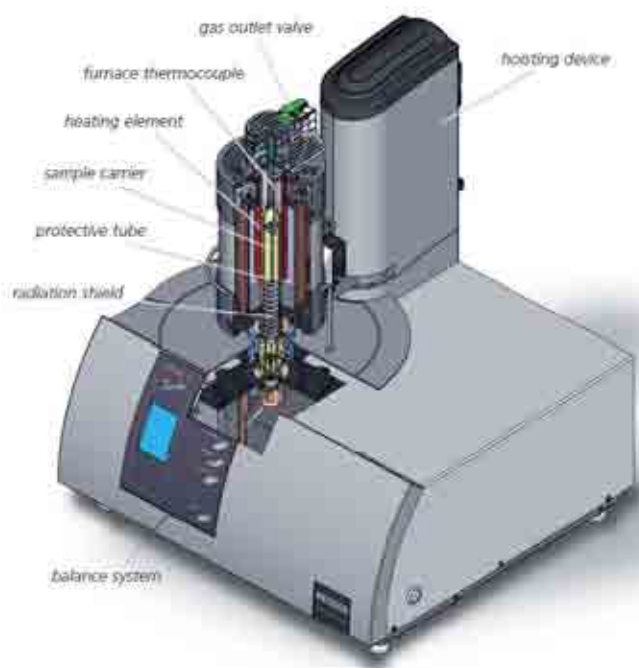
Fig. 2.2.1.1: TGA apparatus.

2.2.2 DTA

Differential thermal analysis (DTA) is a technique to determine changes of phases in materials with respect to temperature. In this technique, the material of study and an inert reference are made to undergo identical thermal cycles. The objective is to measure the difference of temperature between the sample and the reference. This differential temperature is plotted against time or temperature. The change in temperature with respect to the reference can be either exothermic or endothermic. This provides information about transformation of the material with respect to temperature (transitions).

The apparatus consists of a sample holder comprising thermocouples, sample containers and a temperature programmer. One thermocouple is connected to an inert material such as alumina and the other is placed in the crucible containing the

sample under study. Both two thermocouples are connected to a voltmeter. Any change in phase of the sample under study will make a deflection in the voltmeter, when the temperature at which the transition takes place is reached.

As this technique and TGA share common parts in their design and their goal is to heat a sample to see changes, they are commonly integrated in one single apparatus.

2.3 Nitrogen adsorption

2.3.1 Principles

In general, the phenomenon of adsorption consists of the adhesion of gas, liquid or dissolved solids to a surface. The substance that adsorbs is the adsorbate and the underlying material is the adsorbent. The opposite phenomenon is called desorption.

There are two ways in which molecules and atoms can adsorbe to surfaces: physisorption and chemisorption. The interactions responsible for physisorption are Van der Waals interactions. These interactions have long range but they are weak. Typical enthalpy values of physisorption are in the range of 20 kJmol^{-1}. In contrast, in chemisorptions, the probe molecule adheres to the surface by forming a chemical bond. Typical enthalpy values in this case are in the range of 200 kJmol^{-1}. In addition, some molecules adsorb selectively to different planes on surfaces. For example, the selective chemisorption of nitrogen on nickel and palladium has been reported.[140] Moreover, a 2 to 1 ratio has been found between molecules of more strongly adsorbed carbon dioxide and molecules of nitrogen chemisorbed on platinum.[141]

The extent of surface coverage during adsorption is expressed as the fractional coverage θ, where:

$$\theta = \text{Number of adsorption sites occupied/Number of adsorption sites available}$$

On the other hand, the fractional coverage is often expressed in terms of adsorbate volume by:

$$\theta = V/V_\infty$$

where V_∞ is the corresponding volume of adsorbate to complete the monolayer coverage. This volume can be determined by observing the change of fractional coverage with respect to time.

The variation of θ with respect to pressure at a fixed temperature leads to an adsorption isotherm. The amount of adsorbate in the adsorbent is function of its pressure. The quantity adsorbed is normalised by the mass of the adsorbent to allow comparison to other materials. There are many types of isotherms and they agree quite well with experimental data despite their empirical basis. One of them is the BET isotherm, which has its basis in the BET method.

2.3.1.1 BET Method

The BET method is a useful analysis technique to estimate surface areas on materials. BET stands for the initial of the surnames of Stephen Brunauer, Paul Emmett and Edward Teller who aimed to explain the physical adsorption of gas molecules on a solid surface.[142] Their theory is an extension of the Langmuir theory which suggests that adsorption takes place through the following mechanism:

$$A(g) + S \leftrightarrow AS$$
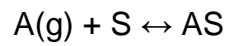
where A is a gas molecule and S is an adsorption site. The direct and inverse rates are K_1 and K_{-1}; and in the overall equilibrium:

$$k = \frac{K_1}{K_{-1}} = \frac{\theta}{(1-\theta)p} \qquad (1)$$

or

$$\theta = \frac{Kp}{1 + Kp} \qquad (2)$$

where p is the partial pressure of the gas. For very low pressures $\theta \approx Kp$ and for high pressures $\theta \approx 1$.

The amount of substance adsorbed, m, will be proportional to θ for a specified adsorbent, so $m = b\theta$, where b is a constant. Then:

$$m = \frac{bKp}{1 + Kp} \qquad (3)$$

which if inverted, yields:

$$\frac{1}{m} = \frac{1}{b} + \frac{1}{bKp} \qquad (4)$$

By plotting $1/m$ against $1/p$, the constants K and b can be determined from the slope and intercept of the line. Knowing K, the fraction of the surface covered, θ, can be calculated.[143]

The Langmuir model is based on the following assumptions:

1. The surface of the adsorbent is uniform; therefore all of the adsorption sites are equivalent.

2. Adsorbed molecules do not interact with each other.

3. All adsorption occurs through the same mechanism.

4. At the maximum adsorption, only a monolayer is formed; molecules of adsorbate do not deposit on other, already adsorbed, molecules of adsorbate, only on the free surface of the adsorbent.

However, there are always imperfections in surfaces, adsorbed molecules are not necessarily inert, and the mechanism is clearly not the same for the very first molecules to adsorb to a surface as for the last. The fourth condition is the most troublesome as frequently more molecules will adsorbed to the monolayer. This problem is addressed by the BET model.

BET theory deals with multilayer adsorption taking into account the following hypothesis:

i. gas molecules physically adsorb on a solid in layers infinitely

ii. there is no interaction between each adsorption layer; and

iii. the Langmuir theory can be applied to each layer.

The corresponding mathematical derivation leads to equations (5) and (6):

$$\frac{1}{v\left[\left(P_0/P\right)-1\right]} = \frac{c-1}{v_m c}\left(\frac{P}{P_0}\right) + \frac{1}{v_m c} \tag{5}$$

$$c = \exp\left(\frac{E_1 - E_l}{RT}\right) \tag{6}$$

where:

P = equilibrium pressure of adsorbate at the temperature of adsorption

P_0 = saturation pressure of adsorbate at the temperature of adsorption

v = adsorbed gas quantity

v_m = monolayer adsorbed gas quantity

c = BET constant

E_1 = heat of adsorption for the first layer

E_l = heat of adsorption for the second and higher layers (heat of liquefaction)

The adsorption isotherm of equation (5) can be plotted as a straight line with $\dfrac{1}{v\left[\left(P_0/P\right)-1\right]}$ on the y axis and $\varphi = \left(\dfrac{P}{P_0}\right)$ on the x axis, according to the experimental results. The plot obtained is called a BET plot (Figure 2.3.1.1.1). The linear relationship of this equation is maintained only in the range of $0.05 < P/P_0 < 0.35$. The value of the slope (A) and the y intercept (I) of the line are used to calculate the monolayer adsorbed gas quantity v_m and the BET constant c. For that means, the following equations are used:

$$v_m = \frac{1}{A + I} \qquad (7)$$

$$c = 1 + \frac{A}{I} \quad (8)$$

The total and specific surface areas (S_{total} and S, respectively) can be evaluated using the following equations:

$$S_{total} = \frac{(v_m N s)}{V} \quad (9)$$

$$S = \frac{S_{total}}{a} \quad (10)$$

where:

N = Avogadro's number

s = adsorption cross section

V = molar volume of adsorbent gas

a = molar mass of adsorbed species
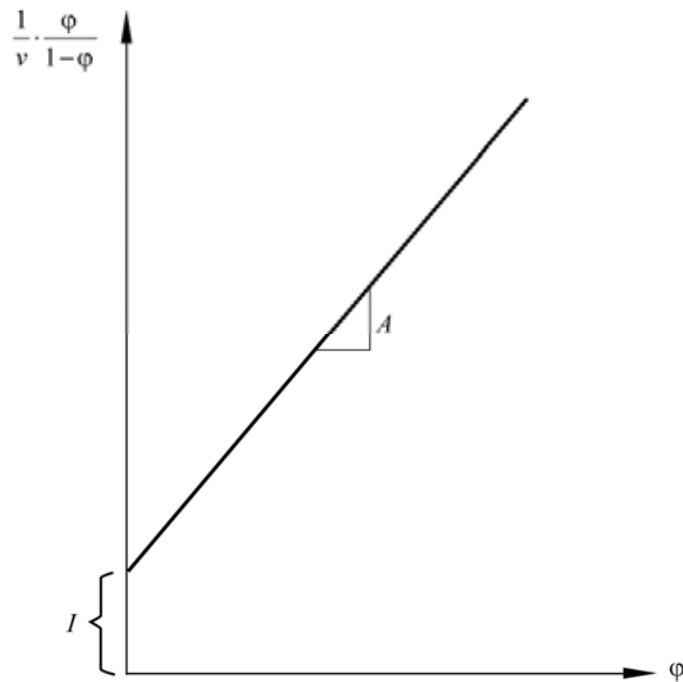
Figure 2.3.1.1.1: Plot BET.

2.3.1.2 BJH Method

BJH stands for the surname of Elliott P. Barrett, Leslie G. Joyner and Paul P. Halenda.[144] Their method consists in computing the pore volume and area distribution from the desorption isotherms of porous materials. It is based on the Kelvin equation of cylindrical pore filling. Their model assumes that the equilibrium between the gas and adsorbed phases during desorption is determined by two mechanisms:

i. physical adsorption on the pore walls, and

ii. capillary condensation.

The calculation may be summarized in the following equation:

$$v_{ads}(x_k) - \sum_{i=1}^{k}[\Delta V_i(r_i] \le r_c(x_k)) + \sum_{i=k+1}^{n} \Delta S_i t_i(r_i > r_c(x_k))$$

where:

v_{ads} = volume of liquid adsorbate (cm^{3}g^{-1})

x_k = relative pressure $\left(\frac{P}{P_o}\right)$ in cm^{3}g^{-1} (STP)

V = volume given in cm^{3}g^{-1}

r_i = pore radius

r_c = inner capillary radius

S = surface area (m^{2}g^{-1})

t = thickness of adsorbed layer

The formula describes that the amount of volume adsorbed at the k-th point in the isotherm is the contribution of the volume in condensate in all pores smaller than some characteristic size (depending on the current relative pressure, x_k) and the volume of adsorbed film on all larger pores at that point.

43

2.3.2 Instrumentation

Prior performing a surface area analysis or pore size measurement, solid surfaces must be freed from physisorbed water and atmospheric gases. Surface cleaning, commonly known as degassing, is carried out by placing a sample of the solid to study in a glass cell and heating it up under a vacuum, or a flow of a dried inert gas. Once clean, the sample is brought to a constant temperature by means of an external bath containing a cryogen (i.e. liquid nitrogen). Then, small amounts of the adsorbate are admitted in steps into the evacuated sample chamber. The gas molecules adsorb on the adsorbent surface and pores. By plotting pressure against adsorbed volume the isotherm is obtained.

2.4 Chromatography

Even though the term chromatography was coined by Mikhail Tsvet during his studies on the separation of plant pigments at the beginning of the 20th Century, there is evidence that some related techniques were developed far before. Nevertheless, it was during the 1940s and 1950s when the principles and techniques of partition chromatography, which led to current technologies, were established.

2.4.1 Principles

Chromatography consists of the separation of compounds in a mixture, which is dissolved in a mobile phase and passed through a stationary phase. The stationary phase separates the different components present in the mixture (analytes) according to differential partitioning between the mobile and stationary phases. The

different partition coefficients of the compounds present in the mixture leads to a differential retention on the stationary phase.

2.4.1.1 Partition coefficient

The partition coefficient is the ratio of concentrations of a compound in the two phases of a mixture of two immiscible solvents at equilibrium (one of the solvents can be a solid). Therefore, these coefficients are a measure of different solubility of the compound between these two solvents.

2.4.2 Techniques by Physical State of Mobile Phase

Chromatography can be preparative or analytical. Whereas the purpose of preparative chromatography is to separate the components of a mixture for their further use (purification), analytical chromatography is carried out mainly for measuring relative proportions of analytes in a mixture. Techniques by physical state of mobile phase for preparative or analytical include gas chromatography (GC) and high pressure liquid chromatography (HPLC).

2.4.2.1 GC

In this technique, the mobile phase is a carrier gas, usually an inert gas such as helium or an unreactive gas such as nitrogen. The stationary phase is a microscopic layer of liquid or polymer on an inert solid support. The separation of the mixtures is based on boiling point (or vapour pressure) differences.

2.4.2.1.1 Operation/Instrumentation

A known volume of gas or liquid is injected into the head of a column containing the stationary phase. This column is placed inside an oven where the temperature of the gas can be controlled. As the carrier gas sweeps the analyte molecules through the column, this motion is inhibited by the adsorption of the analyte molecules either onto the column walls or onto packing materials in the column.

There are two types of column used in GC: packed and capillary. The main difference between them relies in their internal diameters.

The rate at which the molecules progress along the column depends on the strength of adsorption, which in turn depends on the type of molecule and on the stationary phase materials. Since each type of molecule has a different rate of progression, the various components of the analyte mixture are separated as they progress along the column and reach the end of the column at different times (retention time). A detector is used to monitor the outlet stream from the column; thus, the time at which each component reaches the outlet and the amount of that component can be determined.

Generally, substances are identified (qualitatively) by the order in which they emerge (elute) from the column and by the retention time of the analyte in the column. The most common detectors are thermal conductivity detectors (TCD) and flame ionisation detectors (FID). TCD detects components with different thermal conductivity to the carrier gas. TCD is a non-destructive method, whereas FID is a destructive method. It is common to use both of them in-series, as complementary information can be obtained by this means.

Chromatographic data is presented as a chromatogram, which provides a spectrum of peaks for a sample representing the analytes present in a sample eluting from the column at different times. Retention time can be used to identify analytes if the method conditions are constant. The area under the peak is proportional to the amount of analyte present in the chromatogram. By integration, the concentration of an analyte in the original sample can be determined. Concentration can be calculated using a calibration curve created by finding the response for a series of concentrations of analyte, or by determining the relative response factor of an analyte. The relative response factor is the expected ratio of an analyte to an internal standard (or external standard) and is calculated by finding the response of a known amount of analyte and a constant amount of internal standard (a chemical added to the sample at a constant concentration, with a distinct retention time to the analyte).

2.4.2.2 HPLC

In this technique, the mobile phase is a liquid. This phase can be either aqueous solutions containing a buffer or a salt, or miscible combinations of water with organic liquids. There are many different types of stationary phase, such as hydrophobic saturated carbon chains. This stationary phase is attached to the outside of small spherical silica particles.

2.4.2.2.1 Operation/Instrumentation

A small volume of the analyte is introduced in the stream of the mobile phase which is forced through the column by applying high pressure. The motion of the analyte through the column is slowed by specific chemical or physical interactions with the stationary phase as it traverses the length of the column. How much the analyte is slowed depends on the nature of the analyte and on the compositions of the stationary and mobile phases, as well as the flow rate of the mobile phase. The time at which a specific analyte elutes (comes out of the end of the column) is called the retention time. The retention time under particular conditions is considered a reasonably unique identifying characteristic of a given analyte. Commercial HPLCs are equipped with a UV detector.

A separation can take place at isocratic (constant concentration) or gradient elution conditions. The latter decreases the retention of the later eluting components so that they elute faster. The gradient chosen depends on how hydrophobic the analyte is. The gradient separates the analyte mixtures as a function of the affinity of the analyte for the current mobile phase composition relative to the stationary phase. The choice of solvents, additives and gradient depend on the nature of the stationary phase and the analyte. However, different parameters such as the internal diameter of the column, particle size and pore size of the stationary phase, as well as the performance of the pump are important for optimal separation.

2.4.2.3 Chiral Chromatography

To enable chiral separations to take place, either the mobile phase or the stationary phase must themselves be made chiral. For both GC and HPLC, there are chiral columns (with a chiral stationary phase) commercially available.

2.5 AAS

This technique is used to determine the concentration of a specific metal element in a solution.

2.5.1 Principles

As this technique makes use of absorption spectroscopy, it relies heavily in the Beer-Lambert law.

2.5.1.1 Beer-Lambert Law

This law relates the absorption of light to the properties of the material through which the light is travelling. It states that there is a logarithmic dependence between the transmission of light through a substance and the product of the absorption coefficient of the substance and the distance the light travels through the material (the path length). The absorption coefficient can be written as a product of the absorption cross section of the absorber and the density of absorbers. These relations are written in (1) as:

$$T = I/I_0 = e^{-\alpha l} = e^{-\sigma lN} \quad (1)$$

where:

T = transmission

I = intensity of transmitted light

I_0 = intensity of incident light

α = absorption coefficient of the substance

l = path length

σ = cross section of light absorption by a single particle

N = density (number per unit volume) of absorbing particles

The transmission is expressed in terms of an absorbance (A), defined as:

$$A = -\ln(I/I_0) \quad (2)$$

This implies that the absorbance becomes linear with the concentration according to:

$$A = \sigma lN$$

Thus, if the path length and the absorption cross section are known and the absorbance is measured, the number density of adsorbers can be deduced.

50

2.5.2 Instrumentation/Operation

In order to analyse a sample for its atomic constituents, it has to be atomised. The electrons of the atoms in the atomiser can be promoted to higher orbitals for a short amount of time by absorbing a set quantity of energy (i.e. light of a given wavelength). This amount of energy (or wavelength) is specific to a particular electron transition in a particular element, and in general, each wavelength corresponds to only one element. This gives the technique its elemental selectivity. The technique makes use of a flame to atomise the sample. The flame is around 10 cm long. The height of the flame above the burner head can be controlled by adjusting the flow of the fuel mixture. A beam of light passes through this flame at its longest axis (the lateral axis) and hits a detector.

A liquid sample is normally turned into an atomic gas in three steps:

1. Desolvation (Drying): the liquid solvent is evaporated, and the dry sample remains
2. Vaporization (Ashing): the solid sample vaporises to a gas
3. Atomisation: the compounds making up the sample are broken into free atoms.

The source of radiation is hollow cathode lamps. These lamps are filled with argon or neon gas and contain a cylindrical metal cathode and an anode. Gas particles are ionised by applying a high voltage across the anode and cathode. The further increase in voltage makes the gaseous ions acquire enough energy to eject metal atoms from the cathode. Some of these atoms are in excited states and emit light with the characteristic frequency of the metal.

CHAPTER 3. HLCs AS PRECURSORS OF SUPPORTED TA-Ni CATALYSTS

3.1 Definition of HLCs

In general, HLCs is the term used to refer to a family of materials possessing a similar structure to the occurring naturally mixed hydroxycarbonate of Mg and Al: $Mg_6Al_2(OH)_{16}CO_3 \cdot 4H_2O$ (hydrotalcite), which was first discovered in Sweden in 1842. One particular feature of this family of materials is their characteristic structure which consists of sheets of octahedral metal hydroxides containing two metals in different oxidation states, with cations occupying the centre of the octahedra and hydroxide ions the vertices. This array leads to a positive unbalanced charge which is compensated by hydrated anions in the interlayer space (Figure 3.1). Cations in the sheets and anions/water in the interlayer region are randomly distributed.[145, 146]
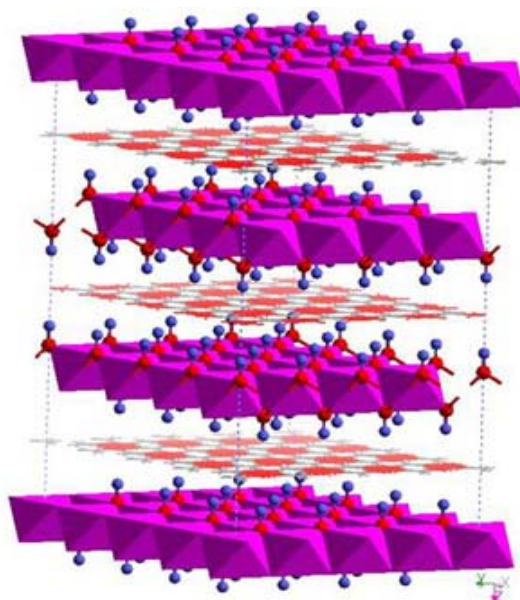
Figure 3.1: Hydrotalcite structure. Cations occupy the centre of the octahedral (in purple) and hydroxide ions the vertices (oxygen in red and hydrogen in blue). Anions and water are placed in the interlayer space.

Depending on the stacking of the sheets, two polytypes of HLCs can be found: one presenting three sheets per unit cell and another showing two sheets per unit cell (rhombohedral and hexagonal symmetry, respectively).[147]

Hydrotalcite crystallises in rhombohedral symmetry and the parameters of the unit cell are a = 3.05 Å and c = 3c' = 22.81 Å, where c' is the thickness of one layer constituted of one layer of octahedral metal hydroxides and one interlayer; c' value is therefore 7.603 Å.[148] The structure of these materials originates from the structure of brucite $Mg(OH)_2$, a mineral naturally occurring (Figure 3.2). In this compound, octahedra share edges to form sheets which stack at the top of the other. The octahedral contains Mg^{2+} in the centre and OH in the vertices. The sheets are kept together by hydrogen bonding. When Mg^{2+} ions are substituted for trivalent ions with not too different anionic radius, a positive charge is generated in the sheets. In order to balance the charge between sheets, anions are incorporated in this region along with water, to give the hydrotalcite structure.[149]

Figure 3.2: Brucite structure (magnesium cation in yellow, oxygen in red and hydrogen in pink).

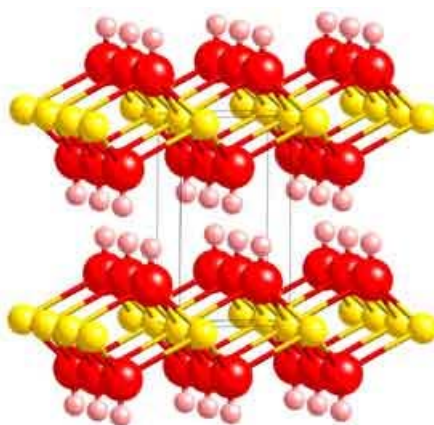The general formula of this type of materials is $[M^{II}_{1-x}M^{III}_x(OH)_2]^{x+}(A^{n-})_{x/n}\cdot yH_2O$; where: $M^{II} = Ni^{2+}$, Mg^{2+}, Zn^{2+}, Cu^{2+}, Fe^{2+} or Co^{2+}; $M^{III} = Al^{3+}$, Cr^{3+}, Fe^{3+}, Mn^{3+}, In^{3+} or Ga^{3+}; $A^{n-} = CO_3^{2-}$, NO_3^-, SO_4^{2-}, Cl^-, Br^-, F^-, OH^-, organic anions, etc., and y = moles of co-intercalated solvent, generally water. When the value of x is varied in the range between 0.2 and 0.33, the result is a large class of isomorphous materials with different physicochemical properties. For natural minerals, the value of x is 0.25 and carbonate is the most common anion. It is also possible to synthesize HLCs with more than two different cations and two different anions.

3.2 Methods of Preparation of HLCs

There are two techniques to synthesise HLCs: coprecipitation and hydrolysis of urea methods.

3.2.1 Coprecipitation Method

The simultaneous precipitation of homogeneous precursors (coprecipitation) is the most reliable and reproducible technique to synthesise HLCs. Moreover, this approach allows the preparation of non-noble metal base catalysts simply and cheaply.

In order to coprecipitate two or more cations, the coprecipitation must be carried out under supersaturation conditions. One way to reach these conditions is by adjusting the pH, which must be equal or higher than that of the most soluble metal hydroxide. In general, there are three ways to carry out the precipitation:

54

i) by increasing pH method, which involves titrating of a solution containing the metal precursors with another solution containing a base NaOH and/or NaHCO$_3$;

ii) by constant pH at low supersaturation method, which is carried out by simultaneous slow addition of both solutions containing the metal precursors and the base; and

iii) by constant pH at high supersaturation method, which consists in the quick addition of the solution containing the metal precursors to the solution containing the base.

After each of these methods, aging or hydrothermal treatments are carried out on the obtained slurries. This step leads to dissociation and, subsequently, to coprecipitation in order to rectify the improper conditions during synthesis. Therefore, no rigorous coprecipitation conditions are needed to develop this type of materials, but some considerations have to be followed in order to obtain pure compounds. The key parameters determining their final structure are both the nature and concentration of cations and anions during synthesis. The ratio between cations must be $0.2 \leq [(M(III)/(M(II)+M(III)] \leq 0.4$ and the ratio between anion species and cations must be $1/n \leq A^{n-}/M(III) \leq 1$ in the final product.

3.2.2 Hydrolysis of Urea Method

Another approach to synthesise HLCs is by the decomposition of organic compounds, i.e. urea.[150-179] The decomposition of urea produces carbonate ions accompanied by a simultaneous increase in the pH, both important factors to

precipitate metal carbonates. The mechanism involves the formation of ammonium cyanate and the further hydrolysis of the cyanate to ammonium carbonate.[180]

$$CO(NH_2)_2 \rightarrow NH_4CNO$$

$$NH_4CNO + 2H_2O \rightarrow (NH_4)_2CO_3$$
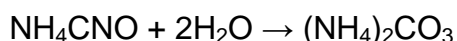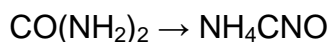
All of the metal hydroxides that form HLC precipitate at pHs between 8 and 10 in highly diluted solutions. The hydrolysis of ammonium to ammonia and carbonate to hydrogen carbonate gives a pH around 9, therefore leading to a suitable pH for precipitating a wide range of metal hydroxides.

3.3 Applications of HLCs

HLCs are useful in applications such as ion exchange and adsorption. For instance, they are useful in the removal of anionic pollutants from water. Their degree of anionic exchange depends on their structural characteristics, i.e. nature of interlayer anion and crystallinity. For example, removal of arsenates, nitrates and phosphates has been done using HLCs containing Zn-Al, Mg-Al and Mg-Fe.[181-186] On the other hand, compounds such as salicylic acid and bactericides have been successfully intercalated in HLCs containing Zn-Al and Mg-Al, respectively.[187-189]

HLCs are widely used in industry as molecular sieves and in medicine they are employed as antacids. In particular, these materials find potential application as

precursors of catalysts, and as catalysts themselves because when they are thermally treated, mixed oxides with high thermal stability and acid-base properties are obtained.[190, 191] In this way, HLCs have been used in catalytic processes such as Aldol,[192] Knoevenagel and Claisen-Schmidt condensations.[193] Moreover, the further reduction of materials containing reducible metals leads to well dispersed metallic particles. Particularly, nickel based catalysts prepared from mixed metal hydroxides have shown effectiveness in hydrogenation reactions . The first report of the catalytic activity of a coprecipitated Ni/Al system in hydrogenation reactions was first claimed in 1924[194] and the first publication claiming hydrogenation activity from a HLC precursor as such appeared in 1975.[195]

Materials prepared by hydrolysis of urea have been used as hosts[150-154, 156, 157, 169-171, 174, 176, 177], nanocomposites[158, 164, 166], and catalysts,[155, 159-161, 167, 168, 172-174, 178, 179] with particular interest in NiAl, NiZnAl and NiMgAl which have found interesting applications in catalysis.[159, 178]

3.4 Experimental

3.4.1 Preparation of TA-Ni Supported Catalysts

3.4.1.1 Supported Ni Obtained from HLCs Synthesised by Coprecipitation

A series of HLCs containing Ni^{2+}, Mg^{2+}, Zn^{2+}, Al^{3+}, Fe^{3+}, and Cr^{3+} were prepared from the metal nitrates using the coprecipitation method.

In the case of Al containing materials, the following combinations and molar ratios were used: Ni/Mg (or Zn) = ∞, 2.94, 1.09 and 0.42, keeping a constant relation of Al (Al/(Ni + Mg (or Zn)) = 0.33).

In the case of Fe containing materials, the following combinations and molar ratios were used: Ni/Mg (or Zn) = ∞ and 2.94, keeping a constant relation of Fe (Fe/(Ni + Mg (or Zn)) = 0.33).

For the series of materials containing Cr, the following combinations and molar ratios were used: Ni/Mg = ∞, 2, 0.875 and 0.5, keeping the relation of Cr constant (Cr/(Ni + Mg) = 0.25).

The synthesis was carried out as follows: an aqueous solution containing the metal precursors in appropriate ratios (with total concentration 0.8 mol dm^{-3}) was added dropwise to another aqueous solution which contained NaOH and Na$_2$CO$_3$, in concentrations 2 and 0.7 mol dm^{-3}, respectively, under vigorous stirring at room temperature. The resulting solution was hydrothermally treated at different temperatures and times in an autoclave (details are given throughout Section 3.5). Finally, the solution was filtered, washed and dried.

The resulting materials were thermally treated in flowing oxygen to obtain the mixed oxide. Subsequent reduction of the solids was carried out in flowing 10% H$_2$ (diluted in N$_2$) in order to develop Ni metal. Different temperatures were used in both thermal treatments steps for which details are given throughout Section 3.5.

3.4.1.2 Supported Ni Obtained from HLCs Synthesised by Urea Hydrolysis

HLCs containing Ni^{2+}, Mg^{2+}, Zn^{2+}, Al^{3+}, Fe^{3+} and Cr^{3+} were prepared from the metal nitrates by means of the urea hydrolysis method.

For the series of materials containing Al, the following combinations and molar ratios were used: Ni/Mg (or Zn) = ∞, 2.94, 1.09 and 0.42, keeping a constant relation of Al (Al/(Ni + Mg (or Zn)) = 0.33).

In the case of Fe containing materials, the following combinations and molar ratios were used: Ni/Mg (or Zn) = ∞ and 2.94, keeping a constant relation of Fe (Fe/(Ni + Mg (or Zn)) = 0.33).

For the series containing Cr, the following molar ratios and combinations were used: Ni/Mg (or Zn) = ∞ and 2. The relation of Cr (Cr/(Ni + Mg (or Zn) = 0.25) was kept constant.

Basically, urea (1.65 mol dm^{-3}) was added to an aqueous solution containing the desired metal precursors in appropriate ratios (total concentration 0.5 mol dm^{-3}).[151] The solution was heated at 90°C under stirring and reflux for 48 hrs, and then filtered, washed and dried at 60°C. In this method there is no need to treat the solutions after synthesis in autoclaves.

The materials were calcined and reduced analogously to the series described above. Details of thermal treatments are given throughout Section 3.5.

3.4.1.3 Chiral Modification of Supported Ni Prepared from HLCs

The reduced supported Ni was dispersed in an aqueous TA solution under stirring and reflux for one hour (values of parameters such as TA concentration, temperature of modification, pH, etc. are given in detail in Section 3.5.4). In some cases, prior to the addition of the catalyst, 0.5 g of sodium bromide was added to the modifying solution. After cooling down, the materials were washed with deionised water (1 x 50 cm^3), methanol (2 x 50 cm^3), and the solvent used during hydrogenation reactions (1 x 50 cm^3), using a centrifuge.

3.4.2 Characterisation of Materials

The HLCs were characterised using powder XRD and TG-DTA-MS. Powder XRD was used during the different stages of the development of the catalysts.

3.4.2.1 Powder XRD Studies

Powder XRD experiments were carried out using a Siemens D5000 X-ray diffractometer using Cu K$_{\alpha 1}$ radiation, λ = 1.54056 Å (40 kV and 30 mA). From the half-width of the Ni (111) peak, the mean crystallite size of the Ni particles was calculated using Scherrer's equation.

Instrumental broadening and zero point errors were not taken into account in the XRD measurements through use of an internal standard.

3.4.2.2 TG-DTA-MS

TG-DTA was carried out using a Netzch STA 449F1 instrument with a Netzch QMS 403C mass spectrometer coupled to it. The materials were heated up to 700°C using a heating rate of 10°C min^{-1} and oxygen as a carrier.

3.4.3 Hydrogenation of MAA over TA-Ni Supported Catalysts Obtained from HLCs Precursors

The hydrogenation of MAA (2 mL) over the obtained catalyst (0.2 g) was carried out in a Parr batch reactor at 100°C for 48 hours under stirring. The initial hydrogen pressure was 10 bar and methanol was used as a solvent. Once hydrogenation was completed, the catalyst was recovered from the solution and the product of reaction was analysed by means of GC and HPLC, for estimating the hydrogenation yield and e.e, respectively. The Trace gas chromatograph was equipped with a FID detector and a Chrompak column (25m x 0.25mm) coated with fused silica (CHIRASIL-DEX, df = 0.25). The Dionex HPLC was equipped with a Chiralpak AD column which contained amylase tris-(3,5-dimethylphenylcarbanate) coated on 10 μm silica gel as stationary phase (250 x 4.6 mm). A 1% IPA in hexane solution was used as eluent. Detection of the species was carried out by means of UV at λ = 210 nm.

3.4.4 Analysis of the Postmodifier Solutions

The extent of TA adsorbed in the solid was measured from the postmodifier solution by means of HPLC. A 0.2 mol dm^3 phosphoric acid aqueous solution was

used as the mobile phase. The machine was equipped with an Acclaim column (120 C_8, 5 μm, 120 Å, 4.6 x 250 mm). Detection of the species was carried out by means of UV at λ = 230 nm.

Measurements of Ni leached out from the solid during chiral modification was carried out by AAS using an Alpha 3 spectrophotometer equipped with a Ni cathode lamp at λ = 310 nm.

3.5 Results and Discussions

3.5.1 Powder XRD

3.5.1.1 Powder XRD Studies of Materials Prepared by Coprecipitation

Powder XRD patterns of the solids containing Ni, Mg and Al in their structure prepared by coprecipitation, are shown in Figures 3.5.1.1.1-3.5.1.1.4. The as synthesised materials were hydrothermally treated at 110°C for 24 and 48 hrs, respectively, using autoclaves.

Figure 3.5.1.1.1: Powder XRD patterns of $Ni_{67}Al_{33}$ synthesised using the coprecipitation method. From bottom to top: as prepared, hydrothermally treated at 110°C for 24 hrs, and hydrothermally treated at 110°C for 48 hrs.

As the degree of crystallinity is directly related to the sharpness and intensity of the peaks in the powder XRD patterns, it can be confirmed that crystallinity in the materials improved after hydrothermal treatment. In these compounds the major effect on crystallinity is normally the regularity in the stacking of the layers. Other factors, such as particle size, may affect crystallinity too. At first sight, there is little difference in the peak intensity when the time is varied from 24 to 48 hours. However, disorder also may be present in the stacking of the layers, lowering thus the symmetry and giving rise to considerable differences in relative intensities.

Figure 3.5.1.1.2: Powder XRD patterns of $Ni_{50}Mg_{17}Al_{33}$ synthesised using the coprecipitation method. From bottom to top: as prepared, hydrothermally treated at 110°C for 24 hrs, and hydrothermally treated at 110°C for 48 hrs.
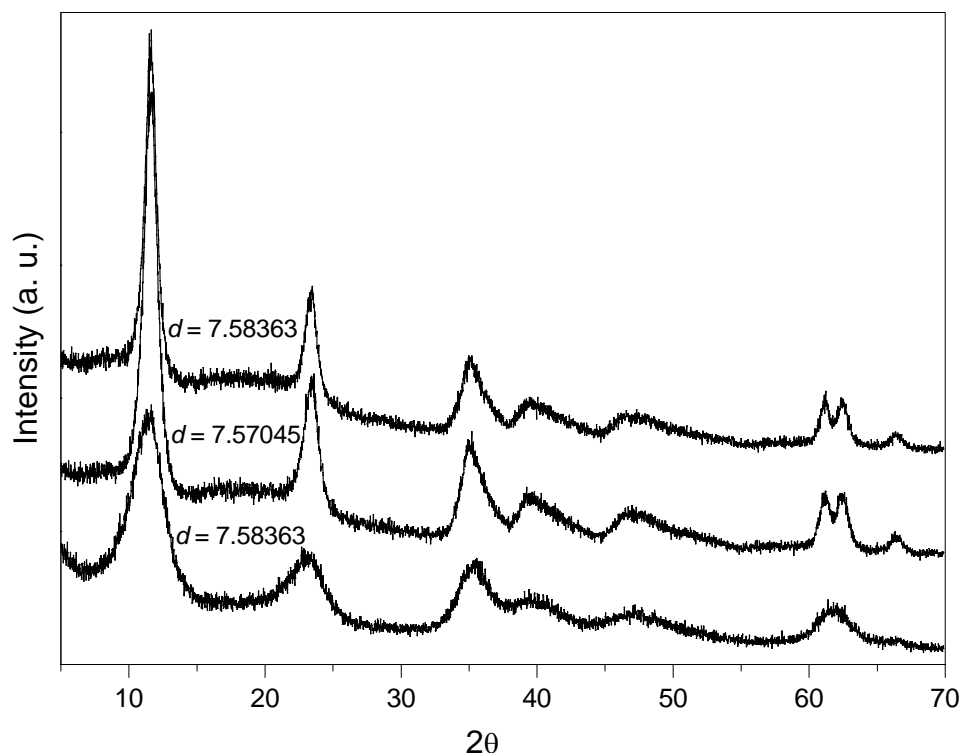
Figure 3.5.1.1.3: Powder XRD patterns of $Ni_{35}Mg_{32}Al_{33}$ synthesised using the coprecipitation method. From bottom to top: as prepared, hydrothermally treated at 110°C for 24 hrs, and hydrothermally treated at 110°C for 48 hrs.
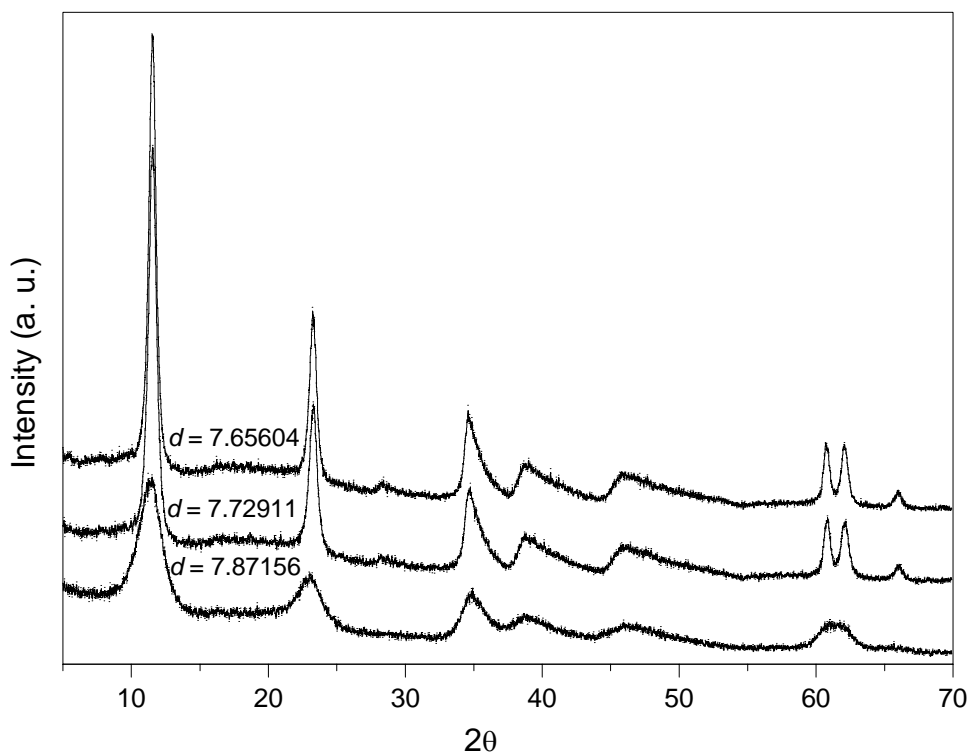
Figure 3.5.1.1.4: Powder XRD patterns of $Ni_{20}Mg_{47}Al_{33}$ synthesised using the coprecipitation method. From bottom to top: as prepared, hydrothermally treated at 110°C for 24 hrs, and hydrothermally treated at 110°C for 48 hrs.

Powder XRD patterns of the solids containing Ni, Zn and Al in their structure prepared by coprecipitation, are shown in Figures 3.5.1.1.5-3.5.1.1.7. Analogously to the previous series, the as synthesised materials were hydrothermally treated at 110°C for 24 and 48 hrs, respectively, using autoclaves.
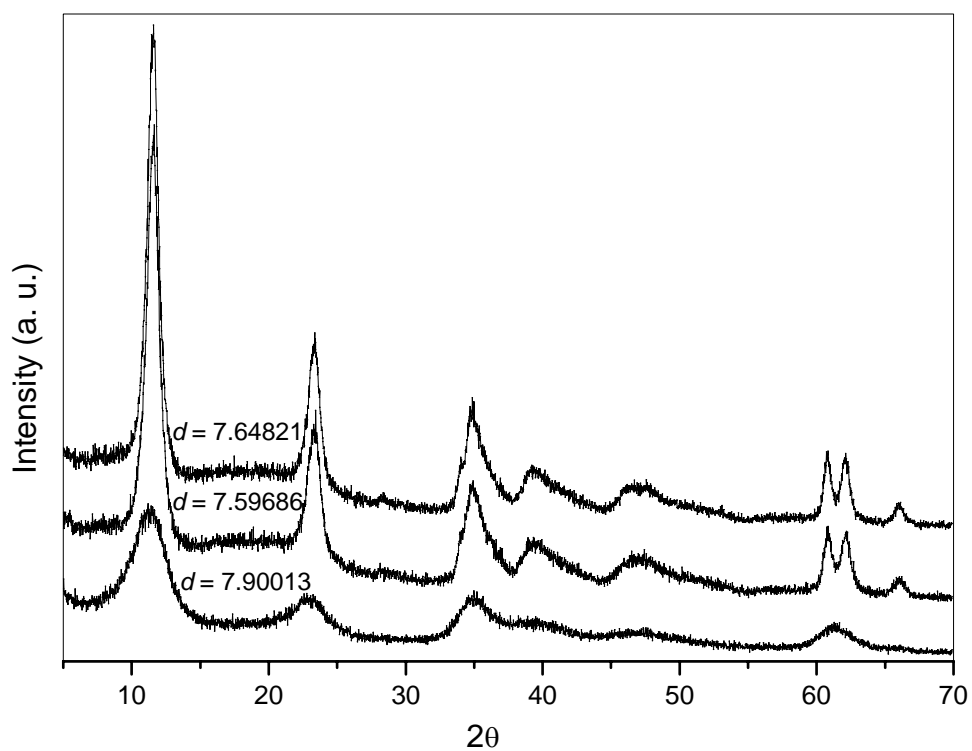
Figure 3.5.1.1.5: Powder XRD patterns of $Ni_{50}Zn_{17}Al_{33}$ synthesised using the coprecipitation method. From bottom to top: as prepared, hydrothermally treated at 110°C for 24 hrs, and hydrothermally treated at 110°C for 48 hrs.
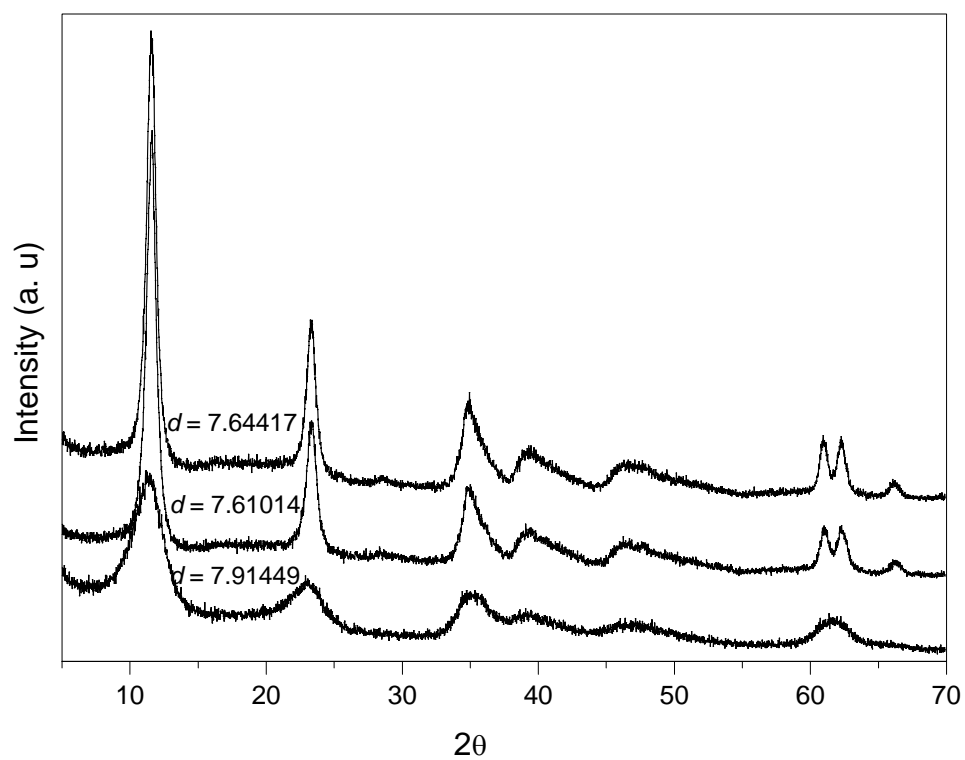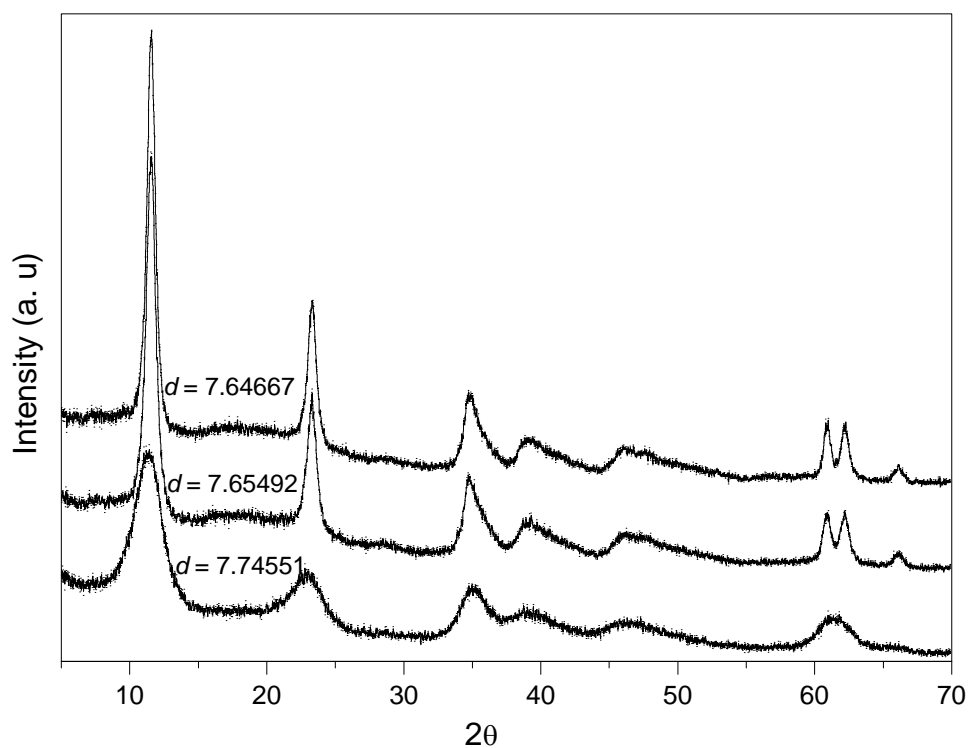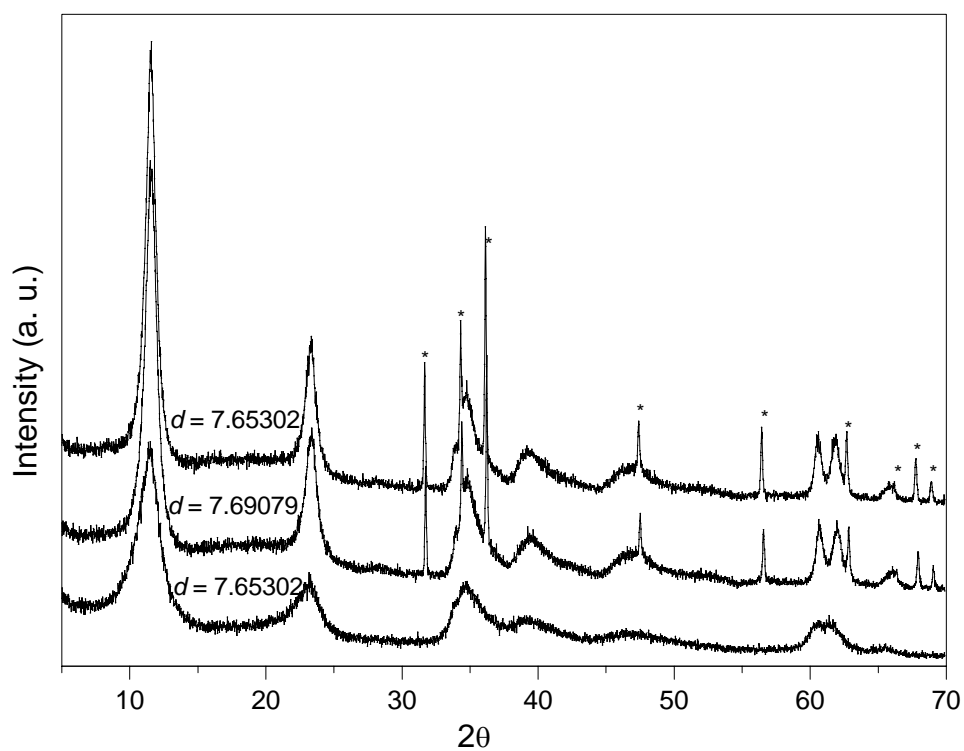
Figure 3.5.1.1.6: Powder XRD patterns of $Ni_{35}Zn_{32}Al_{33}$ synthesised using the coprecipitation method. From bottom to top: as prepared, hydrothermally treated at 110°C for 24 hrs, and hydrothermally treated at 110°C for 48 hrs. *ZnO.
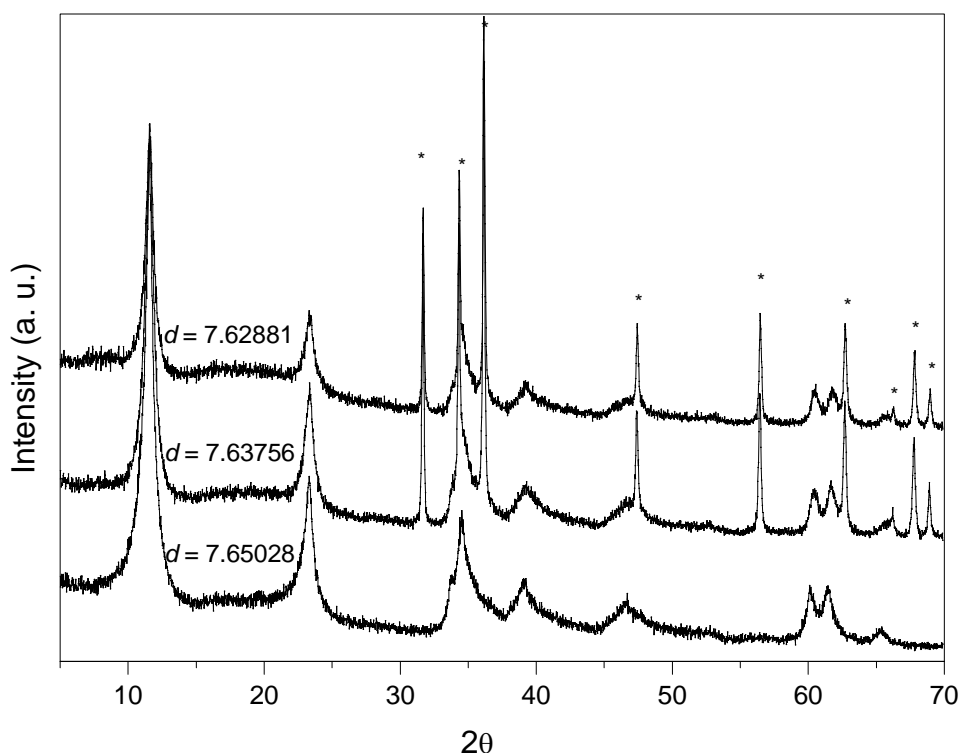
Figure 3.5.1.1.7: Powder XRD patterns of $Ni_{20}Zn_{47}Al_{33}$ synthesised using the coprecipitation method. From bottom to top: as prepared, hydrothermally treated at 110°C for 24 hrs, and hydrothermally treated at 110°C for 48 hrs. *ZnO.

In general, the takovite-like material and Mg-containing materials show the hydrotalcite phase as the only phase present in the materials (Figures 3.5.1.1.1-4). On the contrary, Zn-containing materials show some impurities represented by the ZnO phase (indicated by an asterisk in Figures 3.5.1.1.6 and 3.5.1.1.7), which are more prominent as the amount of Zn increases in the materials and after thermal treatment. This, and the different phases discussed in these studies were identified using the Powder Diffraction File (PDF-4+) database, maintained by the International Centre for Diffraction Data (ICDD).[196]

On the other hand, according to the XRD patterns, some of the materials present a shift in the position of the (003) peak towards higher 2θ values, as the hydrothermal treatment temperature increases (Figures 3.5.1.1.3, 3.5.1.1.4 and 3.5.1.1.7). As a consequence, d value becomes smaller.

It has been mentioned before that the c' value varies depending on the nature of the interlayer anion. According to Miyata,[197] for HLCs containing $(CO_3)^{2-}$, the c' value is approximately 7.65 Å.

The different combinations of cations in our materials, as well as the hydrothermal treatments carried on them have had an effect on c' value. The nature of the metal hydroxide layers varied the strength of hydrogen bonding between OH^- and water and carbonates in the interlayer species. This cause on c' value has been related to the state of hydration in some HLCs too.[198] This effect is also observed on the TG-DTA profiles (Section 3.5.2.1).

Longer times and/or higher temperatures during the hydrothermal processes help to rectify the structure of HLCs. Figure 3.5.1.1.8 shows the effect of temperature on crystallinity of a takovite-like material. The higher the temperature used during the hydrothermal treatment, the better the crystallinity showed by the solid.
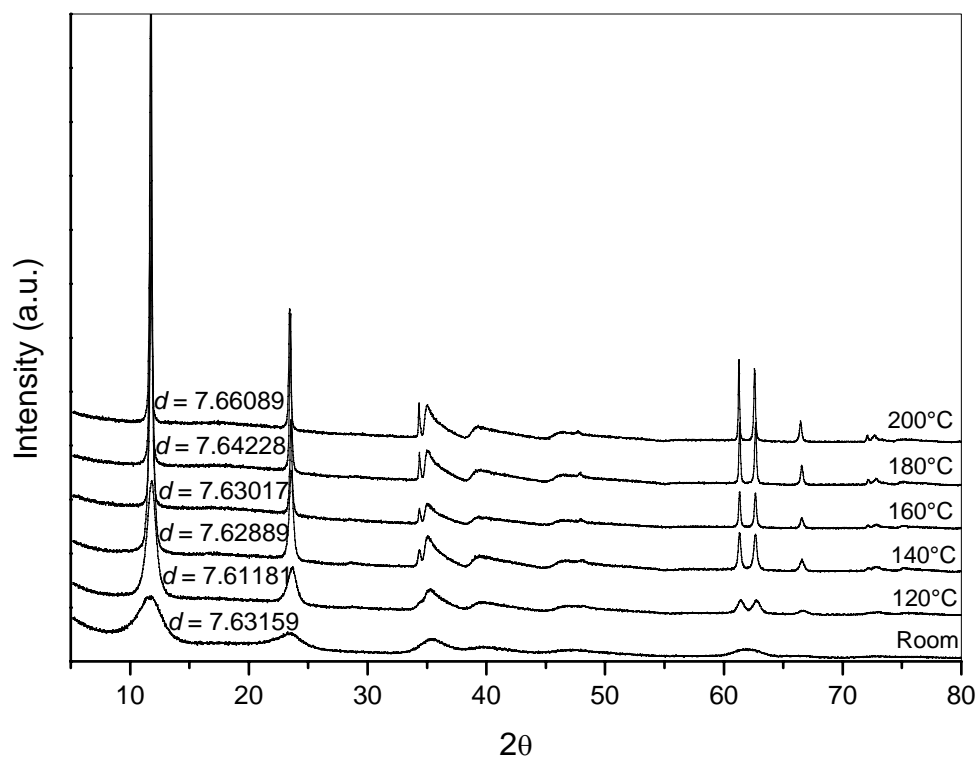
Figure 3.5.1.1.8: Powder XRD patterns of $Ni_{67}Al_{33}$ synthesised using the coprecipitation method, showing the effect of temperature on crystallinity during hydrothermal treatment.
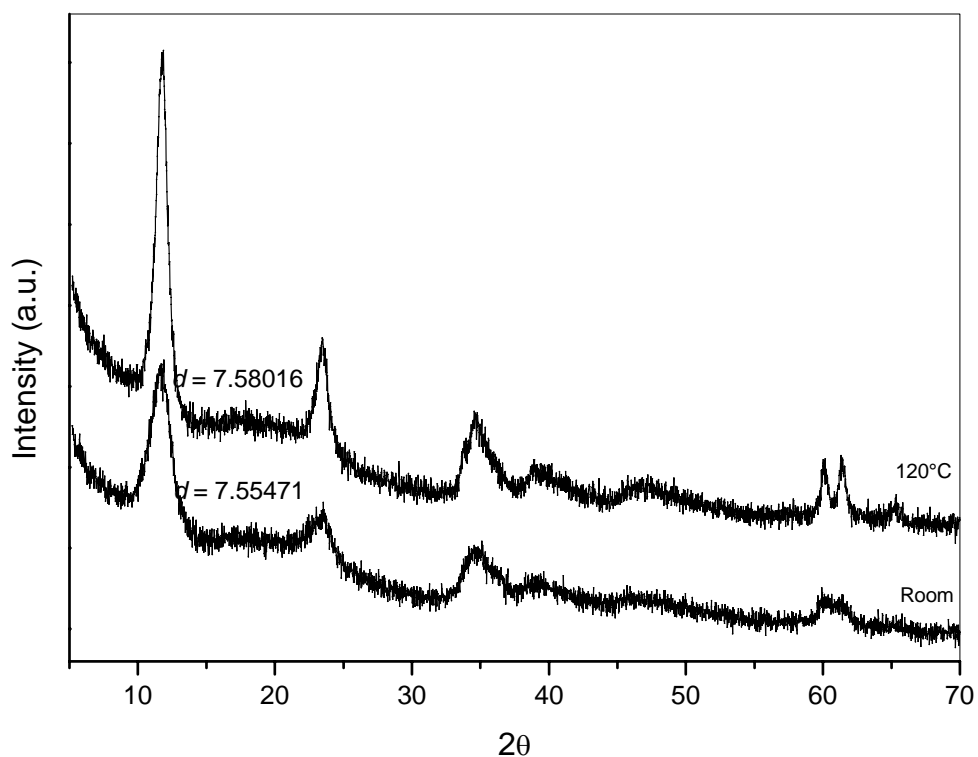
Figure 3.5.1.1.9: Powder XRD patterns of $Ni_{67}Fe_{33}$ synthesised using the coprecipitation method, as synthesised (bottom) and hydrothermally treated at 120°C (top).

Figure 3.5.1.1.9 shows the powder XRD studies carried on a Ni/Fe material. The degree of crystallinity is improved after hydrothermally treated at 120°C. The high background noise is due to fluorescence effects on account of the iron present.
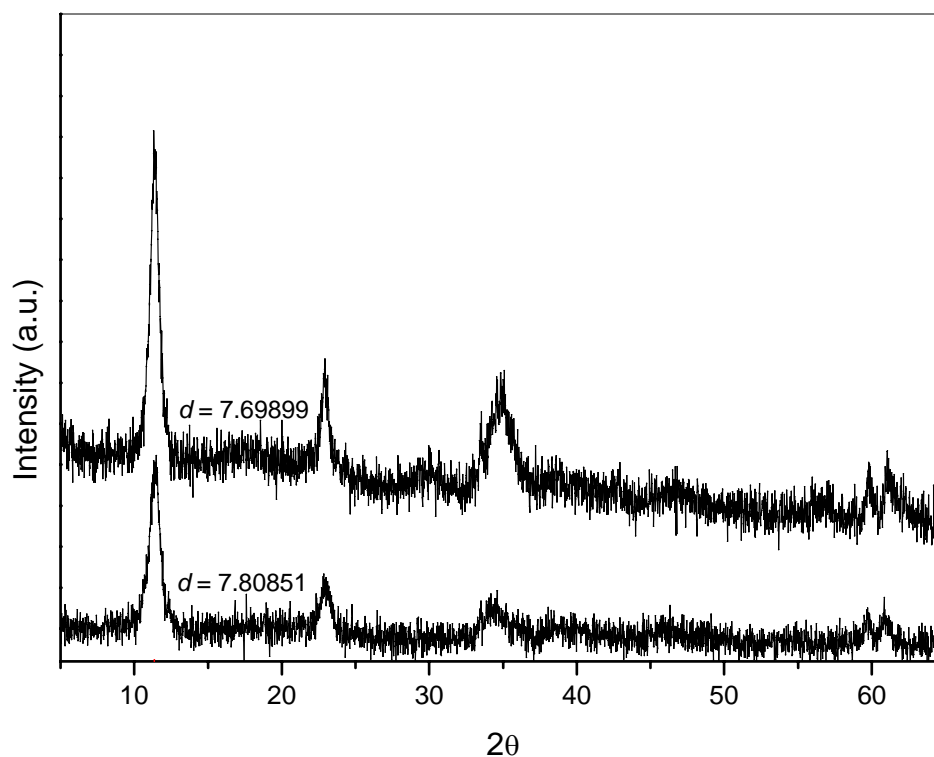
Figure 3.5.1.1.10: Powder XRD patterns of $Ni_{50}Zn_{17}Fe_{33}$ (top) and $Ni_{50}Mg_{17}Fe_{33}$ (bottom), synthesised using the coprecipitation method. Both materials hydrothermally treated at 110°C for 48 hrs.

Figure 3.5.1.1.10 shows the materials containing Mg/Fe and Zn/Fe of the corresponding series. All of them present the characteristic XRD patterns of HLCs without segregation of phases, although the crystallinity of these materials is clearly lower than Ni/Mg/Al and Ni/Zn/Al above discussed.
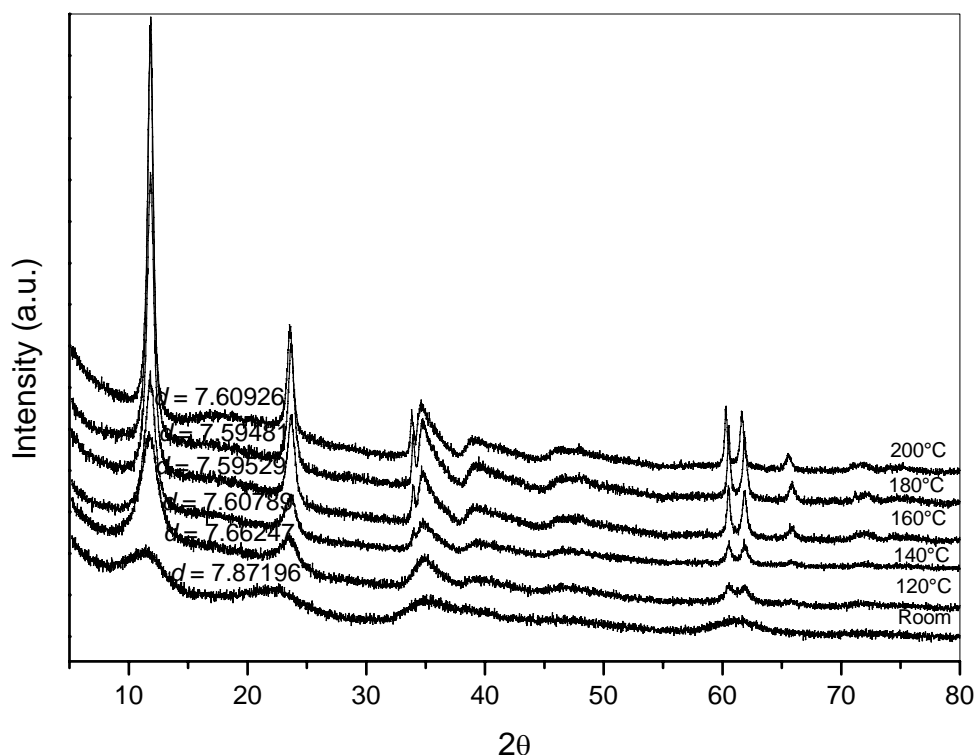
Figure 3.5.1.1.11: Powder XRD patterns of $Ni_{67}Cr_{33}$ synthesised using the coprecipitation method, showing the effect of temperature on crystallinity during hydrothermal treatment.

Figure 3.5.1.1.11 shows the effect of temperature during thermal treatment on a material containing Ni and Cr.

The structure of $Ni_{67}Cr_{33}$ is improved as the temperature of hydrothermal treatment increases. Similar to $Ni_{67}Al_{33}$, it contains just a layered phase in the range of temperatures studied. This material shows a more straight relation between the hydrothermal temperature treatment and interlayer space. The interlayer space becomes linearly smaller as the temperature of hydrothermal treatment increases, except at 200°C.

The incorporation of Mg into Ni/Cr led to materials with layered structures. Their powder XRD patterns are shown in Figures 3.5.1.1.12-14.
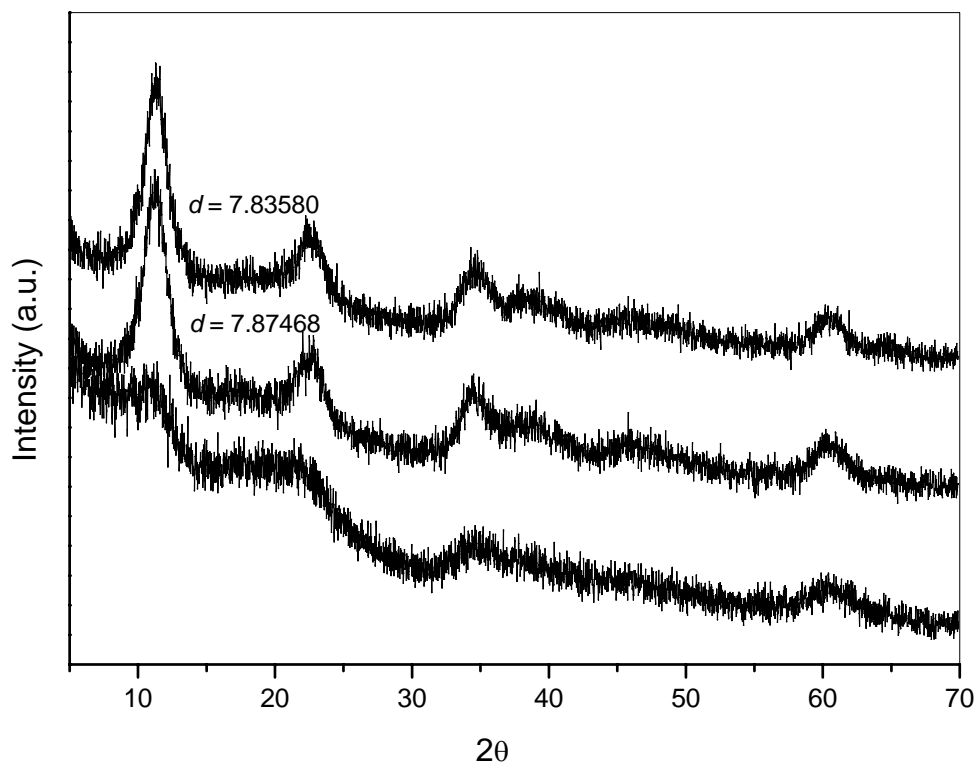
Figure 3.5.1.1.12: Powder XRD patterns of $Ni_{50}Mg_{25}Cr_{25}$ synthesised using the coprecipitation method. From bottom to top: as prepared, hydrothermally treated at 110°C for 24 hrs, and hydrothermally treated at 110°C for 48 hrs.
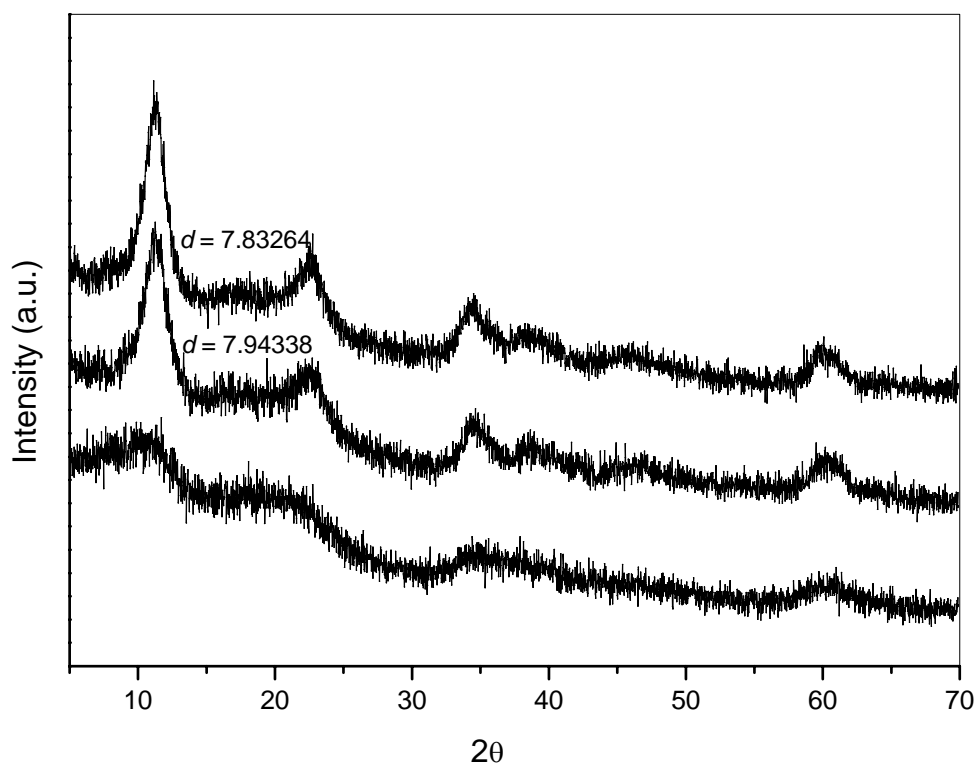
Figure 3.5.1.1.13: Powder XRD patterns of $Ni_{35}Mg_{40}Cr_{25}$ synthesised using the coprecipitation method. From bottom to top: as prepared, hydrothermally treated at 110°C for 24 hrs, and hydrothermally treated at 110°C for 48 hrs.
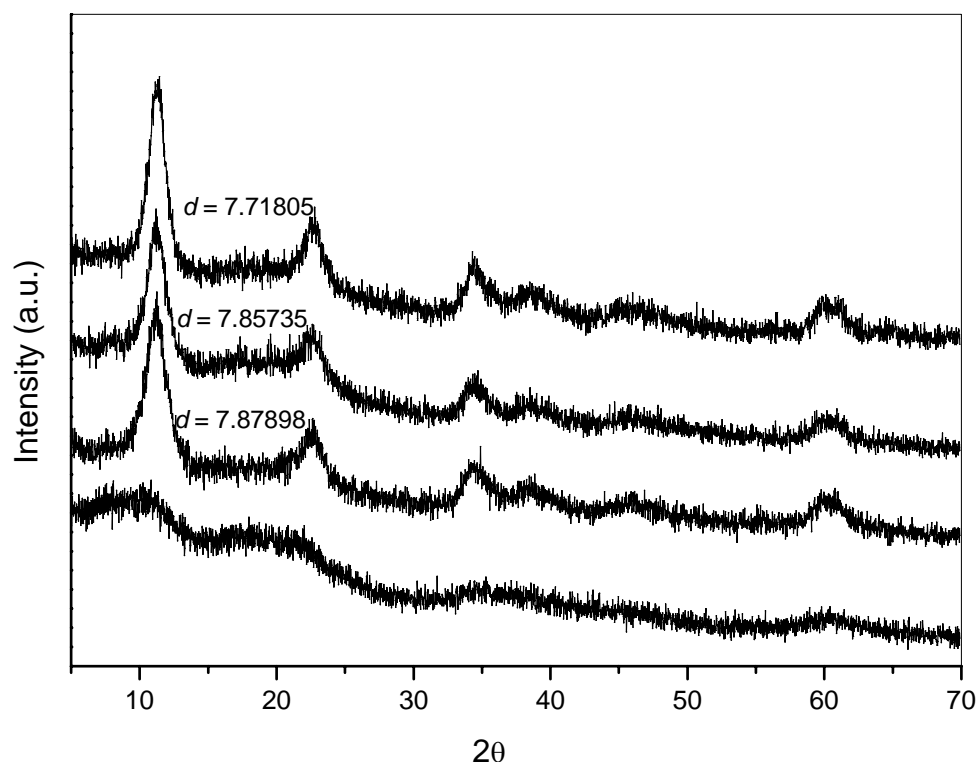
Figure 3.5.1.1.14: Powder XRD patterns of $Ni_{25}Mg_{50}Cr_{25}$ synthesised using the coprecipitation method. From bottom to top: as prepared, hydrothermally treated at 110°C for 24 hrs, hydrothermally treated at 110°C for 48 hrs, and hydrothermally treated at 110°C for 168 hrs.

A prolonged time during hydrothermal treatment (7 days) did not help to improve the crystallinity of $Ni_{25}Mg_{50}Cr_{25}$ (Figure 3.5.1.14).

For this series of materials prepared by coprecipitation, only well defined HLCs obtained were used for further characterisation and catalysis.

In order to determine the temperature at which HLCs decompose to mixed oxides, variable temperature XRD experiments were carried out. The XRD patterns of the materials $Ni_{67}Al_{33}$, $Ni_{67}Fe_{33}$ and $Ni_{67}Cr_{33}$ are shown in Figures 3.5.1.1.15, 3.5.1.1.16 and 3.5.1.1.17, respectively.

77
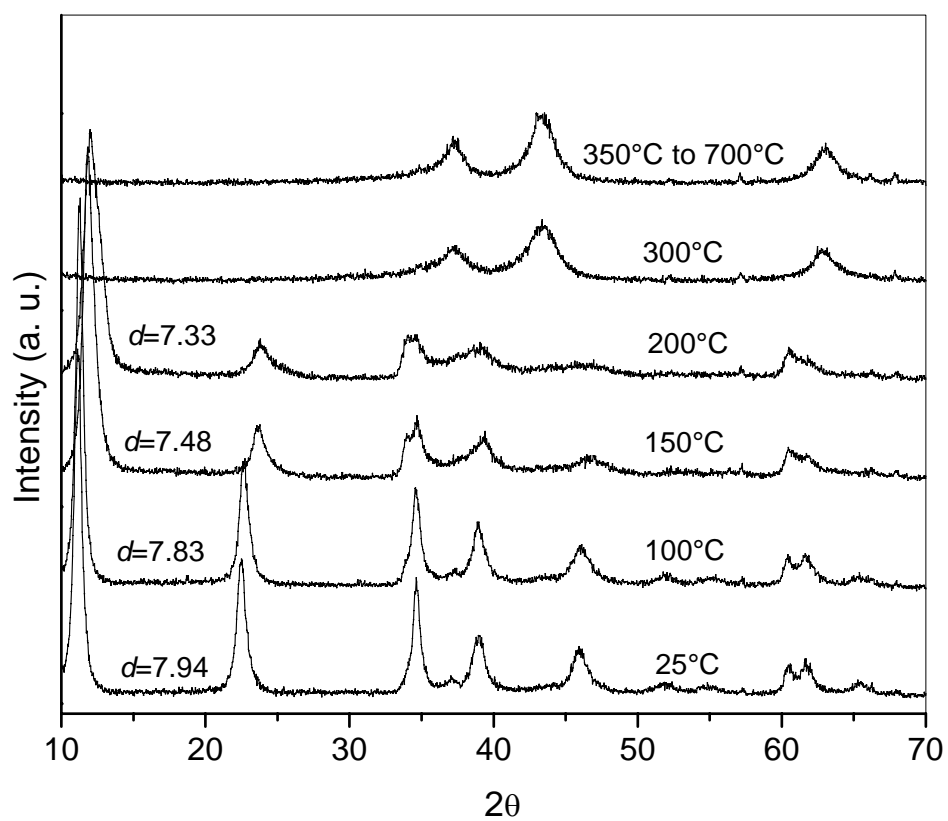
Figure 3.5.1.1.15: Powder XRD patterns of fresh $Ni_{67}Al_{33}$ scanned at different temperatures.
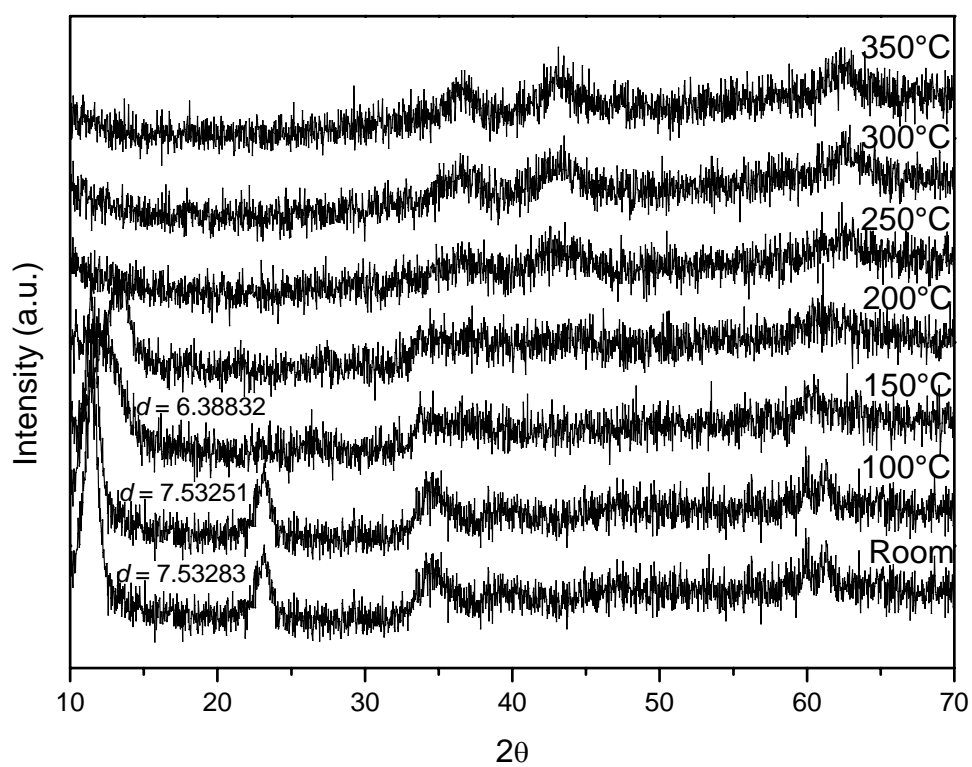
Figure 3.5.1.1.16: Powder XRD patterns of fresh $Ni_{67}Fe_{33}$ scanned at different temperatures.
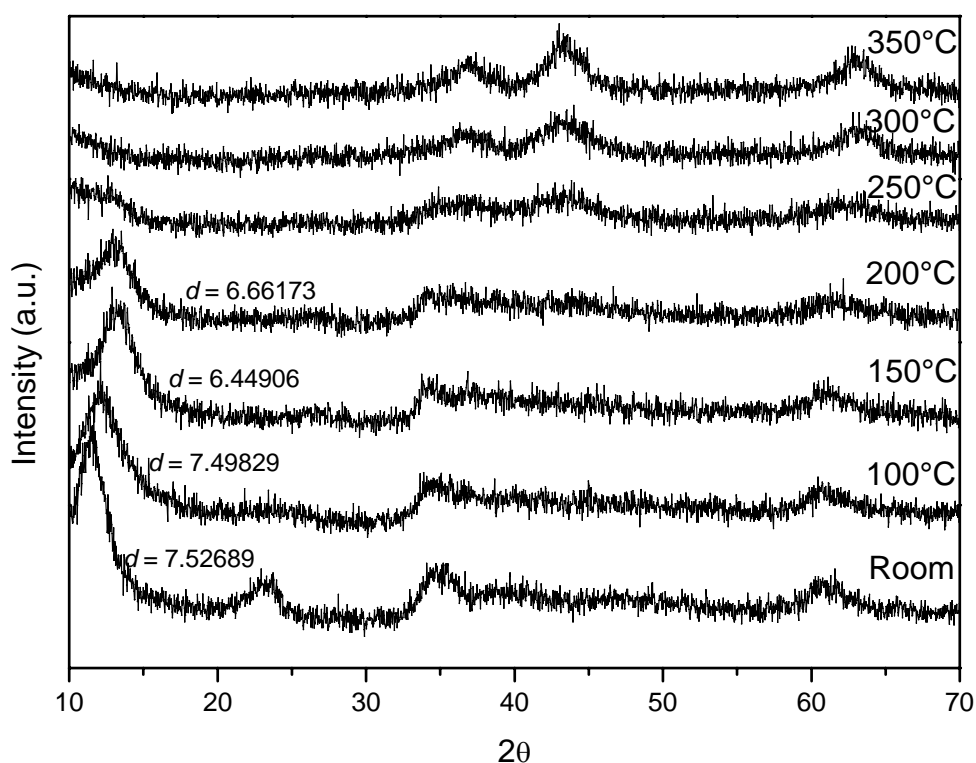
Figure 3.5.1.1.17: Powder XRD patterns of fresh $Ni_{67}Cr_{33}$ scanned at different temperatures.

It can be noticed from the last three Figures (3.5.1.1.15-17) that the layered structure of the materials is lost at 250°C. The decomposition of the layered structure starts at around 200°C. At this temperature HLCs can regenerate their layered structure. From 300°C and above, the phase present in the material is the mixed oxide which has been matched to XRD patterns contained in the PDF-4+ database.[196]

After reduction in 10% H_2/90% N_2, supported Ni metal was formed. Another experiment consisted of reducing the calcined materials in situ by flowing 10% H_2 (diluted in N_2). The temperature was varied in continuing steps of 50°C till 750-800°C. Once the desired temperature was reached, the solids were scanned by XRD. Results of the experiments carried on $Ni_{67}Al_{33}$, $Ni_{67}Fe_{33}$ and $Ni_{67}Cr_{33}$ are shown in Figures 3.5.1.1.18-20, respectively.
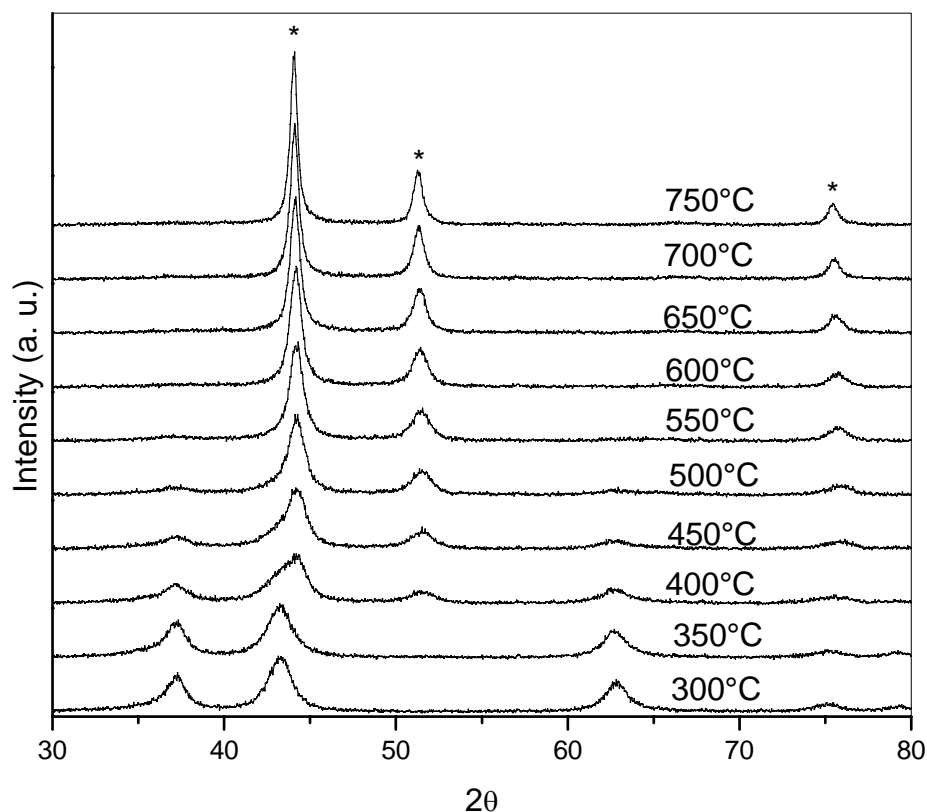
Figure 3.5.1.1.18: Powder XRD patterns of calcined material $Ni_{67}Al_{33}$ at different temperatures of reduction. The material was previously calcined in flowing oxygen at 350°C for 5 hrs. [*]Ni metal.

Figure 3.5.1.1.18 shows the development of metallic Ni on a mixed oxide obtained from a takovite-type material in function of the temperature of reduction.
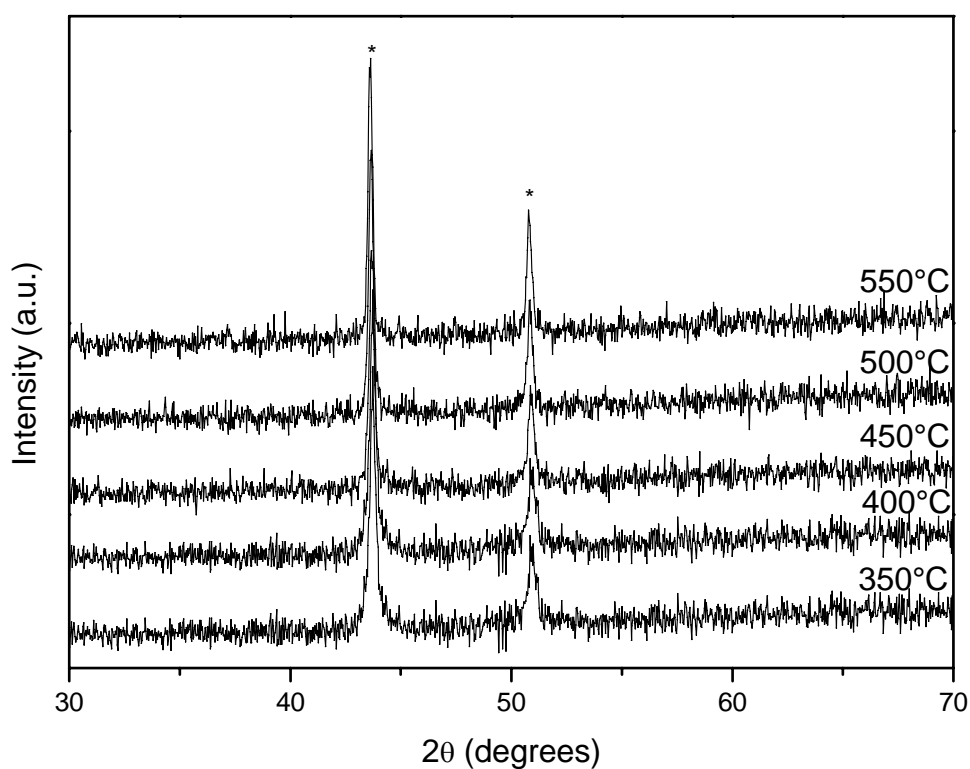
Figure 3.5.1.1.19: Powder XRD patterns of calcined material $Ni_{67}Fe_{33}$ at different temperatures. The material was previously calcined in flowing oxygen at 350°C for 5 hrs. *Ni metal.
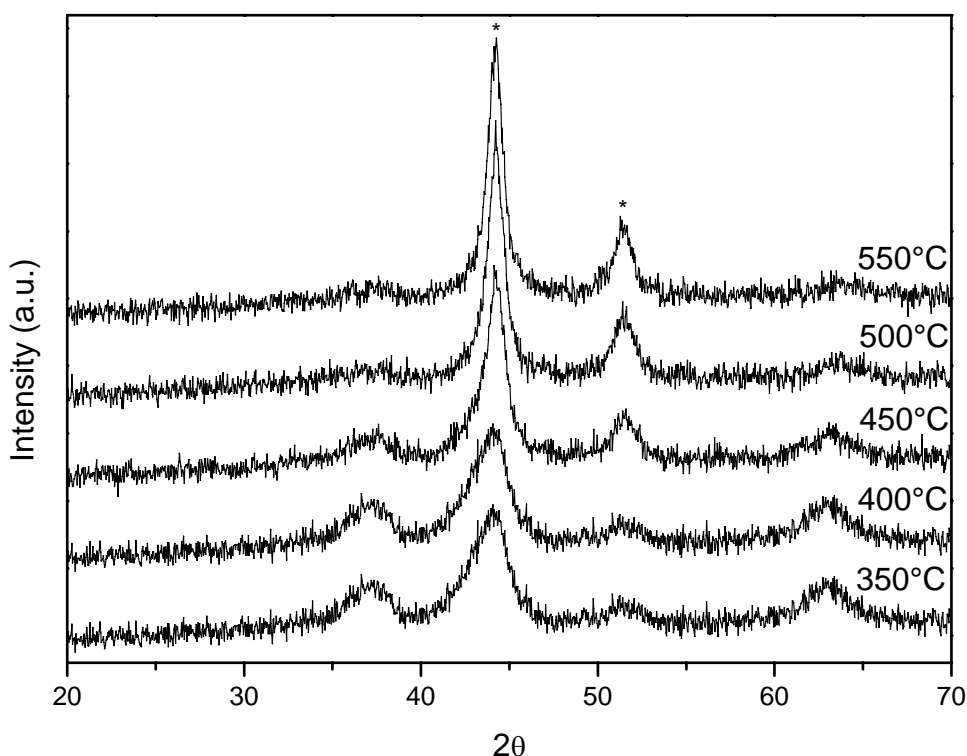
Figure 3.5.1.1.20 Powder XRD patterns of calcined material $Ni_{67}Cr_{33}$ at different temperatures. The material was previously calcined in flowing oxygen at 350°C for 5 hrs. *Ni metal.

Ni metal particle size can be adjusted by varying temperature and/or time during thermal treatments (calcination and reduction). The effect of temperature of reduction on Ni crystallite size of calcined materials with formulas $Ni_{67}Al_{33}$, $Ni_{67}Fe_{33}$ and $Ni_{67}Cr_{33}$ is shown in Tables 3.5.1.1.1-4. Details of the hydrothermal/thermal treatments are described in captions. The crystal size of the metallic particles can be estimated from the full width at half maximum (FWHM) of the peaks due to the Ni metal present, using the Scherrer formula:

$$\tau = k\lambda / \beta_\tau \cos\theta$$

Where:

τ = mean crystal diameter, in Å

K = slope factor = 0.9

λ = 1.54056 Å (Cu)

β_τ = line broadening (FWHM) measured in radians

T(°C)	$2\theta_1$	$2\theta_2$	FWHM$_1$	FWHM$_2$	τ_1(nm)	τ_2(nm)	τ(nm)
600	44.2568	51.4884	1.1212	1.4291	9.89	8.92	9.40±0.47
650	44.2222	51.4200	1.0805	1.3740	10.25	9.27	9.76±0.49
700	44.1936	51.4030	0.9904	1.2439	11.18	10.23	10.70±0.53
750	44.1521	51.3532	0.9351	1.2327	11.84	10.31	11.07±0.55

Table 3.5.1.1.1: Mean Ni crystallite size with respect to temperature of reduction of a calcined material with starting formula $Ni_{67}Al_{33}$. The material was hydrothermally treated at 120°C for 24 hrs, and calcined in flowing oxygen at 400°C for 4 hrs.

T(°C)	$2\theta_1$	$2\theta_2$	$FWHM_1$	$FWHM_2$	τ_1(nm)	τ_2(nm)	τ(nm)
450	44.0415	51.5521	2.0178	1.4770	5.47	8.64	7.05±0.35
500	44.2718	51.4963	1.3446	1.7304	8.25	7.37	7.81±0.39
550	44.2978	51.4932	1.1152	1.5011	9.95	8.5	9.22±0.46
600	44.2674	51.4909	1.0159	1.3332	10.92	9.57	10.24±0.51
650	44.2488	51.4564	0.9384	1.2441	11.81	10.24	11.02±0.55
700	44.2142	51.4490	0.8554	1.1653	12.95	10.93	11.94±0.60
750	44.1906	51.4197	0.8174	1.1614	13.55	10.96	12.25±0.61

Table 3.5.1.1.2: Mean Ni crystallite size with respect to temperature of reduction of a calcined material with starting formula $Ni_{67}Cr_{33}$. The material was hydrothermally treated at 200°C for 24 hrs, and calcined in flowing oxygen at 400°C for 4 hrs.

T(°C)	$2\theta_1$	$2\theta_2$	FWHM$_1$	FWHM$_2$	τ_1(nm)	τ_2(nm)	τ(nm)
400	44.3666	51.6310	0.8195	1.1752	13.56	10.89	12.22±0.61
450	44.3669	51.6326	0.8191	1.1731	13.56	10.91	12.23±0.61
500	44.3365	51.6201	0.7128	0.9170	15.58	13.95	14.76±0.74
550	44.2720	51.5488	0.3415	0.4603	32.48	27.75	30.11±1.50
600	44.2449	51.5231	0.3125	0.4263	35.48	29.95	32.71±1.63
650	44.2146	51.4867	0.3104	0.3775	35.70	33.79	34.74±1.74
700	44.1744	51.4490	0.2797	0.3740	39.60	34.06	36.83±1.84
750	44.1460	51.4197	0.2554	0.3304	43.34	38.53	40.93±2.04

Table 3.5.1.1.3: Mean Ni crystallite size with respect to temperature of reduction of a calcined material with starting formula Ni$_{67}$Cr$_{33}$. The material was hydrothermally treated at 120°C for 24 hrs, and calcined in flowing oxygen at 350°C for 5 hrs.

T(°C)	$2\theta_1$	$2\theta_2$	$FWHM_1$	$FWHM_2$	τ_1(nm)	τ_2(nm)	τ(nm)
400	43.8882	51.1000	0.3441	0.4238	32.06	29.85	30.95±1.54
450	43.8414	51.0434	0.2885	0.3774	38.17	33.47	35.82±1.80
500	43.7915	50.9868	0.2455	0.3127	44.82	40.35	42.58±2.13
550	43.7490	50.9375	0.2333	0.2578	47.13	48.89	48.01±2.40
600	43.7093	50.9043	0.2078	0.2402	52.88	52.45	52.66±2.63
650	43.6702	50.8504	0.2006	0.2263	54.74	55.60	55.17±2.75
700	43.6437	50.8178	0.1911	0.2330	57.44	53.96	55.70±2.78

Table 3.5.1.1.4: Mean Ni crystallite size with respect to temperature of reduction of a calcined material with starting formula $Ni_{67}Fe_{33}$. The material was hydrothermally treated at 120°C for 24 hrs, and calcined in flowing oxygen at 350°C for 5 hrs.

From the previous Tables (3.5.1.1.1-4) it can be seen that the Ni particle size is a function of temperature of reduction, the former increases with respect to the latter. The comparison between the values obtained on a material of a given composition, in which hydrothermal and thermal temperatures treatments were varied, reveals that both thermal processes have an effect on Ni particle size too (Tables 3.5.1.1.2 and 3.5.1.1.3).

Ni particle sizes of Ni/Mg/Al and Ni/Zn/Al series prepared using standardised conditions of calcinations and reduction steps are summarized in Tables 3.5.1.1.5 and 3.5.1.1.6, respectively.

Ni/Mg ratio	Hydrothermal treatment	Ni crystallite size (nm)[a]
∞	none	50
∞	110°C for 24 hrs	21
∞	110°C for 48 hrs	22
2.94	none	20
2.94	110°C for 24 hrs	31
2.94	110°C for 48hrs	19
1.09	none	20
1.09	110°C for 24 hrs	22
1.09	110°C for 48 hrs	19
0.42	none	14
0.42	110°C for 24 hrs	17
0.42	110°C for 48 hrs	14

Table 3.5.1.1.5: Values of Ni particle sizes of the series of materials containing Ni/Mg/Al prepared by coprecipitation. The materials were calcined in flowing oxygen at 700°C for 7 hrs and reduced in flowing 10% hydrogen (in nitrogen) at 750°C for 7 hrs. [a]The error in measuring the width at half height is 0.125°. Ni crystallite size calculation error is about ±5%.

There is no direct correlation between the increments in content of Mg in the materials or with respect to the hydrothermal treatment of a given material (Table 3.5.1.1.5).

Ni/Zn ratio	Hydrothermal treatment	Ni crystallite size (nm)[a]
2.94	none	30
2.94	110°C for 24 hrs	28
2.94	110°C for 48hrs	37
1.09	none	-
1.09	110°C for 24 hrs	-
1.09	110°C for 48 hrs	-
0.42	none	-
0.42	110°C for 24 hrs	-
0.42	110°C for 48 hrs	-

Table 3.5.1.1.6: Values of Ni particle sizes of the series of materials containing Ni/Zn/Al prepared by coprecipitation. The materials were calcined in flowing oxygen at 700°C for 7 hrs and reduced in flowing 10% hydrogen (in nitrogen) at 750°C for 7 hrs. [a]The error in measuring the width at half height is 0.125°. Ni crystallite size calculation error is about ±5%.

With the exception of $Ni_{50}Zn_{17}Al_{33}$, the Ni(111) peak overlapped with the other peaks of the phases developed in the Ni/Zn/Al series which made it not possible to determine the Ni crystallite size of the rest of the series.

3.5.1.2 Powder XRD Studies of Materials Prepared by Urea Hydrolysis Method

Powder XRD patterns of the materials synthesised with Ni/Mg/Al in their structure as well as the takovite-like material (Ni-Al-CO_3) are shown in Figure 3.5.1.2.1. It can be seen that the XRD patterns are typical of those of HLCs, and that it is the only phase existing in the materials.
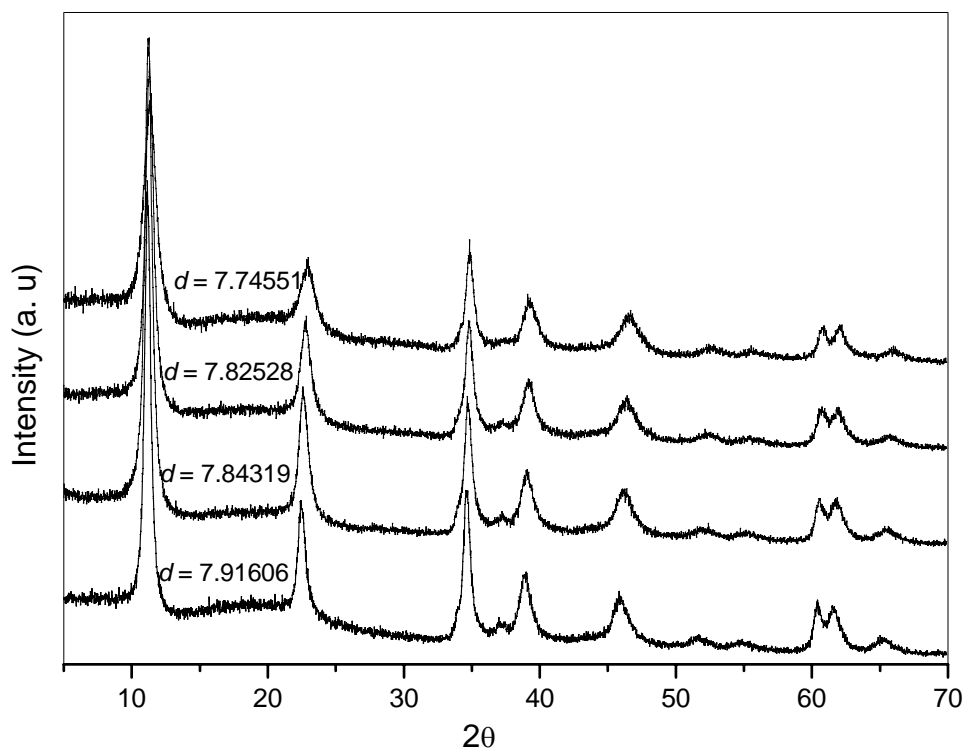
Figure 3.5.1.2.1: Powder XRD patterns of the series Ni/Mg/Al synthesised by hydrolysis of urea. Bottom to top: Ni/Mg =∞, 2.94, 1.09 and 0.42; and Al/(Ni+Mg)=0.33.

The *d* spacing of the Ni/Mg/Al series shifts towards smaller values as Mg is incorporated into the materials.

The materials of the series Ni/Zn/Al show the XRD pattern characteristic of HLCs (Figure 3.5.1.2.2). In addition, the XRD data show traces of ZnO which are more prominent as the amount of Zn increases in the solid. They are compared against the takovite-like material XRD pattern.
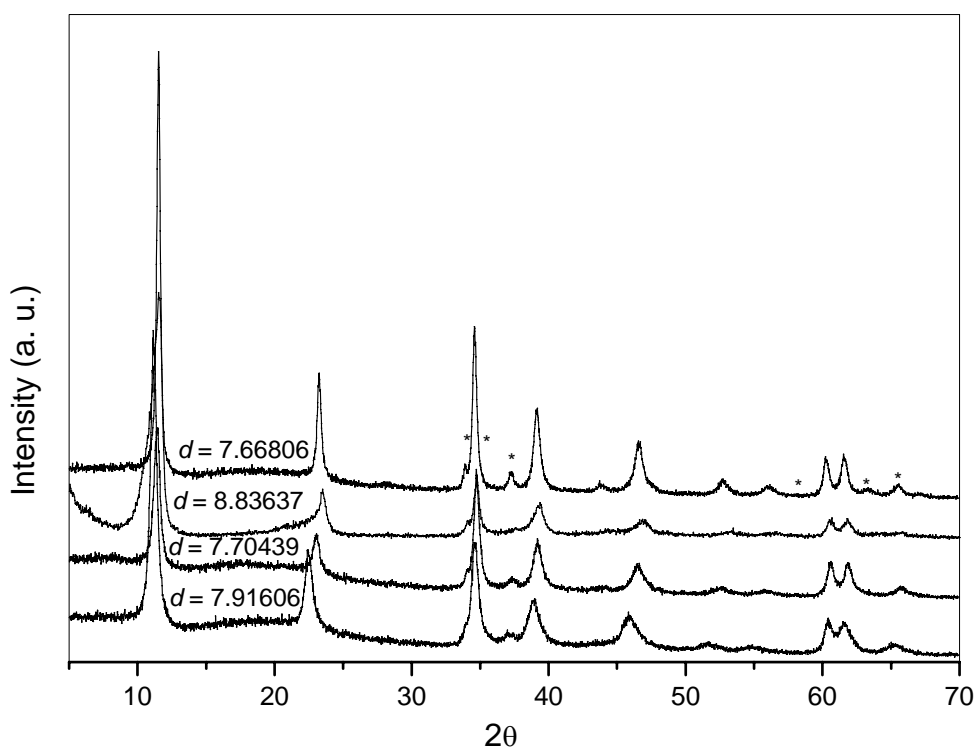
Figure 3.5.1.2.2 Powder XRD patterns of the series Ni/Zn/Al synthesised by hydrolysis of urea. Bottom to top: Ni/Zn =∞, 2.94, 1.09 and 0.42; and Al/(Ni+Zn)=0.33. *ZnO.

It is well known that the ionic radii, the nature of the cation itself and its ratio in the material formulation, are key synthetic parameters to obtain pure HLCs. However, in some cases, a pure HLC is not essential and the presence of other species may have beneficial effects during catalysis. The presence of ZnO in the solids of the Ni/Zn/Al series could have had a beneficial effect in enantioselectivity and this will be discussed further in Section 3.5.4.2.

Figure 3.5.1.2.3 shows the powder XRD patterns of the series of materials containing Ni, Mg (or Zn) and Fe, prepared by hydrolysis of urea. It can be clearly noticed that this method of preparation of HLCs is not the most appropriate for this specific combination of metals. The pH set during synthesis by hydrolysis of urea is not suitable to precipitate HLCs containing Fe.
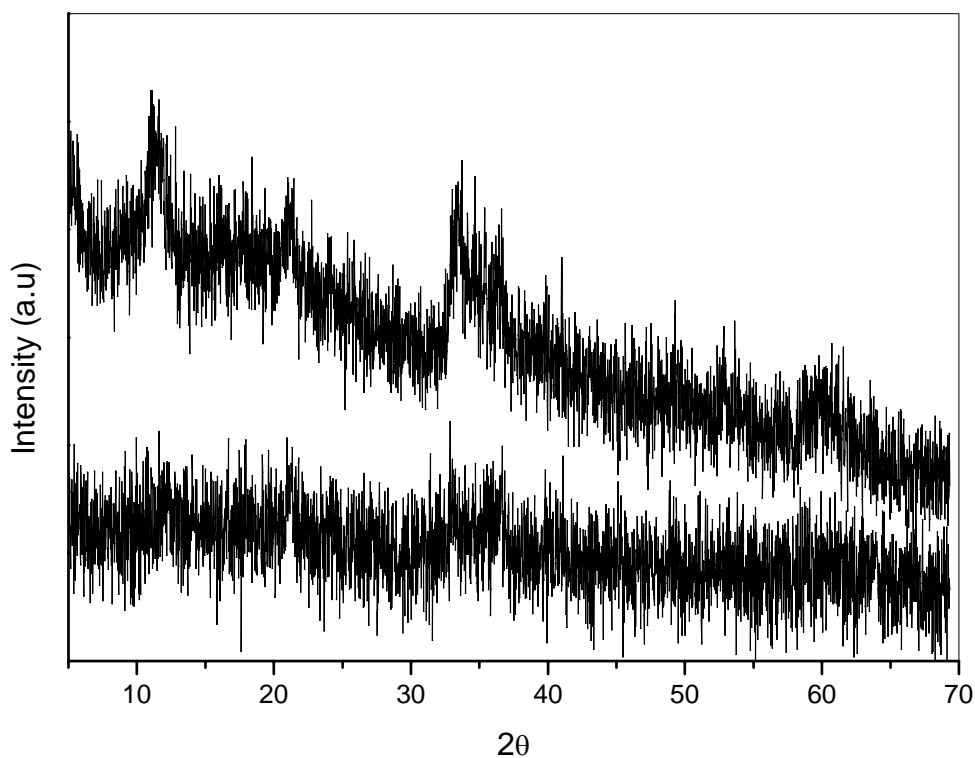
Figure 3.5.1.2.3: Powder XRD patterns of the series Ni/Mg(Zn)/Fe synthesised by hydrolysis of urea. Bottom: $Ni_{50}Mg_{17}Fe_{33}$, and top: $Ni_{50}Zn_{17}Fe_{33}$.

Figure 3.5.1.2.4 shows the powder XRD patterns of the series of materials containing Ni, Mg (or Zn) and Cr, obtained by urea. Once again, the use of this method was not successful for precipitating HLCs containing Cr.
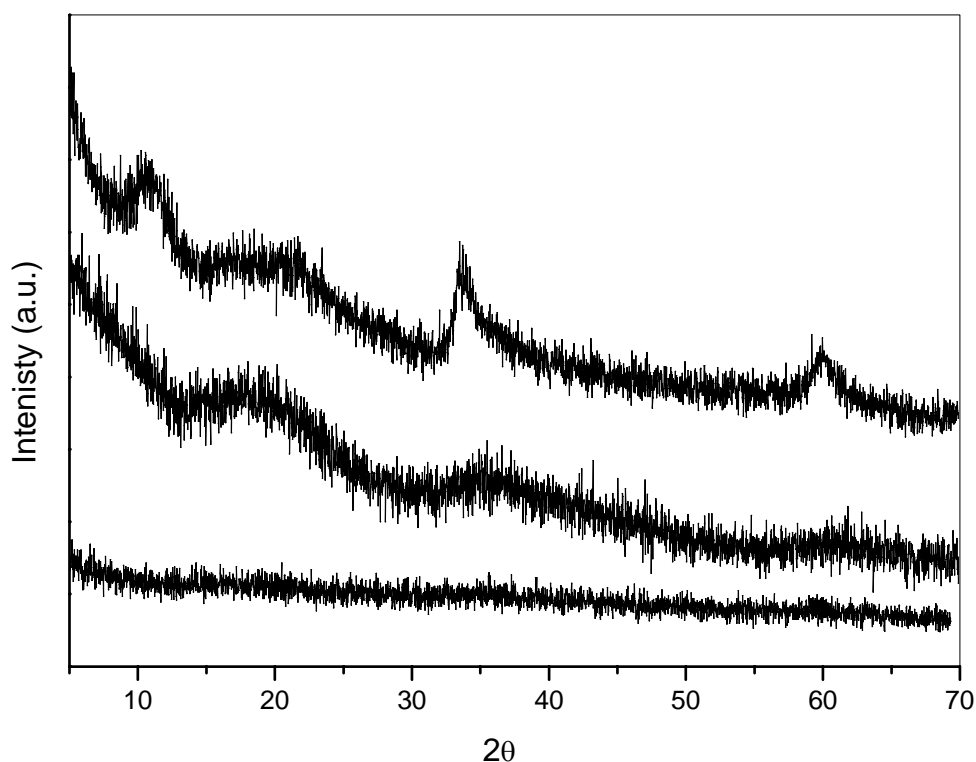
Figure 3.5.1.2.4: Powder XRD patterns of the series Ni/Mg(Zn)/Cr synthesised by hydrolysis of urea. Bottom to top: $Ni_{67}Cr_{33}$, $Ni_{50}Mg_{25}Cr_{25}$ and $Ni_{50}Zn_{25}Cr_{25}$.

Analogously to the series prepared by coprecipitation, experiments of XRD at variable temperature were done over fresh materials of this series. Results are shown in Figures 3.5.1.2.5-11.
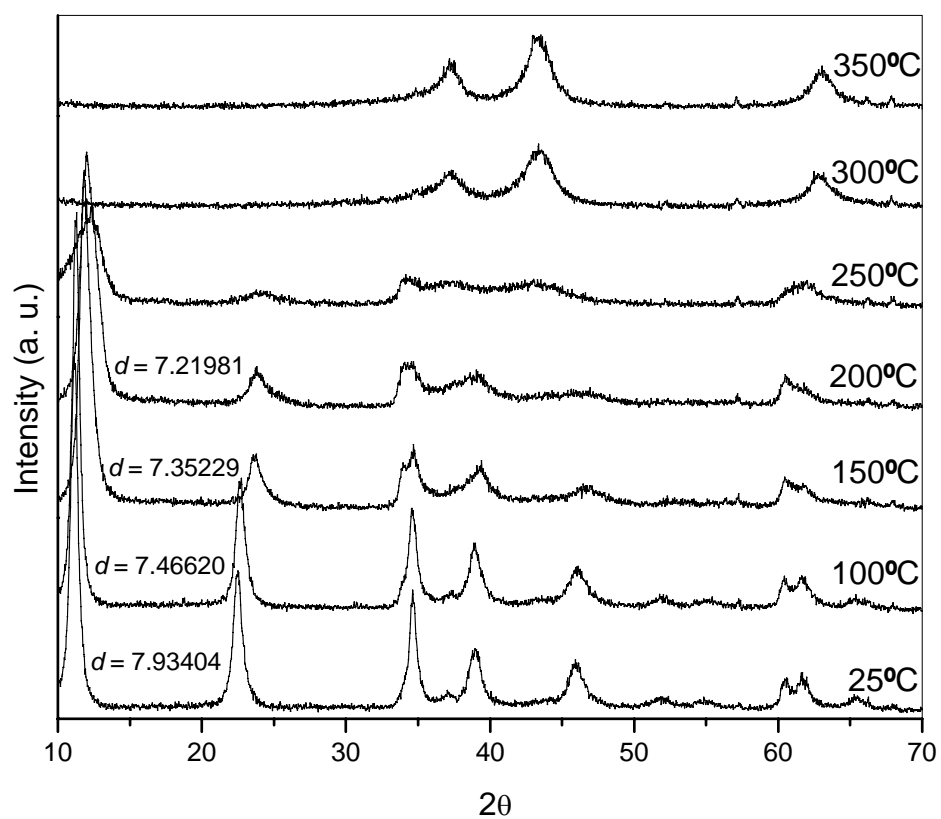
Figure 3.5.1.2.5: Variable temperature XRD studies over $Ni_{67}Al_{33}$ prepared by urea hydrolysis method.
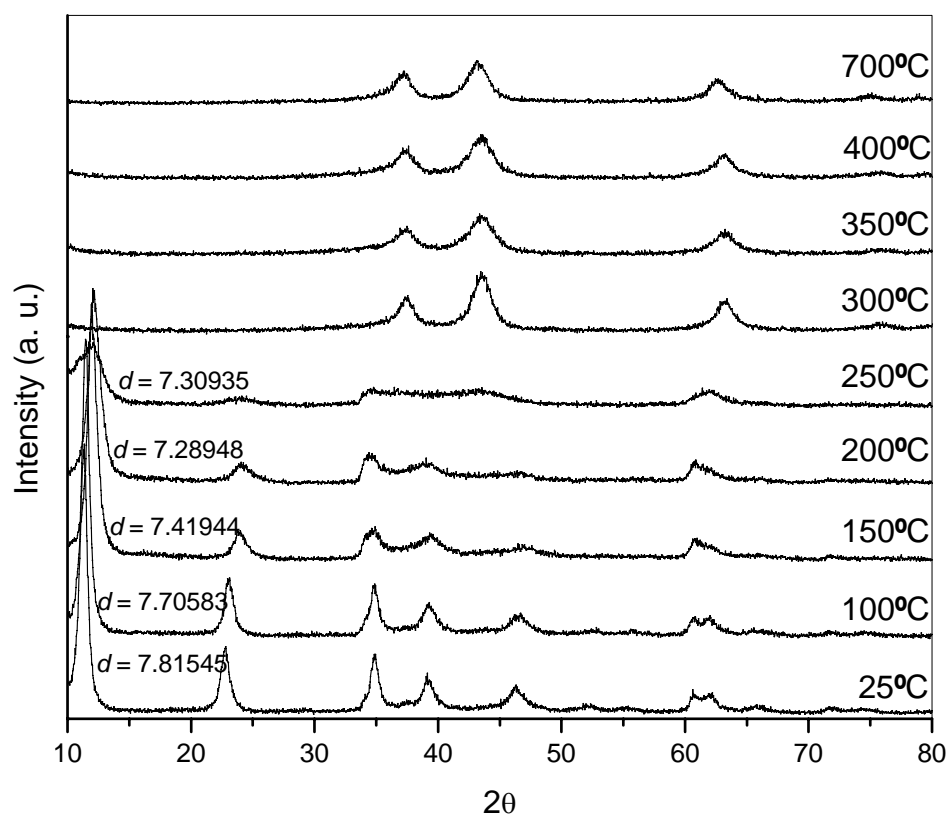
Figure 3.5.1.2.6: Variable temperature XRD studies over $Ni_{50}Mg_{17}Al_{33}$ prepared by urea hydrolysis method.
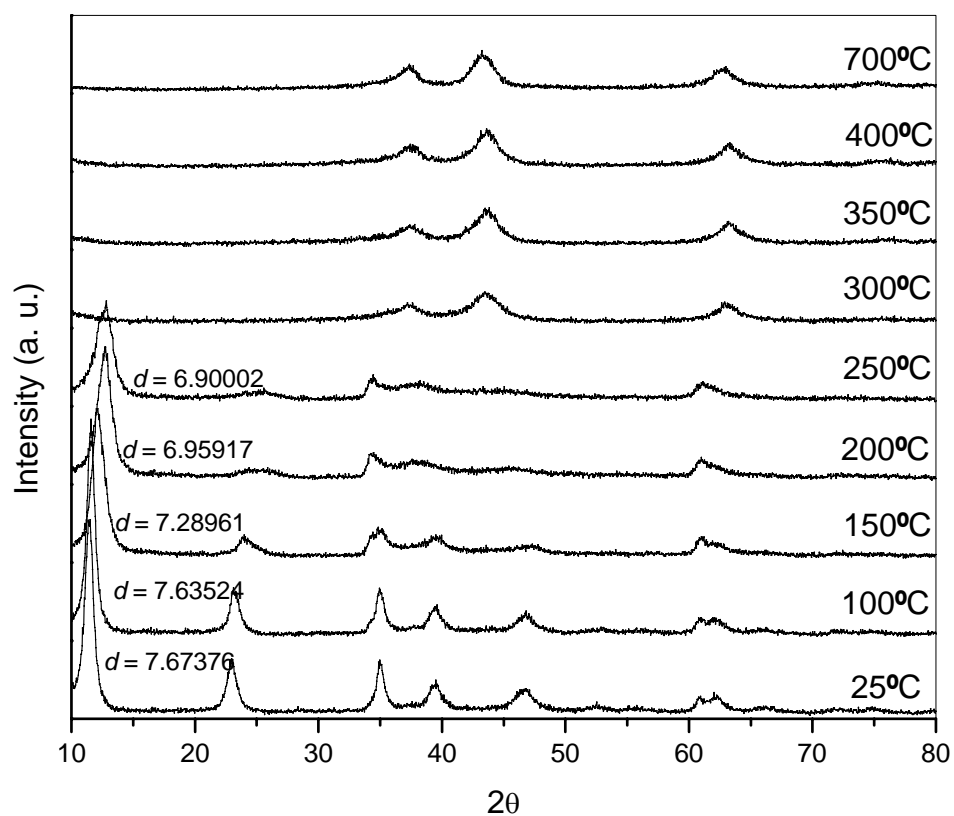
Figure 3.5.1.2.7: Variable temperature XRD studies over $Ni_{35}Mg_{32}Al_{33}$ prepared by urea hydrolysis method.
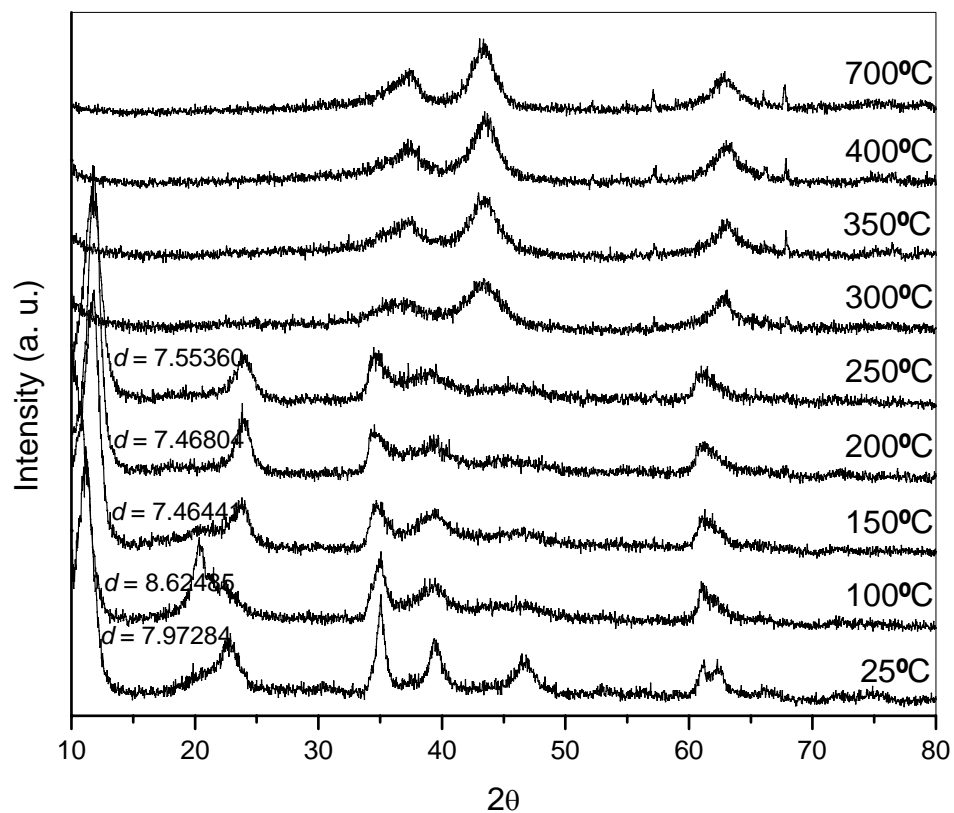
Figure 3.5.1.2.8: Variable temperature XRD studies over $Ni_{20}Mg_{47}Al_{33}$ prepared by urea hydrolysis method.

The following d values are labeled on the figure:

- $d = 7.55360$
- $d = 7.46804$
- $d = 7.46441$
- $d = 8.62485$
- $d = 7.97284$

The traces are labeled (top to bottom): 700°C, 400°C, 350°C, 300°C, 250°C, 200°C, 150°C, 100°C, 25°C.
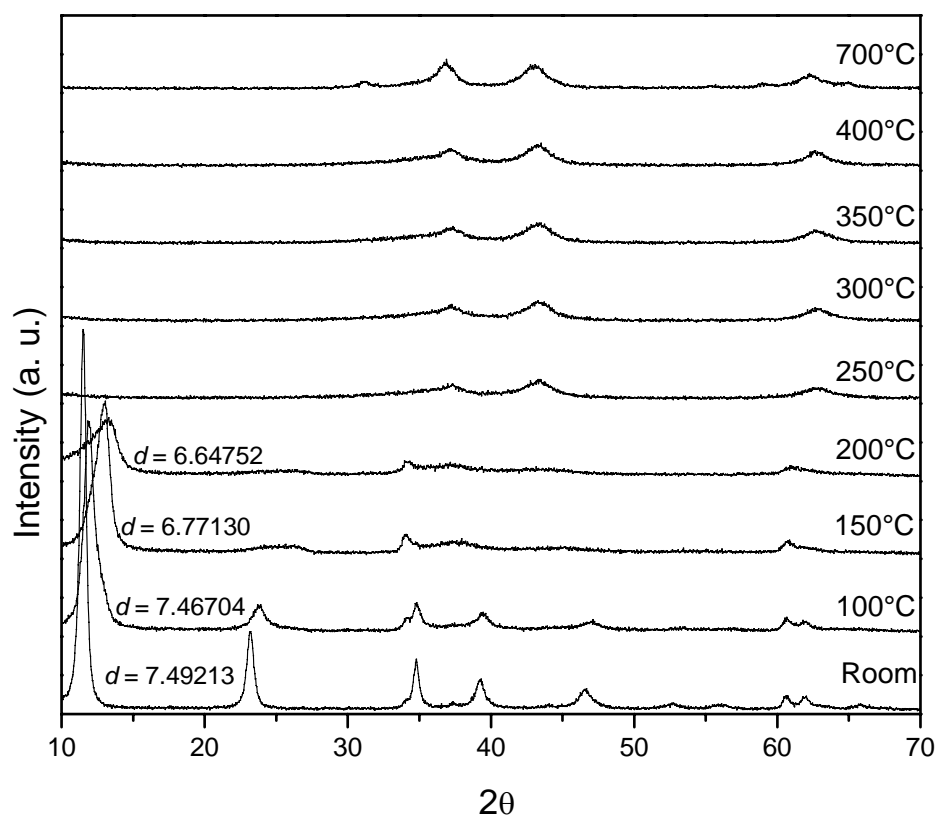
Figure 3.5.1.2.9: Variable temperature XRD studies over $Ni_{50}Zn_{17}Al_{33}$ prepared by urea hydrolysis method.
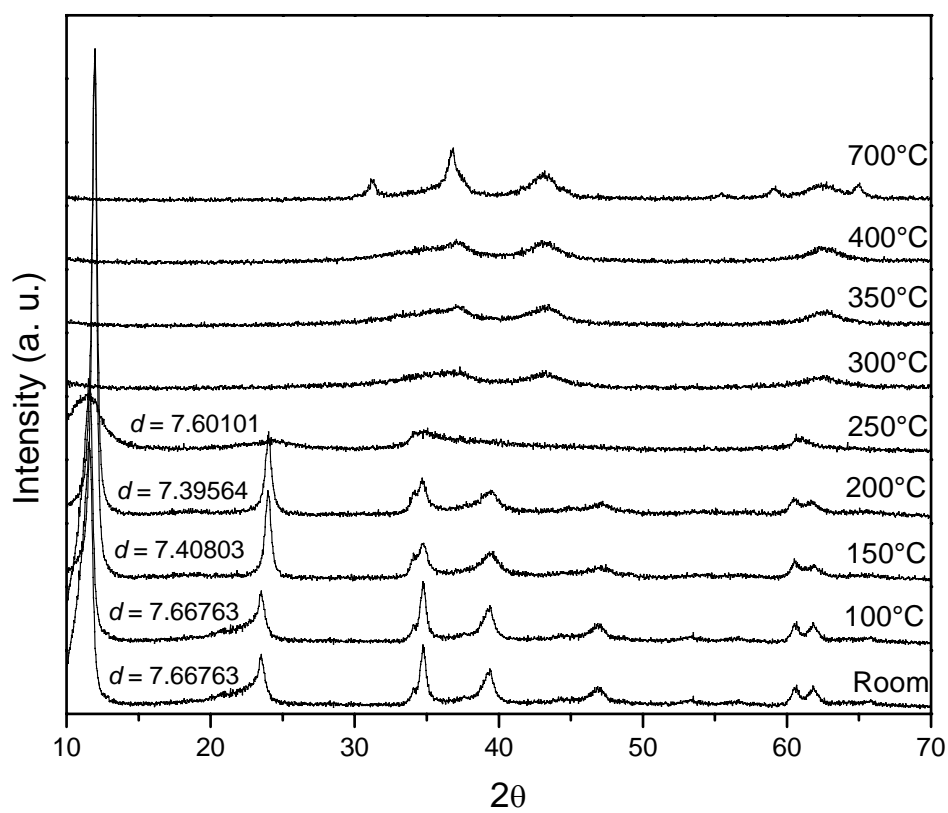
Figure 3.5.1.2.10: Variable temperature XRD studies over $Ni_{35}Zn_{32}Al_{33}$ prepared by urea hydrolysis method.
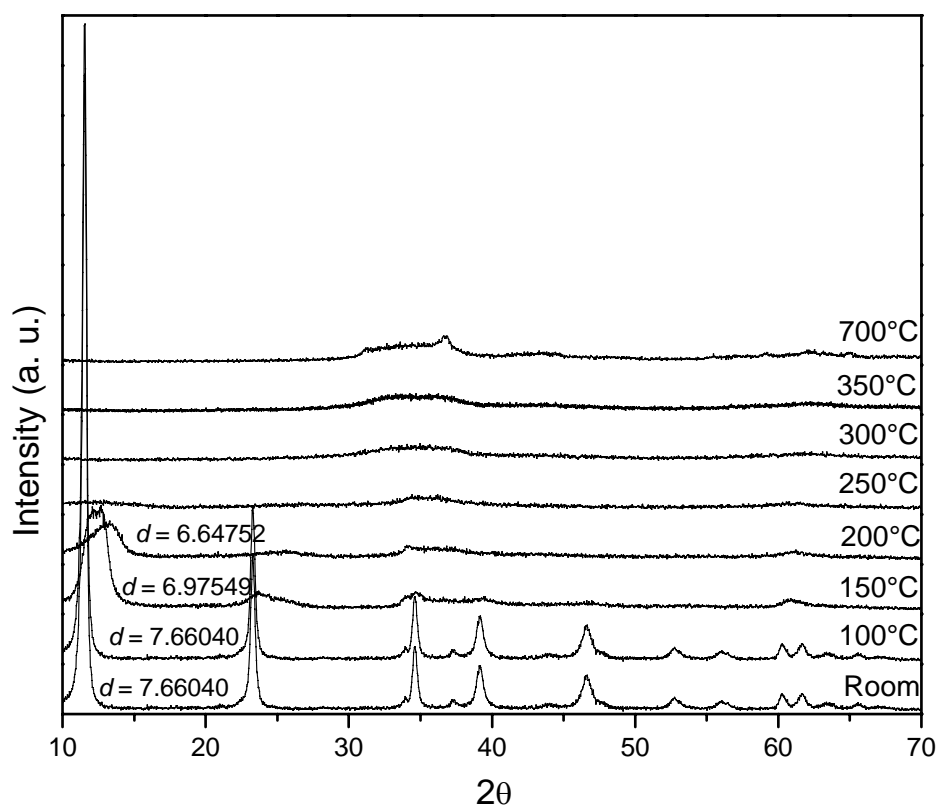
Figure 3.5.1.2.11: Variable temperature XRD studies over $Ni_{20}Zn_{47}Al_{33}$ prepared by urea hydrolysis method.

After calcination in flowing oxygen, the XRD data of the Ni/Mg/Al series revealed mixed oxides of $MgNiO_2$/MgO·NiO (or MgO·3NiO) and spinels of $NiAl_2O_4$ (or $MgAl_2O_4$) (Figure 3.5.1.2.12). For the Ni/Zn/Al series, ZnO·NiO phases and $ZnAl_2O_4$ (or $NiAl_2O_4$) were formed (Figure 3.5.1.2.13). No peaks ascribed to Al oxides were identified in either of the series, which could indicate either the formation of amorphous Al oxides or Al ions dissolved in the matrix of MgO·NiO, ZnO·NiO and/or in the spinel phases. As the amount of Mg increases in the corresponding materials, the peaks of spinel phases become more prominent. Similarly, as more Zn is

incorporated in the structure, the peaks due to the presence of ZnO·NiO, ZnO (zincite) and $ZnAl_2O_4$ (or $NiAl_2O_4$) become more evident.

It can be noticed that the intensity of the MgO·NiO (ZnO·NiO) peaks decreases as the amount of Mg (Zn) is increased. This behaviour corresponds to the formation of spinels. It is not possible to tell from the XRD pattern whether Mg, Zn or Ni discarded from the network forms the spinels, or whether the spinel contains a mixture of the two M^{2+} cations present.
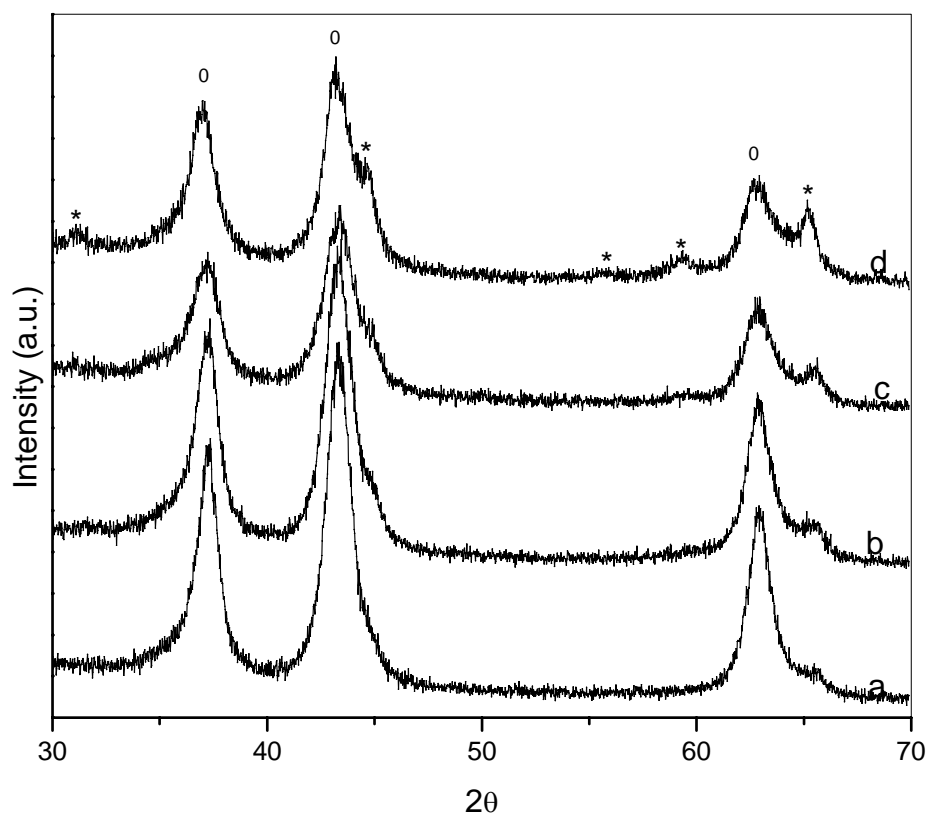
Figure 3.5.1.2.12: XRD patterns of the materials of the series Ni/Mg/Al prepared by hydrolysis of urea, calcined at 700°C for 7 hrs. a) Ni/Mg = ∞, b) Ni/Mg = 2.94, c) Ni/Mg = 1.09 and d) Ni/Mg = 0.42; Al/(Ni+Mg) = 0.33. ^{0}MgO·NiO and *$MgAl_2O_4$ (or $NiAl_2O_4$).
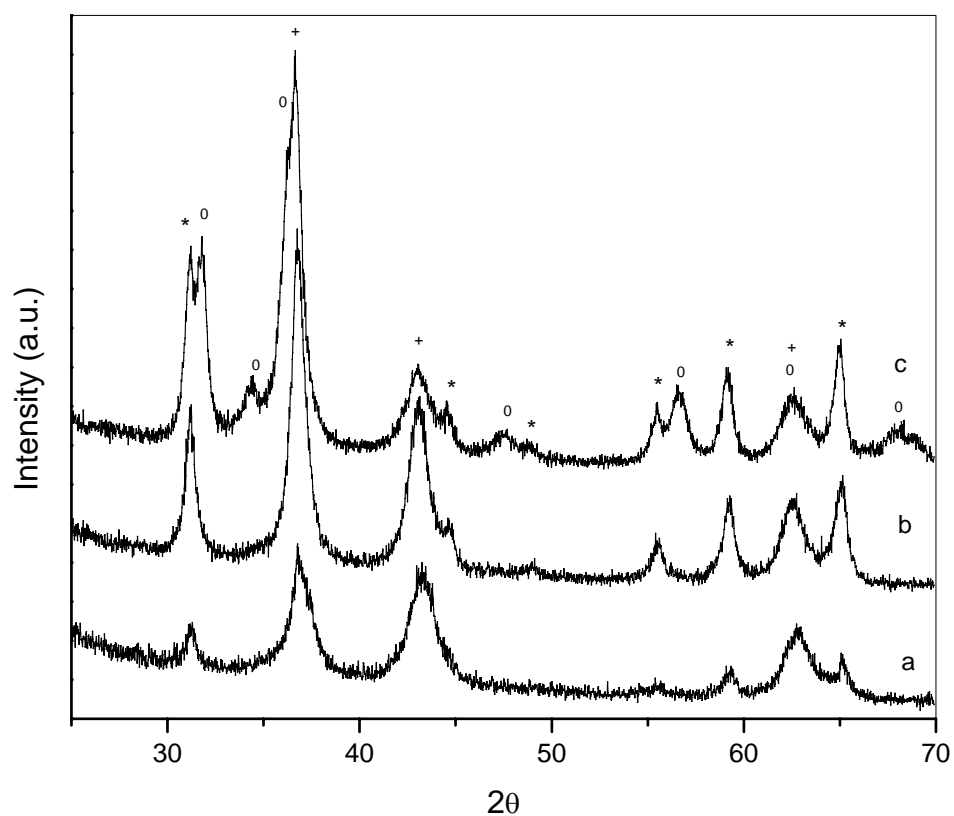
Figure 3.5.1.2.13: XRD patterns of the materials of the series Ni/Zn/Al prepared by hydrolysis of urea, calcined at 700°C for 7 hrs. a) Ni/Zn = 2.94, b) Ni/Zn = 1.09 and c) Ni/Zn = 0.42; Al/(Ni+Zn) = 0.33. [+]ZnO·NiO, [0]ZnO and [*]$ZnAl_2O_4$ (or $NiAl_2O_4$).

Figures 3.5.1.2.14 and 3.5.1.2.15 show the XRD patterns of the reduced materials of both series.
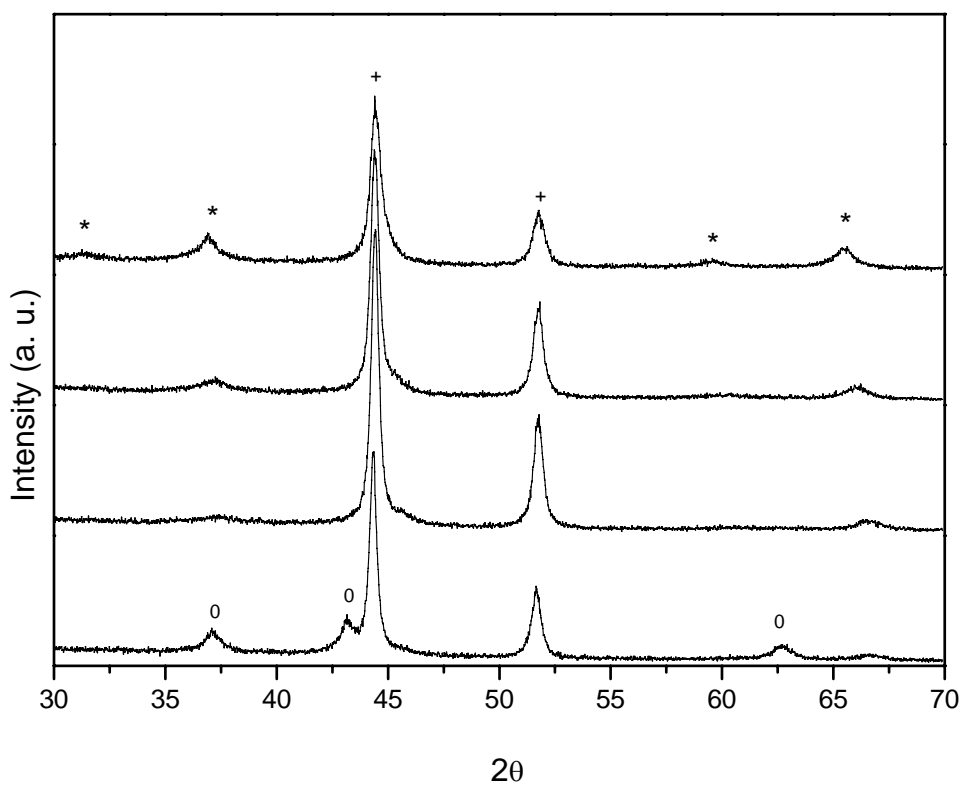
Figure 3.5.1.2.14: XRD patterns of the series materials containing Ni/Mg/Al prepared by urea hydrolysis, calcined at 700°C and reduced at 750°C, in flowing oxygen and flowing 10% hydrogen, respectively. Both thermal treatments were carried out for 7 hrs. Bottom to top: Ni/Mg = ∞, 2.94, 1.09 and 0.42 (Al/(Ni+Mg) = 0.33). ^{0}NiO, *Al$_2$MgO$_4$, MgAl$_2$O$_4$ and/or NiAl$_2$O$_4$, and $^+$metallic Ni.
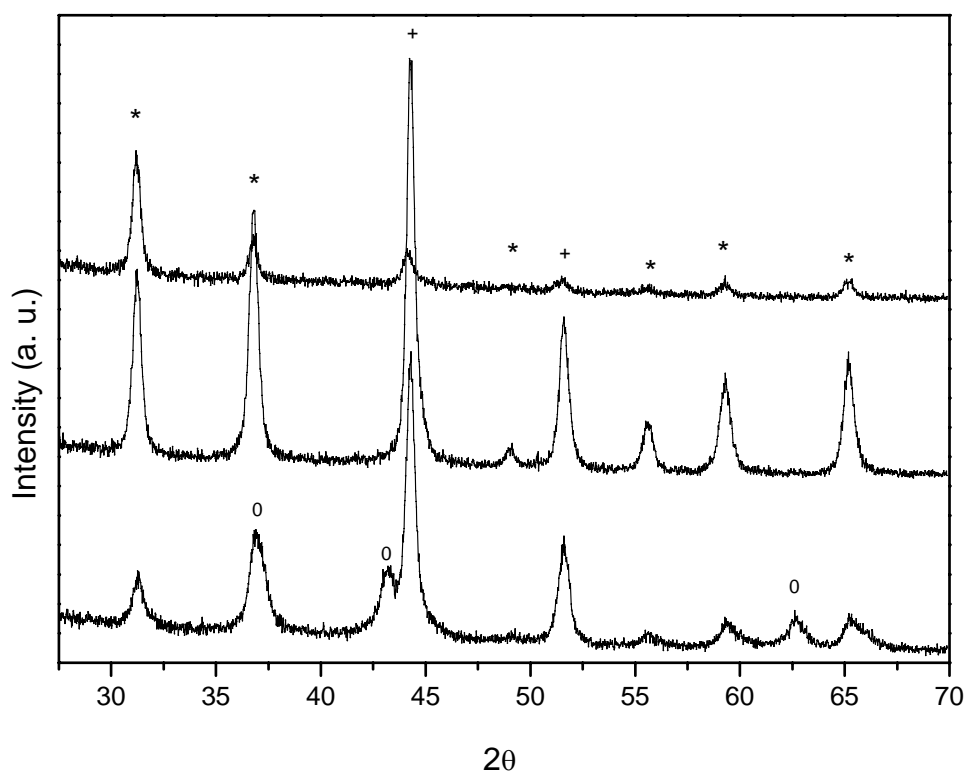
Figure 3.5.1.2.15: XRD patterns of the series materials containing Ni/Zn/Al prepared by urea hydrolysis, calcined at 700°C and reduced at 750°C, in flowing oxygen and flowing hydrogen, respectively. Both thermal treatments were carried out for 7 hrs. Bottom to top: Ni/Zn = ∞, 2.94, 1.09 and 0.42 (Al/(Ni+Zn) = 0.33). ^{0}NiO (or ZnO·NiO), *ZnAl$_2$O$_4$ or NiAl$_2$O$_4$, and $^+$metallic Ni.

From Figure 3.5.1.2.14 it can be seen that traces of NiO remain after reduction of the Takovite-like material. As Mg is introduced into the structure, spinels are more prominent. This behaviour is seen as well for the analogous series containing Zn (Figure 3.5.1.2.15). The solid with starting formula Ni/Zn = 2.94 shows a NiO (or ZnO·NiO) phase apart from the spinel phase.

From the half width of the Ni peaks, the crystal size of the metallic particles of both series, Ni/Mg/Al and Ni/Zn/Al, was estimated. The results are shown in Table 3.5.1.2.1.

Ni/M ratio Al = 0.33	Ni crystallite size (nm)	Ni/ Zn ratio Al = 0.33	Ni crystallite size (nm)[a]
∞	27.0	∞	27.0
2.94	26.5	2.94	20.1
1.09	24.2	1.09	24.0
0.42	19.5	0.42	20.5

Table 3.5.1.2.1: Ni crystallite size for the series of materials synthesised by urea hydrolysis method. [a]The error in measuring the width at half height is 0.125°. Ni crystallite size calculation error is about ±5%.

From Table 3.5.1.2.1 it can be noticed that for the series Ni/Mg/Al, the higher the amount of Ni present in the material, the larger the Ni crystallite size. However, this is not true for the series Ni/Zn/Al as there are minor variations in the trend. This divergence can be explained in terms of two possible different factors such as particle size or even difference in reducibility of NiO or (ZnO·NiO) species. The Ni crystallite sizes of both series are in the range of ~20-30 nm.

3.5.2 TG-DTA

In general, the thermal behaviour of HLCs is characterised by two endothermic transitions observed by DTA. The first one corresponds to the loss of interlayer water. This step is reversible and therefore, the structure of the HLC is not affected. The second at higher temperature corresponds to the loss of hydroxyl groups and anions. There is evidence that shows at this point the HLC can still be regenerated from a layered oxide but once temperature is raised a little more, the HLC is irrecoverable. The quantitative and qualitative properties of both transitions depend on many factors such as the ratio between the different cations and the type of anions present in the material, as well as the different processes that the materials passed through during their synthesis and the atmosphere used during analysis.

3.5.2.1 TG-DTA of the Series of Materials Prepared by Coprecipitation

Figures 3.5.2.1.1-12 show the TG-DTA of the materials of the series Ni/Mg/Al prepared by coprecipitation.

In general, the DTA of the samples synthesised without any post hydrothermal treatment (as prepared) show two endothermic peaks and a shoulder. The first peak is centred at ca. 100°C, the shoulder around 190°C and the second peak at ca. 365°C. The latter shift to a higher temperature as the amount of Mg increases in the material. Details of the temperature at which these transitions take place are summarised in Table 3.5.2.1.1. The hydrothermal treatment after synthesis led to an improvement in crystallinity, which was observed by XRD studies in Section 3.5.1.1.

This structural tuning is mirrored in the DTA profile of the materials too. Samples hydrothermally treated at 110°C show another well defined endothermic peak at ca. 250°C. Moreover, the transition observed initially at around 100°C in the fresh samples takes place at a higher temperature (ca. 150°C) after hydrothermal treatment. Special cases are the materials $Ni_{67}Al_{33}$ and $Ni_{50}Mg_{17}Al_{33}$, in which another endothermic peak at a temperature below 100°C is observed.
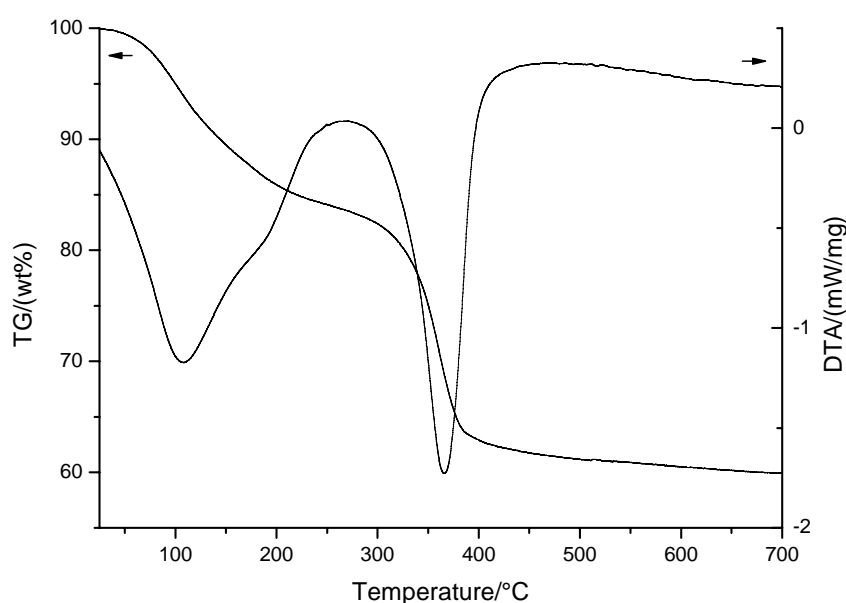
Figure 3.5.2.1.1: TG-DTA of the material $Ni_{67}Al_{33}$ as prepared.
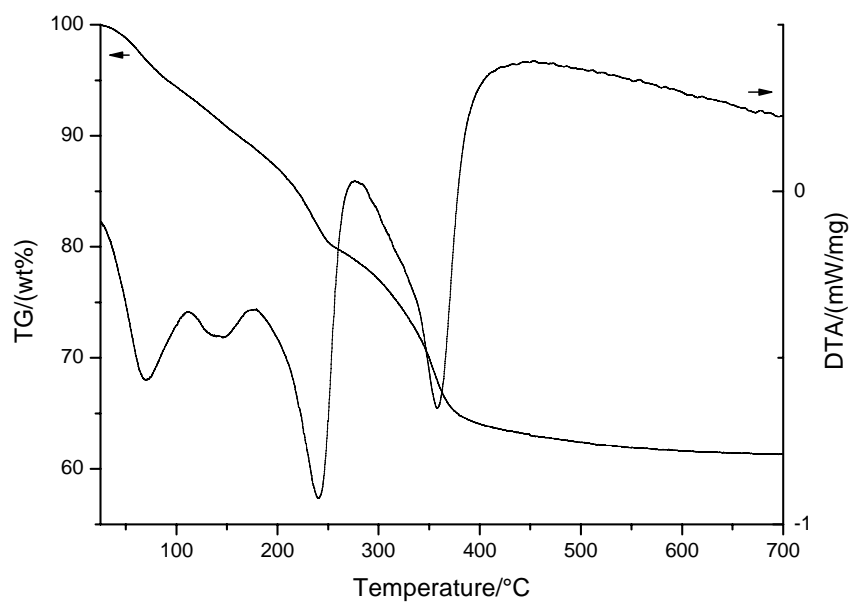
Figure 3.5.2.1.2: TG-DTA of the material Ni$_{67}$Al$_{33}$ hydrothermally treated at 110°C for 24 hrs.
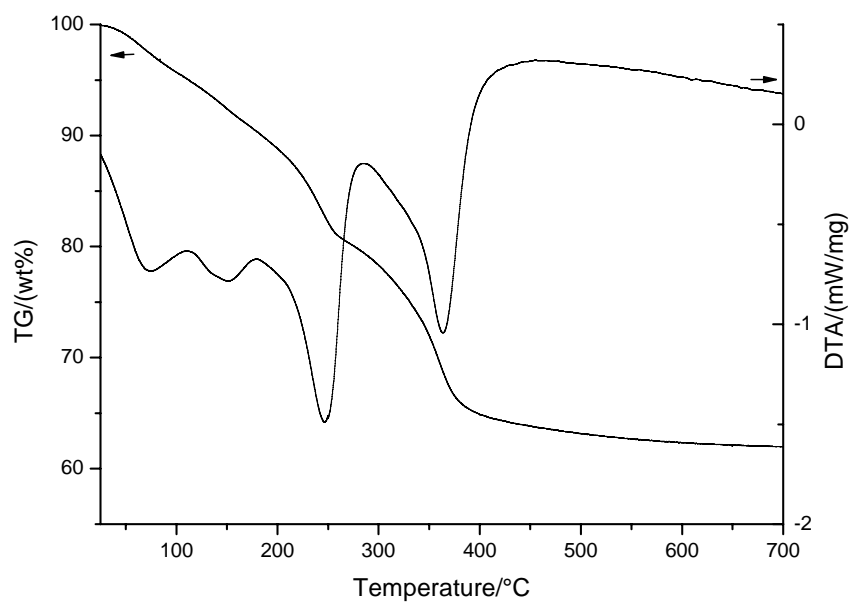
Figure 3.5.2.1.3: TG-DTA of the material Ni$_{67}$Al$_{33}$ hydrothermally treated at 110°C for 48 hrs.
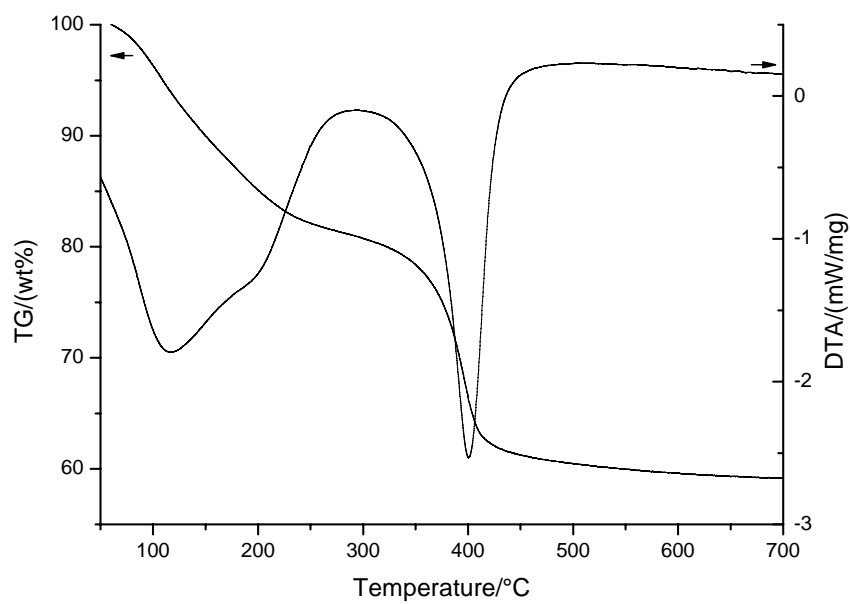
Figure 3.5.2.1.4: TG-DTA of the material $Ni_{50}Mg_{17}Al_{33}$ as prepared.
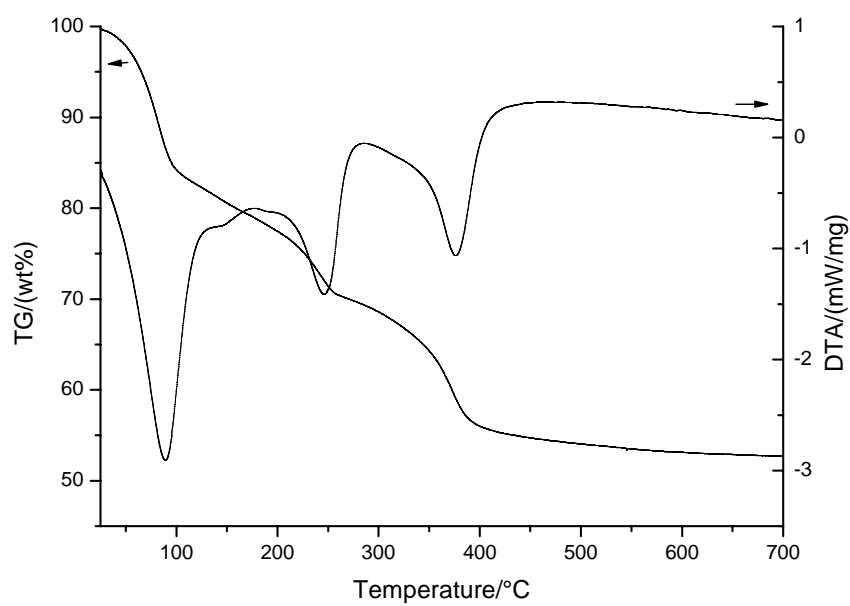
Figure 3.5.2.1.5: TG-DTA of the material $Ni_{50}Mg_{17}Al_{33}$ hydrothermally treated at 110°C for 24 hrs.
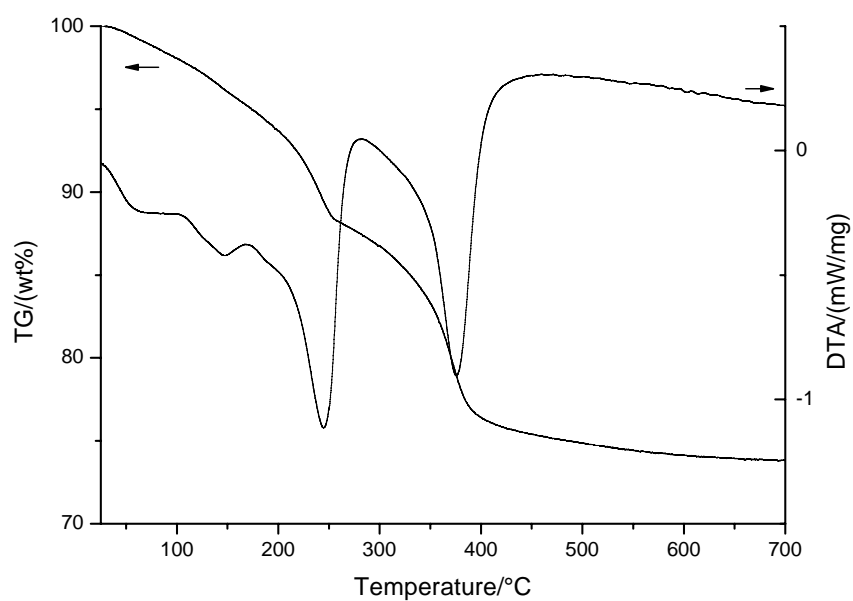
Figure 3.5.2.1.6: TG-DTA of the material $Ni_{50}Mg_{17}Al_{33}$ hydrothermally treated at 110°C for 48 hrs.
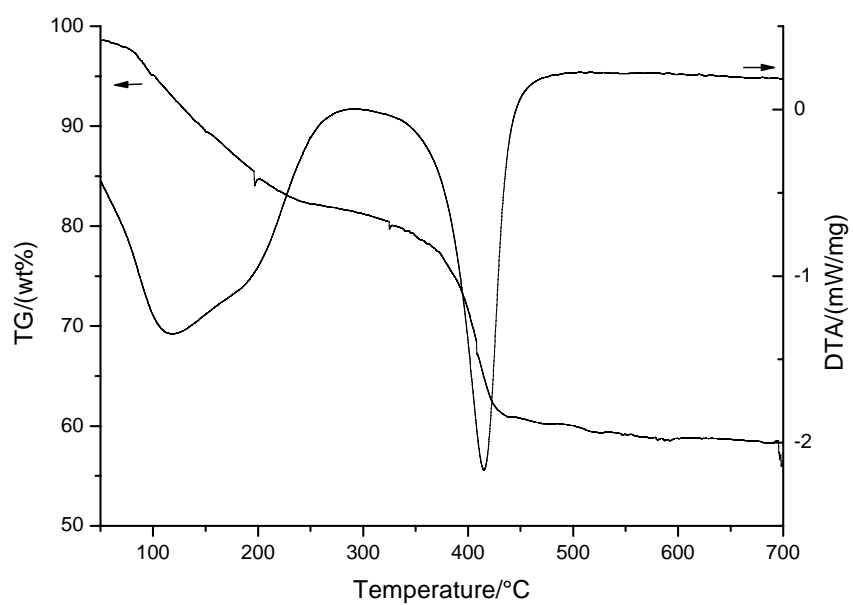
Figure 3.5.2.1.7: TG-DTA of the material $Ni_{35}Mg_{32}Al_{33}$ as prepared.
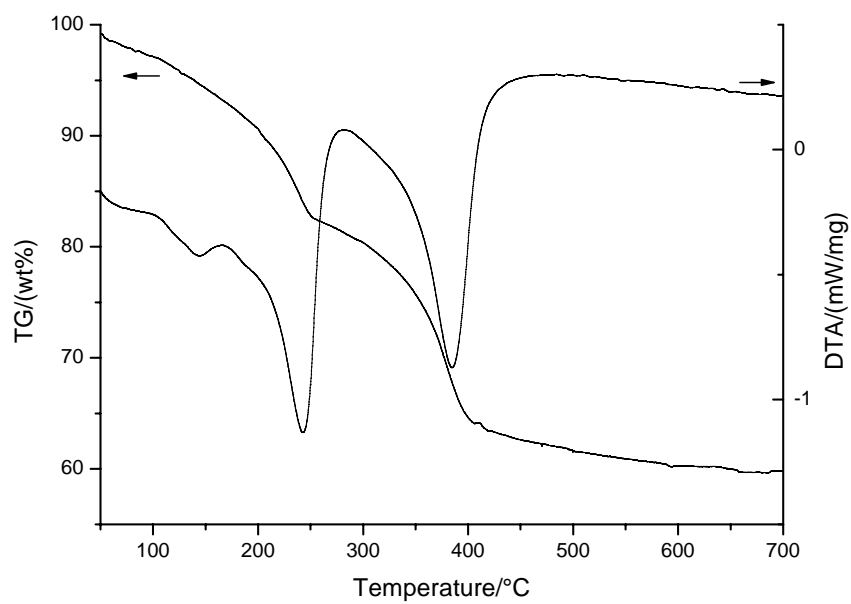
Figure 3.5.2.1.8: TG-DTA of the material Ni$_{35}$Mg$_{32}$Al$_{33}$ hydrothermally treated at 110°C for 24 hrs.
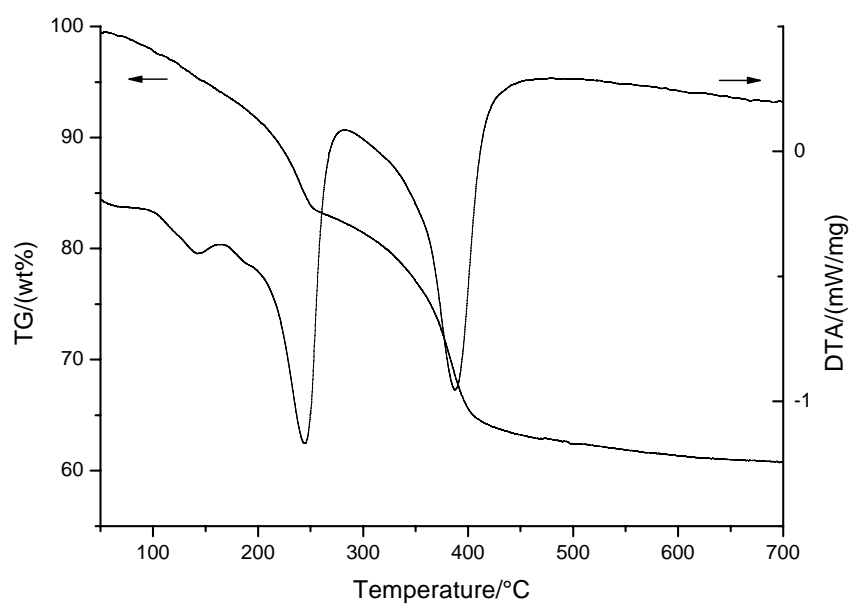
Figure 3.5.2.1.9: TG-DTA of the material Ni$_{35}$Mg$_{32}$Al$_{33}$ hydrothermally treated at 110°C for 48 hrs.
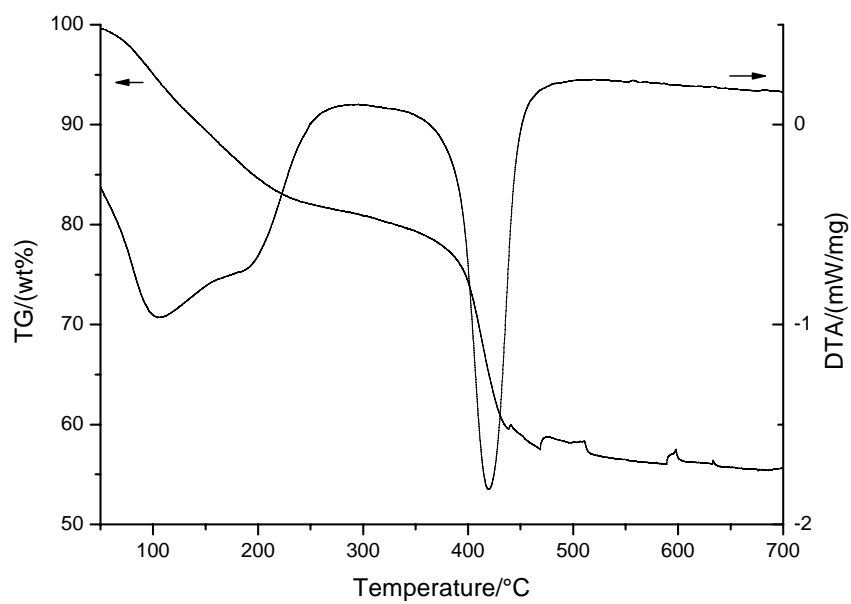
Figure 3.5.2.1.10: TG-DTA of the material $Ni_{20}Mg_{47}Al_{33}$ as prepared.
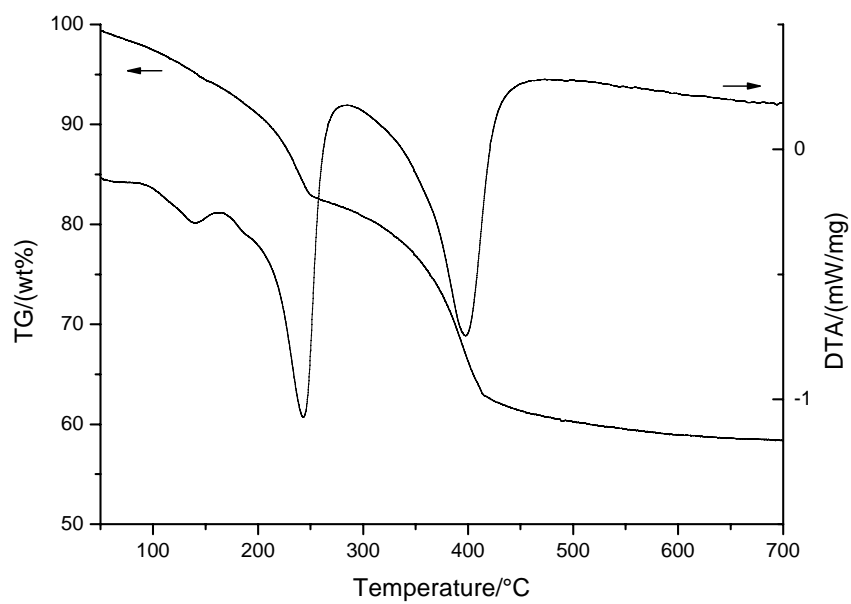
Figure 3.5.2.1.11: TG-DTA of the material $Ni_{20}Mg_{47}Al_{33}$ hydrothermally treated at 110°C for 24 hrs.
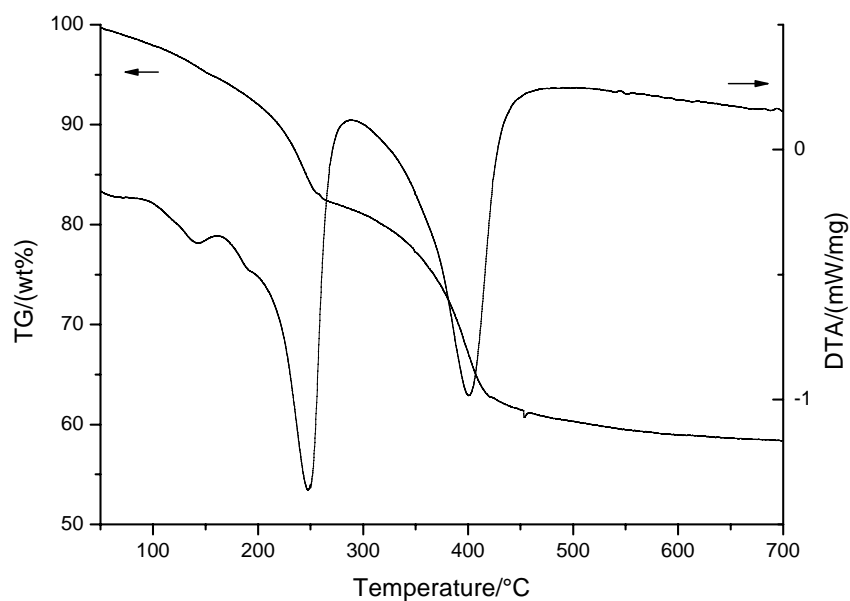
Figure 3.5.2.1.12: TG-DTA of the material $Ni_{20}Mg_{47}Al_{33}$ hydrothermally treated at 110°C for 48 hrs.

Material	Transition I[a]	Shoulder	Transition II[a]	Transition III[a]	Transition IV[a]
$Ni_{67}Al_{33}$	105	190	365	-	-
$Ni_{67}Al_{33}$[b]	69	-	142	240	357
$Ni_{67}Al_{33}$[c]	70	-	150	245	362
$Ni_{50}Mg_{17}Al_{33}$	116	195	400	-	-
$Ni_{50}Mg_{17}Al_{33}$[b]	89	-	146	245	376
$Ni_{50}Mg_{17}Al_{33}$[c]	62	-	147	246	375
$Ni_{35}Mg_{32}Al_{33}$	115	190	415	-	-
$Ni_{35}Mg_{32}Al_{33}$[b]	142	-	240	383	-
$Ni_{35}Mg_{32}Al_{33}$[c]	141	-	245	387	-
$Ni_{20}Mg_{47}Al_{33}$	102	190	418	-	-
$Ni_{20}Mg_{47}Al_{33}$[b]	138	-	243	397	-
$Ni_{20}Mg_{47}Al_{33}$[c]	142	-	244	401	-

Table 3.5.2.1.1: Transition temperatures (minima) of the materials of the series Ni/Mg/Al prepared by coprecipitation determined by DTA. [a](°C). [b]Hydrothermally treated at 110°C for 24 hrs. [c]Hydrothermally treated at 110°C for 48 hrs.

Details of weight losses with respect to temperature that are observed in the different inflections taking place during TGA are shown in Table 3.5.2.1.2.

Material	T(°C)/wt(%)	T(°C)/wt(%)	T(°C)/wt(%)	T(°C)/wt(%)	T(°C)/wt(%)	T(°C)/wt(%)
$Ni_{67}Al_{33}$[a]	205/15	298/3	390/19	-	-	700/3
$Ni_{67}Al_{33}$[b]	250/20	375/15	-	-	-	700/4
$Ni_{67}Al_{33}$[c]	255/20	382/15	-	-	-	700/4
$Ni_{50}Mg_{17}Al_{33}$[a]	233/18	330/3	412/17	-	-	700/3
$Ni_{50}Mg_{17}Al_{33}$[b]	95/15	219/9	262/6	331/4	393/10	700/4
$Ni_{50}Mg_{17}Al_{33}$[c]	206/7	250/5	304/3	391/9	-	700/3
$Ni_{35}Mg_{32}Al_{33}$[a]	226/17	340/2	434/19	-	-	700/2
$Ni_{35}Mg_{32}Al_{33}$[b]	248/18	297/2	349/5	400/10	-	700/6
$Ni_{35}Mg_{32}Al_{33}$[c]	248/17	309/3	402/15	-	-	700/4
$Ni_{20}Mg_{47}Al_{33}$[a]	246/17	323/4	440/19	412/17	-	700/5
$Ni_{20}Mg_{47}Al_{33}$[b]	249/17	320/4	414/17	-	-	700/4
$Ni_{20}Mg_{47}Al_{33}$[c]	256/17	313/2	418/17	-	-	700/5

Table 3.5.2.1.2: weight losses with respect to temperature of the initial sample weight of the materials of the series Ni/Mg/Al prepared by coprecipitation determined by TGA. [a]As prepared. [b]Hydrothermally treated at 110°C for 24 hrs. [c]Hydrothermally treated at 110°C for 48 hrs.

Figures 3.5.2.1.13-16 show the TG-DTA of the materials of the series Ni/Mg/Cr hydrothermally treated at 110°C for 48 hrs.

These materials are less crystalline than the previous series, which has been discussed in the corresponding XRD studies (Section 3.5.1.1). In general, the DTA profiles show two endothermic peaks without any regular trend as the amount of Mg incorporated in the materials is increased.
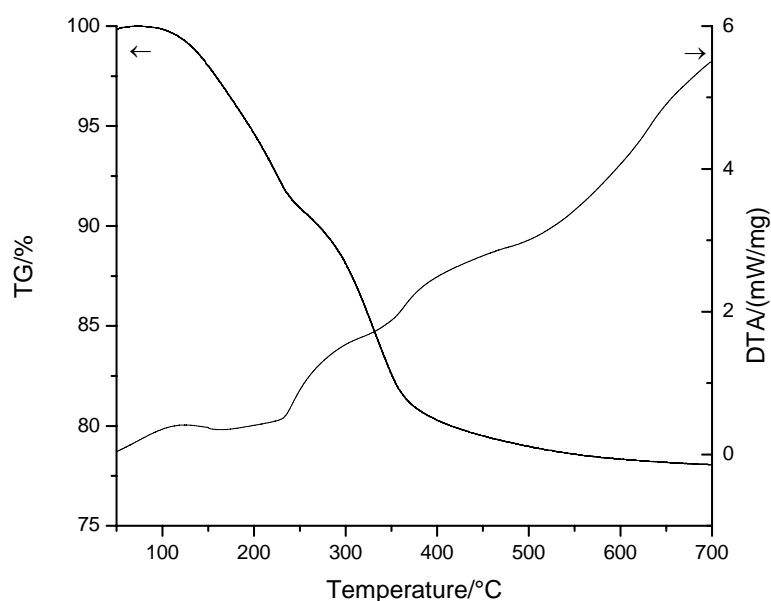
Figure 3.5.2.1.13: TG-DTA of the material $Ni_{67}Cr_{33}$ hydrothermally treated at 110°C for 48 hrs.

The DTA of $Ni_{67}Cr_{33}$ shows three broad endothermic transitions in the temperature ranges of 105-280°C, 295-370°C and 390-700°C, respectively. According to the TGA, the first thermal transition embraces a weight loss of 10% from the initial sample weight. The second thermal transition leads to a weight loss of 8%. The third thermal transition is accompanied by a weight loss of 4%. The total weight loss at 700°C is therefore 22% (Figure 3.5.2.1.13).
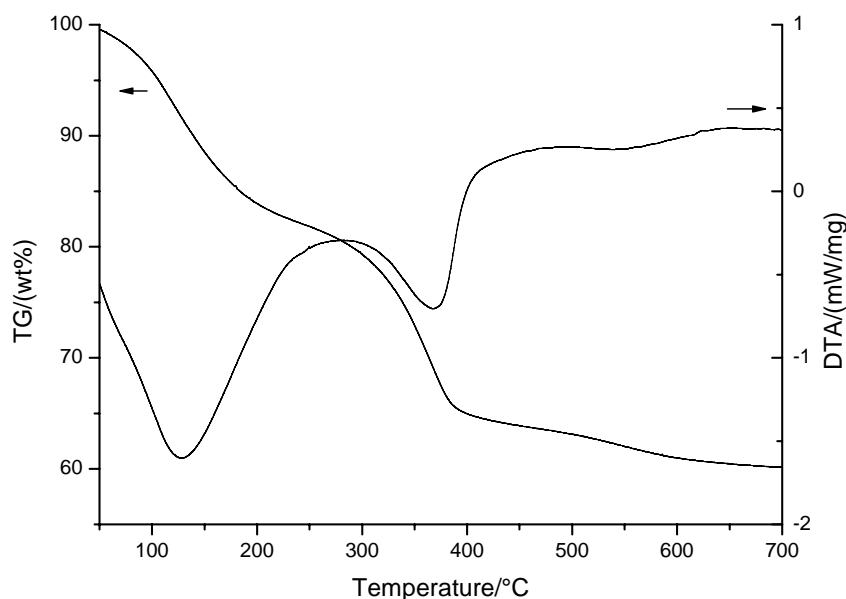
Figure 3.5.2.1.14: TG-DTA of the material $Ni_{50}Mg_{25}Cr_{25}$ hydrothermally treated at 110°C for 48 hrs.

The DTA profile of the material $Ni_{50}Mg_{25}Cr_{25}$ shows two endothermic transitions with minimum centred at 128°C and at 368°C, respectively; and a not well defined endothermic transition in the range 463-635°C (Figure 3.5.2.1.14). The TGA reveals a weight loss of 19% at the end of the first thermal transition (ca. 288°C), from the initial weight of the sample. At the end of the second thermal transition (at ca. 383°C), a further loss of 15% is seen. A further weight loss of 6% corresponds to the third transition. The sample has lost 40% of its initial weight at 700°C.

The DTA profile of the material $Ni_{35}Mg_{40}Cr_{25}$ reveals an endothermic transition with minimum centred at 115°C and a shoulder at ca. 200°C, an endothermic transition with minimum at 365°C, and a not well defined transition in the range 492-615°C. On the other hand, the TGA profile shows different inflections up to 257, 257-424 and 424-585°C, which correspond to weight losses of 20, 16 and 4% from the original weight of the sample, respectively. The total weight loss is therefore 40% at 700°C (Figure 3.5.2.1.15).
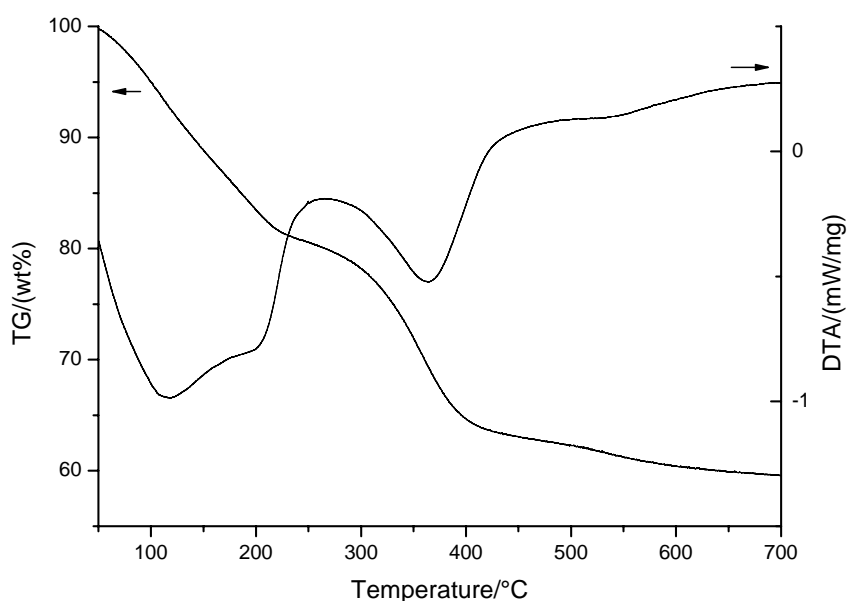
Figure 3.5.2.1.15: TG-DTA of the material $Ni_{35}Mg_{40}Cr_{25}$ hydrothermally treated at 110°C for 48 hrs.

The material labelled as Ni$_{25}$Mg$_{50}$Cr$_{25}$ presents an endothermic transition with minimum centred at 110°C, a shoulder at ca. 200°C, an endothermic transition with minimum centred at 379°C, and a not well defined endothermic transition in the range 501-635°C; and three gradual weight losses of 22, and 16 and 5% as the material was heated through the range of temperature studied. These weight losses took place at 284, 411 and 700°C, respectively. All of these details are obtained from its TG-DTA profile (Figure 3.5.2.1.16).
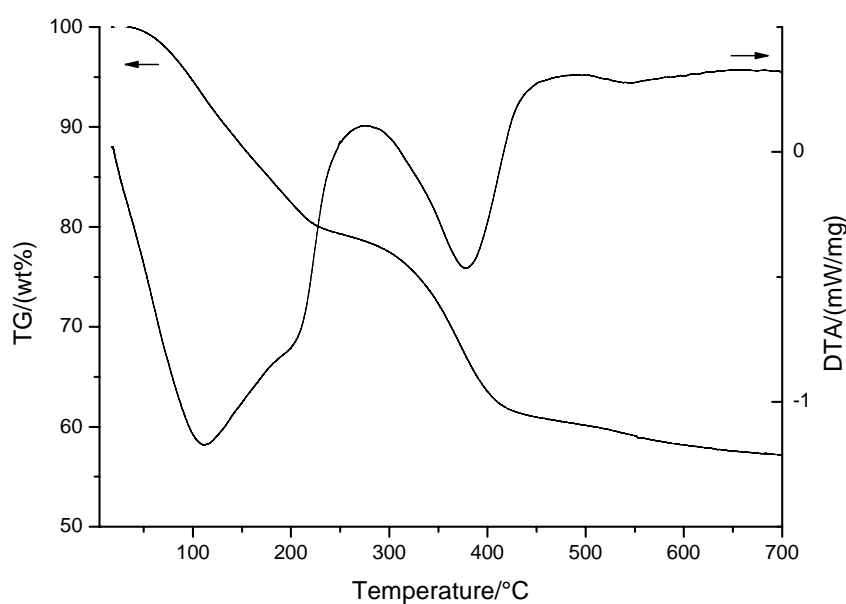
Figure 3.5.2.1.16: TG-DTA of the material Ni$_{25}$Mg$_{50}$Cr$_{25}$ hydrothermally treated at 110°C for 48 hrs.

Figures 3.5.2.1.17-22 show the DT-TGA profiles and mass spectra (MS) of the series of the materials containing Fe prepared by the coprecipitation method.
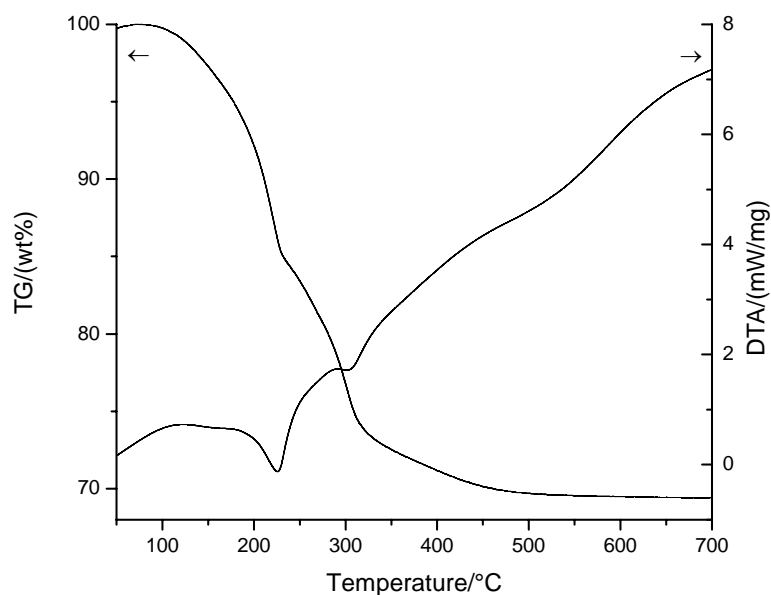
Figure 3.5.2.1.17: TG-DTA of the material $Ni_{67}Fe_{33}$ hydrothermally treated at 120°C for 24 hrs.

$Ni_{67}Fe_{33}$ DTA profile exhibits four endothermic transitions, the first one in the range 127-176°C, the second one with minimum centred at 230°C, the third one with minimum centred at and 306°C, and the fourth one in the range 457-582°C. The TGA profile shows weight losses of 26, further 4 and further 1% of the initial sample weight at 315, 457 and 700°C, respectively (Figure 3.5.2.1.17).

MS shows the removal of water and CO_2 from the material. Water is released in three stages according to the mass spectrum: a big peak with maximum centred at 220°C and a broad shoulder at lower temperature, a small peak with maximum at 265°C and another peak with maximum centred at 300°C; whereas CO_2 from carbonate species are released at around 300°C (Figure 3.5.2.1.18).
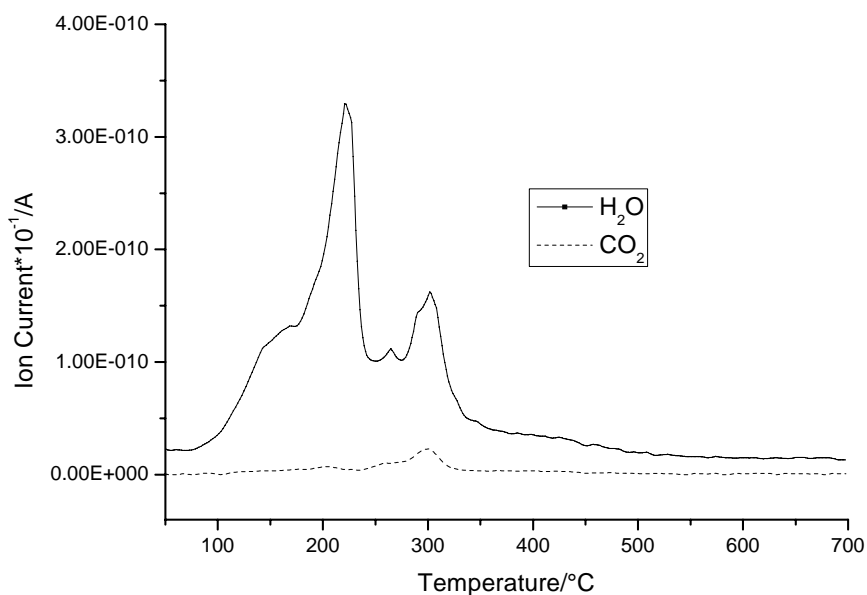
Figure 3.5.2.1.18: MS of the material $Ni_{67}Fe_{33}$ hydrothermally treated at 120°C for 24 hrs.

When Mg was incorporated to the Ni/Fe structure, the thermal transitions are as follows: one in the range 130-175°C, another with minimum centred at 227°C, the next one with minimum centred at 330°C, and another in the range 462-630°C. Weight losses of 14, 12, and 4 % are seen at 234, 341 and 530°C, respectively. The species delivered are water (with a broad shoulder at temperature below the maximum), and water/OH anions along with CO_2; from lower to higher temperature peaks, respectively. The total weight loss of the sample at 700°C is 30% (Figures 3.5.2.1.19 and 3.5.2.1.20).
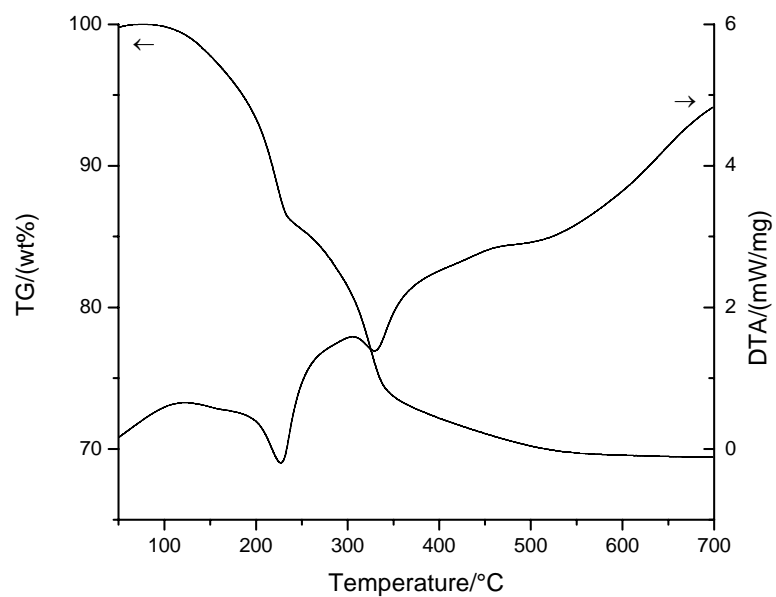
Figure 3.5.2.1.19: TG-DTA of the material $Ni_{50}Mg_{17}Fe_{33}$ hydrothermally treated at 110°C for 48 hrs.
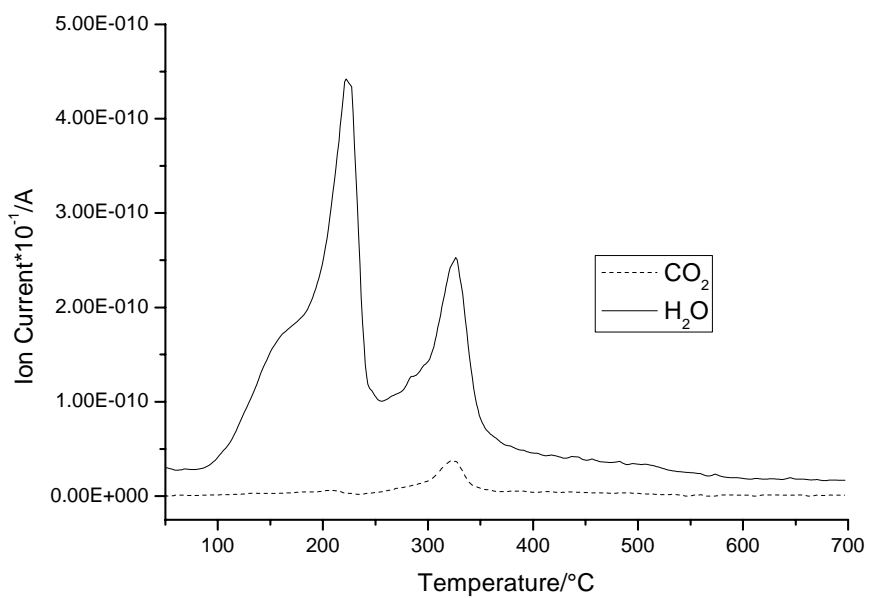
Figure 3.5.2.1.20: MS of the material $Ni_{50}Mg_{17}Fe_{33}$ hydrothermally treated at 110°C for 48 hrs.

Figures 3.5.2.1.21 and 3.5.2.1.22 show the TG-DTA and MS of the material Ni/Zn/Fe, respectively.
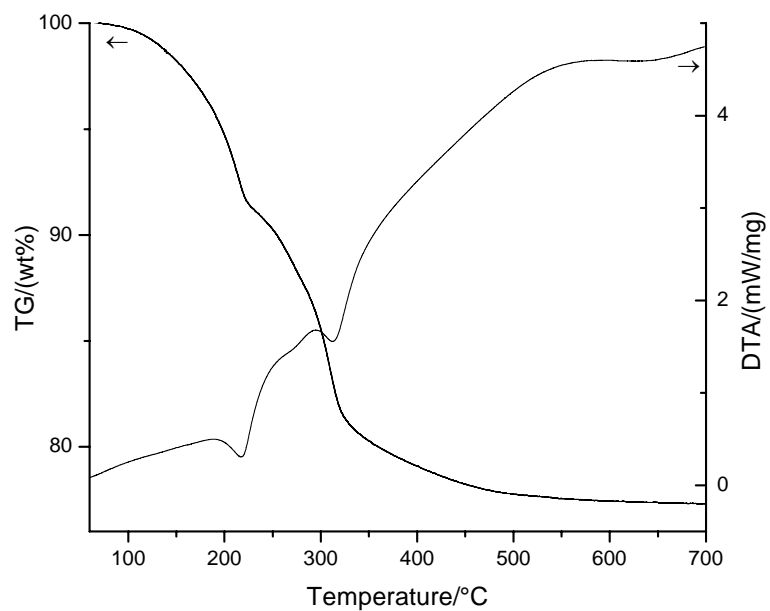
Figure 3.5.2.1.21: TG-DTA of the material $Ni_{50}Zn_{17}Fe_{33}$ hydrothermally treated at 110°C for 48 hrs.
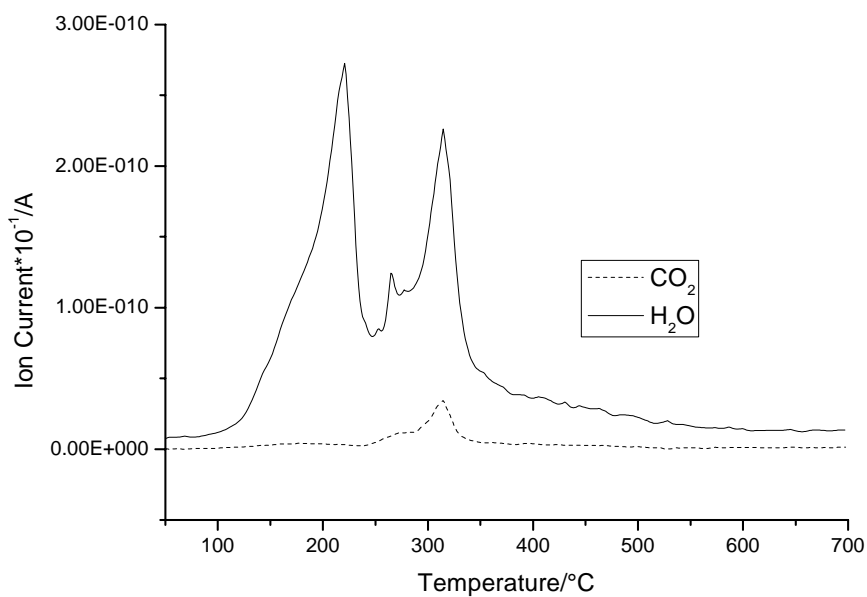
Figure 3.5.2.1.22: MS of the material $Ni_{50}Zn_{17}Fe_{33}$ hydrothermally treated at 110°C for 48 hrs.

When Zn replaces Mg, the DTA is as follows: an endothermic transition peak takes place with minimum centred at 217°C, an endothermic transition in the range 259-279°C, an endothermic transition peak with minimum centred at 312°C, and another one in the range 600-675°C. The matching species for the transitions are water, water/OH and CO_2. The weight losses for the corresponding thermal transitions are 8, 10, 4 and 1%, respectively. The total weight loss at 700°C is 23% (Figures 3.5.2.1.21 and 3.5.2.1.22).

3.5.2.2 TG-DTA of the Series of Materials Prepared by Hydrolysis of Urea

For HLCs containing Mg-Al-CO_3, Miyata[199] has observed three thermal transitions. Those are attributed to loss of interlayer water, loss of water from structural hydroxyl groups and to the decomposition of interlamellar carbonate species. These transitions have been found to be dependent on aluminium content.

For our materials containing Ni-Mg-Al-CO_3 prepared by hydrolysis of urea, we have found two thermal transitions instead: one corresponding to loss of interlayer water and the other due to the loss of both water from structural hydroxyl groups and interlamellar CO_2 species released simultaneously.

The TG-DTA of the series Ni/Mg/Al is shown in Figures 3.5.2.2.1-4. The species released from the solids were identified by MS.
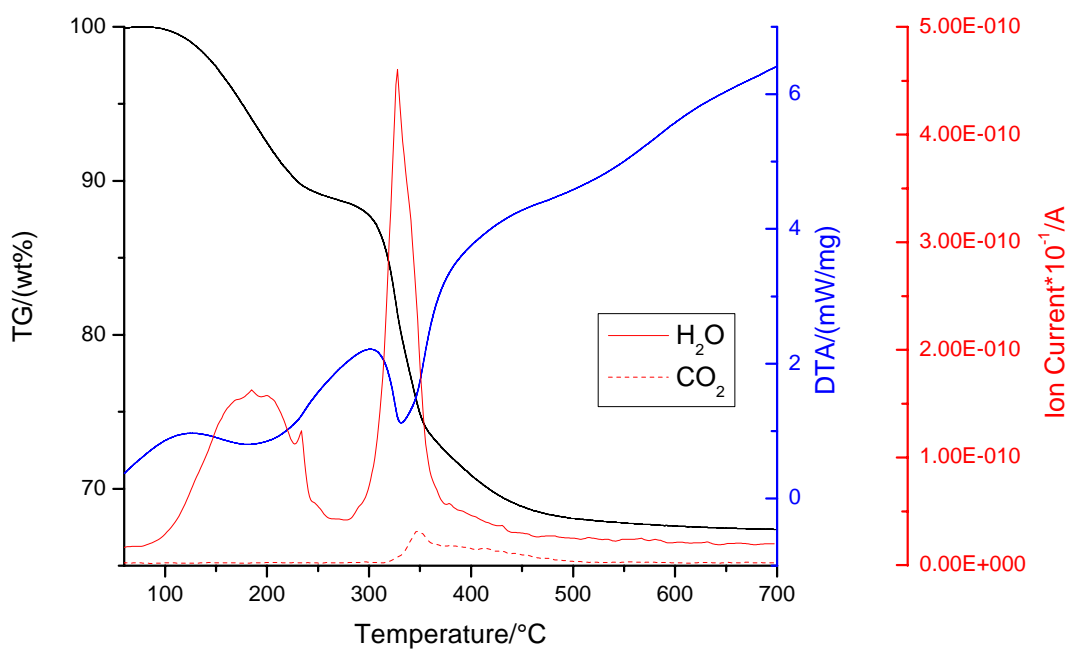
Figure 3.5.2.2.1: TG-DTA-MS of the material $Ni_{67}Al_{33}$.
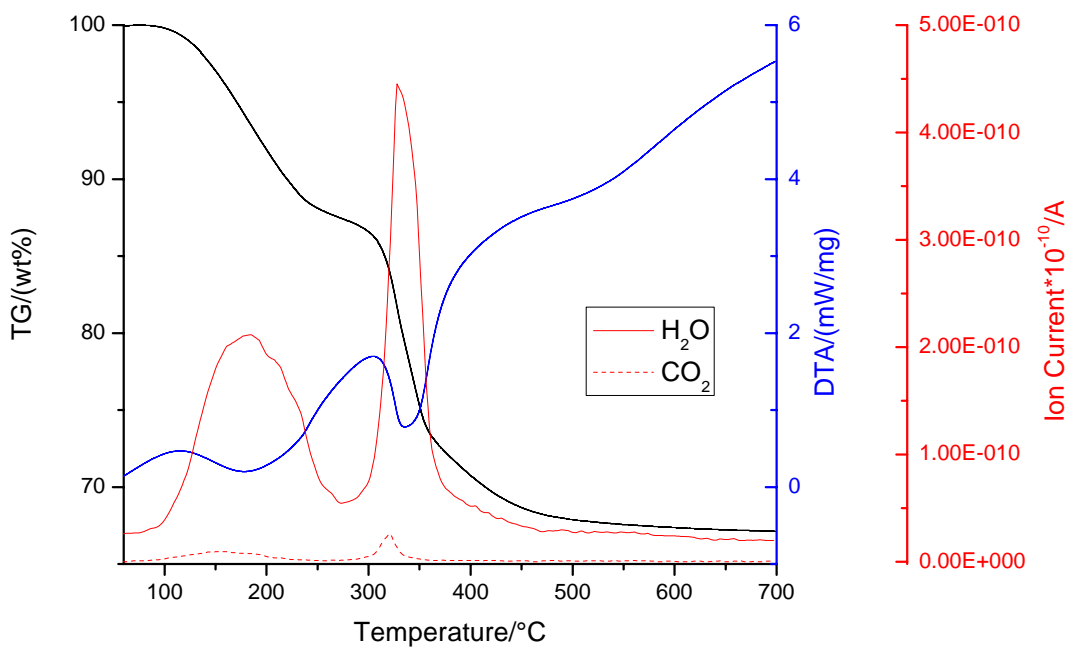
Figure 3.5.2.2.2: TG-DTA-MS of the material $Ni_{50}Mg_{17}Al_{33}$.
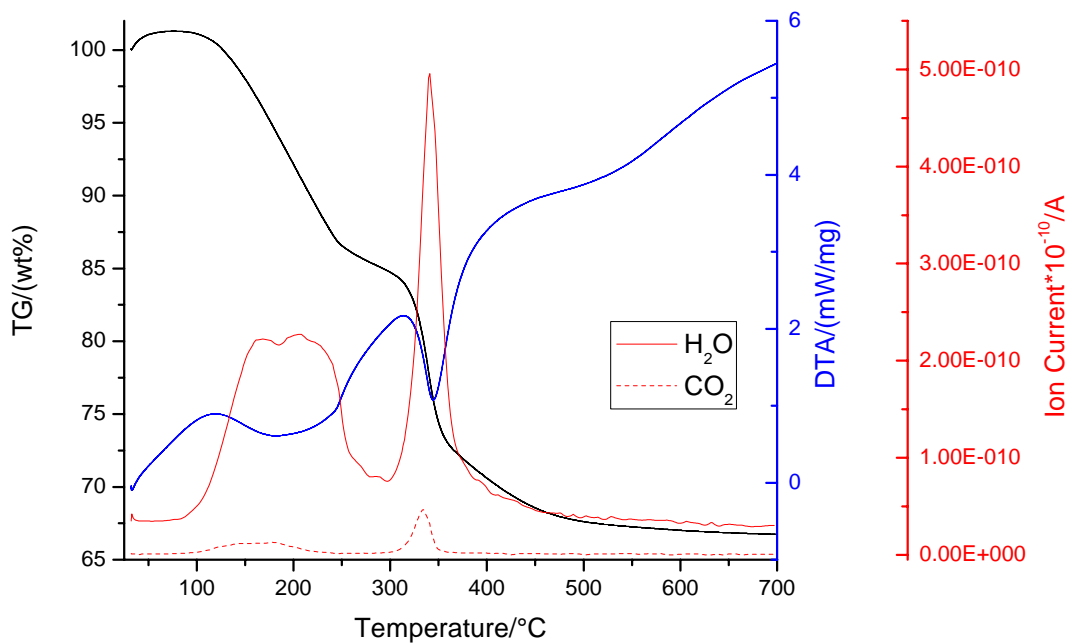
Figure 3.5.2.2.3: TG-DTA-MS of the material $Ni_{35}Mg_{32}Al_{33}$.
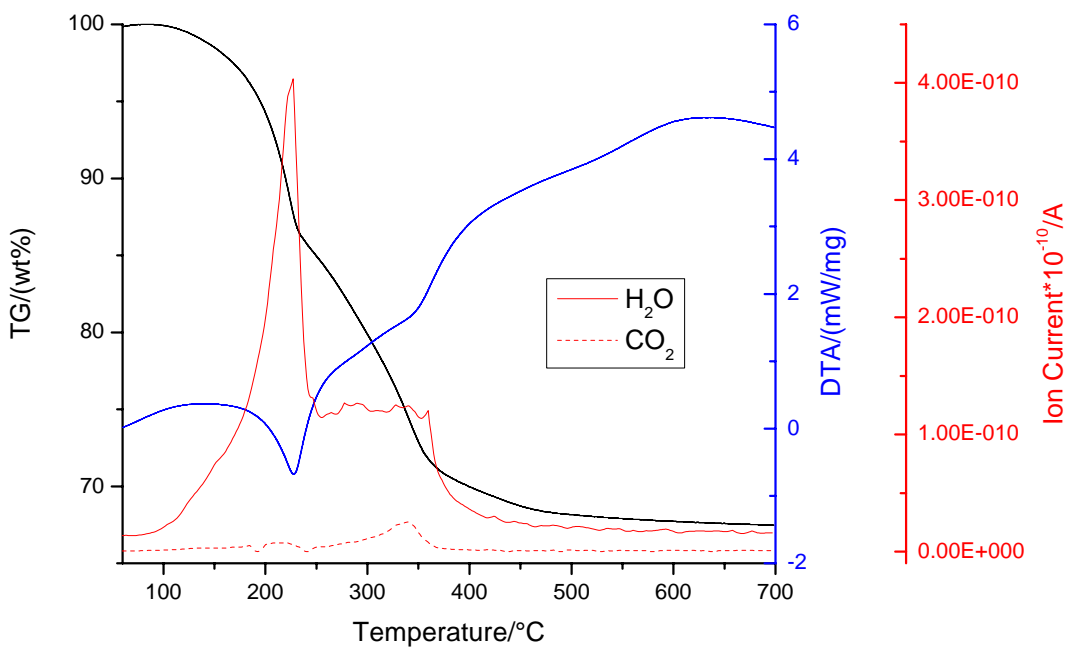
Figure 3.5.2.2.4: TG-DTA-MS of the material $Ni_{20}Mg_{47}Al_{33}$.

From the DTA's of the Figures (3.5.2.2.1-4), it can be seen that the exact position of the endothermic peaks varies with respect to Ni/Mg ratio in the samples. The minima at which these transitions take place are shown in Table 3.5.2.2.1.

Ni/Mg ratio	Transition I (°C)	Transition II (°C)
∞	201	331
2.94	205	338
1.09	212	344
0.42	228	350

Table 3.5.2.2.1: Details of thermal transitions of HLCs containing Ni-Mg-Al-CO3-H_2O.

In general, for the series Ni/Mg/Al, as the amount of Mg present increases, thermal transitions take place at higher temperature.

Moreover, all of the materials of this series present another transition in the range of temperatures of ~450-600°C.

The TGA of the material without Mg in its structure shows a weight loss of 10% of the initial sample weight at ca. 237°C. This weight loss is due to removal of water which was confirmed by MS. The removal of water carries on till the temperature of 275°C, with a further 1% of weight loss. A further 14% loss of the sample weight at 351°C has been attributed to the simultaneous removal of water and carbonate species. MS confirms that the natures of the species expelled from the material are water and CO_2. The removal of water and CO_2 carries on up to 500°C where a further total weight loss of 6% is observed. The total weight loss is 32% at 700°C.

The TGA of the material with Ni/Mg ratio equal to 2.94 shows a weight loss of 7% of the initial sample weight at 239°C. Removal of water is attributed to this loss according to the MS data. Removal of water carries on till 277°C and a further weight loss of 1% is seen by 293°C. A further weight loss of 18% takes place by 358°C, and another weight loss of 5% is observed by 437°C. Water and CO_2 have been released from the material at this range of temperature. At 700°C, 33% of the initial weight sample has been lost.

The TGA of the solid with starting Ni/Mg ratio equal to 1.09 shows the first weight loss at 246°C, which corresponds to a 7% loss of the initial sample weight. The next weight loss of further 2% takes place at 302°C. At 354°C, a 17% weight loss is seen. At 451°C, a further 6% weight loss occurs. At the temperature of 700°C, 33% of the initial weight has been lost. Carbonate species and water are seen by MS.

For the material with Ni/Mg ratio equal to 0.42 the first weight loss of 13%, due to the removal of water, takes place at 231°C. Another weight loss of 15% takes place at 255°C. A further weight loss of 4% occurs at 469°C. At 700°C, the total weight loss is 32.5.

In summary, for this series of materials, the following conclusions can be drawn:

i. as the amount of Mg increases in the sample, the first two transitions take place at higher temperatures; and

ii. decomposition of the materials to mixed oxide phases starts at ca. 190°C and finishes at 350-400°C, which is confirmed by XRD studies.

The DT-TGA-MS results of the series Ni/Zn/Al are shown in Figures 3.5.2.2.5-7.
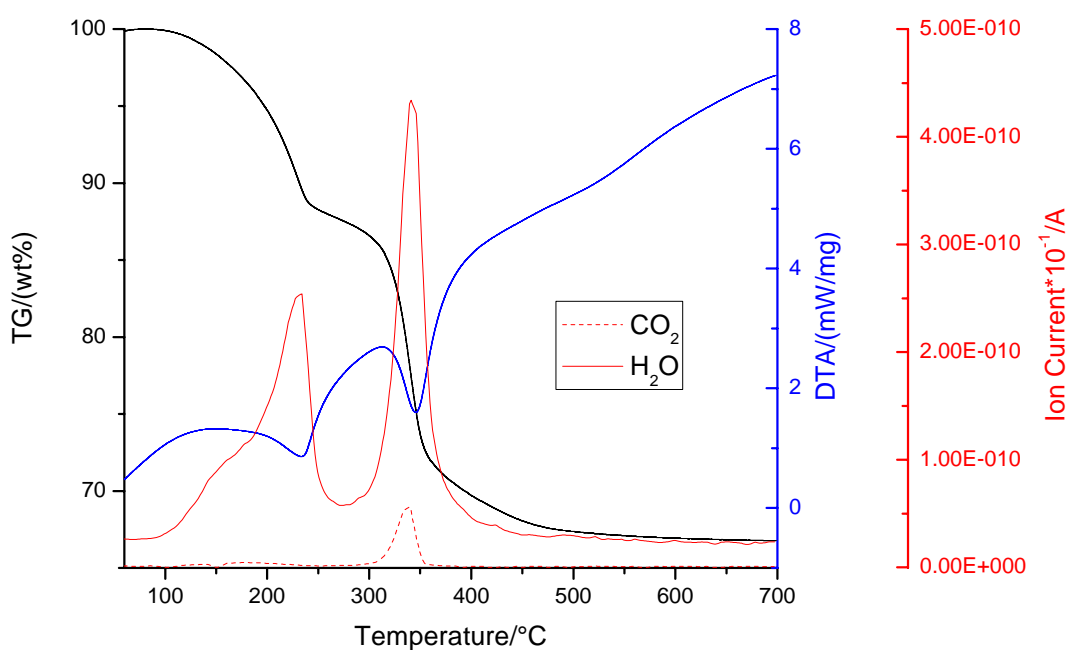
Figure 3.5.2.2.5: TG-DTA-MS of the material $Ni_{50}Zn_{17}Al_{33}$.
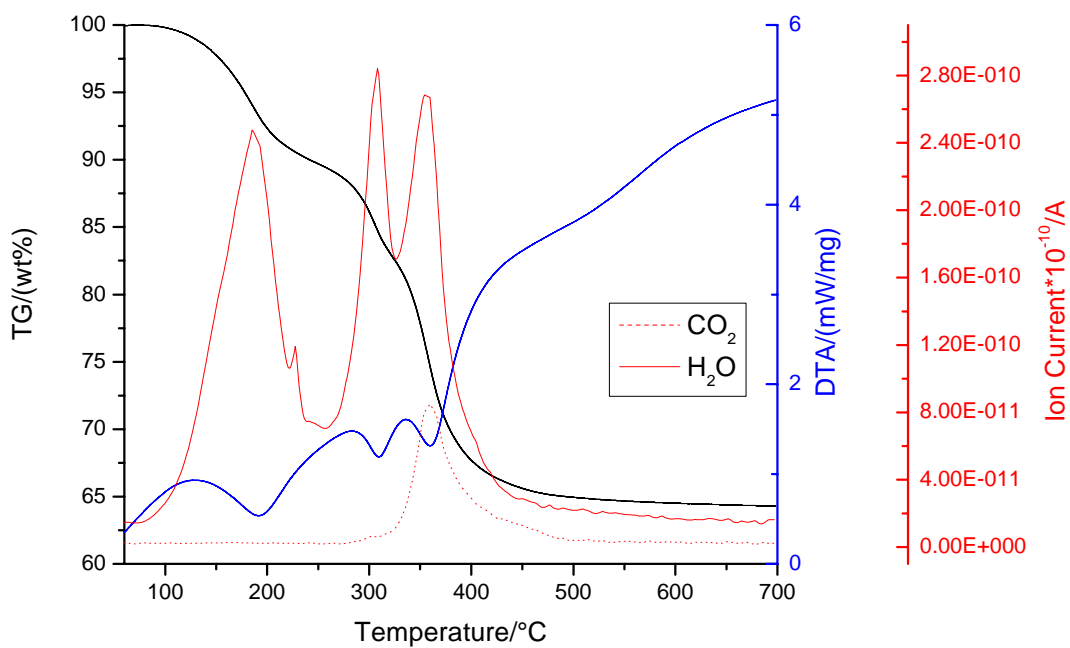
Figure 3.5.2.2.6: TG-DTA-MS of the material $Ni_{35}Zn_{32}Al_{33}$.
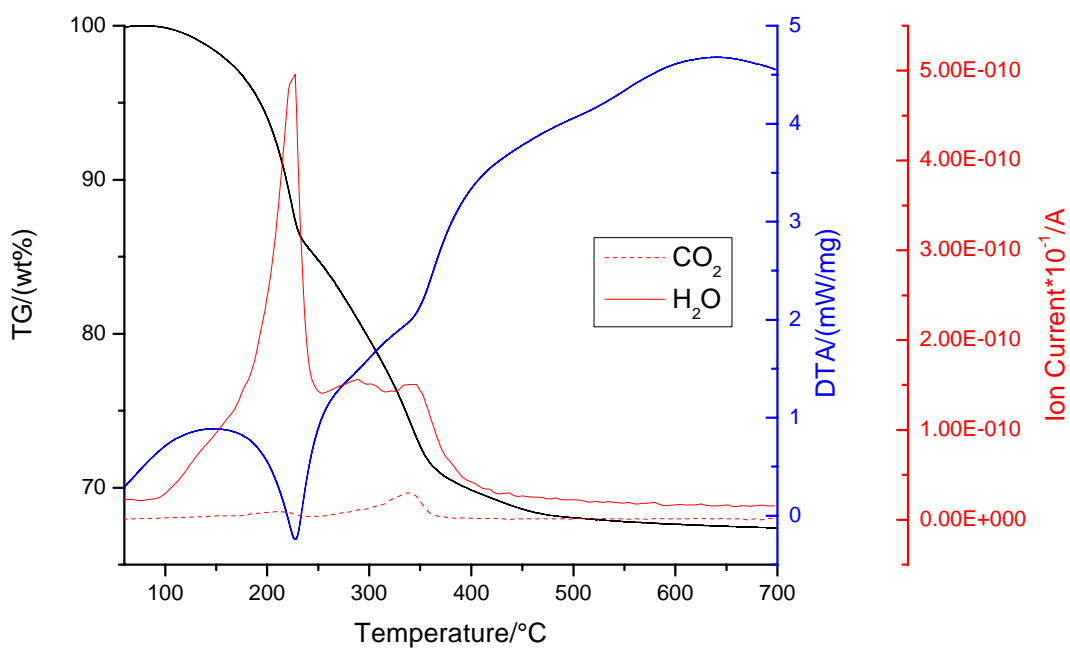
Figure 3.5.2.2.7: TG-DTA-MS of the material $Ni_{20}Zn_{47}Al_{33}$.

Details of the temperature at which transitions take place are given in Table 3.5.2.2.2.

Ni/Zn ratio	Transition I (°C)	Transition II (°C)	Transition III (°C)	Transition IV (°C)
2.94	234[*]	345[*]	476-568[**]	-
1.09	192[*]	309[*]	361[*]	473-566[**]
0.42	227[*]	314-358[**]	491-555[**]	-

Table 3.5.2.2.2: Details of thermal transitions of HLC containing Ni-Zn-Al-CO3-H_2O. [*]Minimum. [**]Range.

The TGA of the sample with Ni/Zn ratio equal to 2.94 shows a 13% weight loss by 290°C. By 355°C, the sample loses further 15% of its weight. A further weight loss of 4% takes place by 454°C. According to the MS profile, the first transition of the DTA is due to removal of solely water, while the second transition embraces the loss of water and carbonate species present in the galleries of the solid. At 700°C, the total weight loss is 33%.

For the material Ni/Zn = 1.09, weight losses of 9, 2, 5, 16 and 3% take place by 216, 272, 310, 395 and 456°C, respectively. The total weight loss at 700°C is 35%. MS reads water and carbonate species on the first thermal transition, water on the second thermal transition; and water and carbonate species on the third thermal transition of its TGA.

For the material Ni/Zn = 0.42, weight losses of 14, 14, and 4% take place by 231, 358 and 471°C, respectively. The total weight loss at 700°C is 33%.

3.5.3 Chiral Modification

Before exploring the effect of the most important variables of chiral modification on enantioselectivity (i.e. TA concentration and pH), the effect of Ni crystallite size will be discussed. This parameter has been found to be of paramount importance in supported and unsupported systems.

3.5.3.1 Ni Crystallite Size Effect on Enantioselectivity

According to Nitta et al.,[93] for unsupported nickel catalysts, enantioselectivity improves as nickel crystallite size increases. This phenomenon was observed in a series of Ni/SiO$_2$ catalysts, where Ni crystallite size was enhanced with an increase in Ni loading during synthesis.[95] The catalytic properties of these materials improved rapidly with increase in Ni loading up to 50% Ni wt. and then remained almost constant. Precipitation conditions such as temperature, stirring, Na$_2$CO$_3$/Ni ratio and ageing time all have an effect in Ni crystallite size for that particular system and the authors argue that narrow crystallite size distribution containing around 10 nm crystallites seems to be suitable for obtaining catalysts with high enantioselectivity in the hydrogenation of MAA. At the same time, they have proved that the enantiodifferentiation ability of supported catalysts also depends on the reduction conditions.[95, 98] A Ni/Al$_2$O$_3$ catalyst exhibited considerably high enantioselectivity

when reduced under relatively mild conditions. On the other hand, for a series of Ni/α-Al$_2$O$_3$ catalysts (40% Ni wt.), Osawa et al.[111, 200] found that the optical yield in the asymmetric hydrogenation of MAA was linked to the mean Ni crystallite size as this increased proportionally to the temperature of reduction, attaining the maximum optical yields at 500-600°C. The researchers concluded that a Ni crystallite size of about 50 nm would provide a suitable surface for the effective enantiodifferentiation with the aid of TA.

In order to figure out the Ni crystallite size effect of the catalysts prepared from HLC precursors on enantioselectivity, a takovite-like material was thermally treated to vary the particle size at constant metal loading. As Ni species are less reducible when calcination temperature increases,[201] higher temperatures of reduction were required when a higher calcination temperature was used. The results of the catalytic properties related to the thermal treatments and Ni crystallite sizes are shown in Table 3.5.3.1.1 (details of reaction are shown in caption).

T_{cal} (°C)	T_{Red} (°C)	τ (nm)	% Conv	% e.e.
350	550	39	79	8
500	675	47	80	10
700	750	27	97	12

Table 3.5.3.1.1: Conditions of reaction: 0.2g of fresh reduced catalyst was modified with a 0.2 ML^{-1} TA aqueous solution. The pH of the modifier solution was adjusted in advanced to 5.1. 5 mL of MAA and 10 mL methanol were used as substrate and solvent, respectively; in the hydrogenation of MAA. Temperature of operation was 100 °C and initial H$_2$ pressure was 10 bar. Reaction time was 48 hrs.

The parameters used for hydrogenation reaction (shown in the caption of Table 3.5.3.1.1) were the same as for TA-RaNi catalyst tested by Kukula et al.[81] (scaled down by a factor of ten). For those studies, the highest value of enantioselectivity was achieved with an initial concentration of TA of ca. 0.2 ML^{-1} during chiral modification.

From Table 3.5.3.1.1 it can be seen that the best results in the hydrogenation are obtained when the material was thermally treated under the most severe conditions. Both activity and enantioselectivity are improved as the temperature in both thermal treatments is increased. From these results it can be noticed that there is indeed a correlation between e.e. and Ni particle size. Moreover, the best catalytic properties were found in Ni particle sizes around 20-30 nm. Catalyst designed with a Ni particle size < 12 nm did not show enantiodifferentiation ability.

3.5.3.2 Effects of Variation of TA Concentration on Enantioselectivity

Another experiment was designed to use different initial TA concentrations during modification to figure out if this would have any effect on the catalytic properties of the materials. A catalyst calcined at 700°C and reduced at 750°C (both treatments during 7 hours) prepared from the takovite-like material precursor was modified by varying TA concentration in the range of 0.02, 0.05, 0.1, 0.2 and 0.3 ML^{-1}, using water as solvent and an initial pH of 5.1. The temperature of modification was kept at 100°C. The modification was carried out for one hour. The catalyst did not show any difference in enantioselectivity when tested in the hydrogenation of MAA, for which the e.e. was found to be ca. 12% for all samples (Table 3.5.3.2.1). Replacing TA for

its antipode gave the same e.e. value but the product was sign reversed (Table 3.5.3.2.2). Modification with optically inactive meso-TA yielded a racemic product mixture (e.e. = 0).

[TA]/ML^{-1}	%e.e.(R)
0.02	12
0.05	12
0.1	11
0.2	12
0.3	11

Table 3.5.3.2.1: Effect of D-TA concentration used during modification on e.e. using a catalyst prepared form the precursor HLC Ni$_{67}$Al$_{33}$. Water was used as the medium of reaction and the pH of the solution was adjusted to 5.1. The temperature of reaction was 100°C.

[TA]/ML^{-1}	%e.e.(S)
0.02	12
0.05	12
0.1	11
0.2	12
0.3	12

Table 3.5.3.2.2: Effect of L-TA concentration used during modification on e.e. using a catalyst prepared form the precursor HLC Ni$_{67}$Al$_{33}$. Water was used as the medium of reaction and the pH of the solution was adjusted to 5.1. The temperature of reaction was 100°C.

It has been stated that enantioselectivity of TA-Ni catalyst is strongly dependent on TA concentration during modification.[38, 103, 107] Keane and Webb[107] reported a direct relation between e.e. and initial TA concentrations over a Ni supported-silica catalyst (11.9% w/w). The optimum concentration increased as the temperature of modification decreased from 100°C to room temperature. Moreover, the number of TA molecules adsorbed was found to be higher using more concentrated TA solutions during modification reaction.

3.5.3.3 Dependence of pH on Enantioselectivity during Catalyst Modification

A catalyst prepared from the takovite-like material precursor (which was previously calcined at 700°C and reduced at 750°C for 7 hours in both cases) was modified with an invariable concentration of TA (0.05 ML^{-1}), using water as solvent, over a wide range of initial pH values: 3.2, 5.1, 7, 9, 11 and 13. The temperature of modification was kept at 100°C. The modification was carried out for one hour. The catalyst did not show difference in e.e. when tested in the hydrogenation of MAA, with the e.e. value again centred at 12% (Table 3.5.3.3.1).

pH$_{mod}$	%e.e.(R)
3.2	12
5.1	12
7	11
9	11
11	12
13	12

Table 3.5.3.3.1: Effect of pH used during modification on e.e. using a catalyst prepared from the HLC precursor Ni$_{67}$Al$_{33}$. Water was used as the medium of reaction and the pH and the temperature of reaction was 100°C. [TA] = 0.05 ML^{-1}. The time of reaction was 1 hr.

It has been stated that enantioselectivity of a modified catalyst is strongly dependent on the pH of the solution containing the modifier. Moreover, It has been speculated that pH may govern the mode of TA adsorption.[107] A pH of 5 is the optimal for the Izumi catalyst modified with acidic reagents.[51] In the case of Ni supported on α-Al$_2$O$_3$, Osawa et al.[111] found two maxima at pH's 3.2 and ca. 5. Bennett et al.,[202] found two maxima using Ni supported on silica in the same model reaction at 3.2 and ca. 9. For studies carried on similar materials, Keane[107] found no pH dependence with the overall reaction at low temperatures (T < 300 K) and low TA concentrations ([TA] < 0.01 ML^{-1}) during modification.

3.5.4 Catalytic Test

3.5.4.1 Catalysts Prepared from HLCs Precursors (Coprecipitation Method)

0.2 g of the reduced Ni supported catalysts were dispersed in an aqueous 0.05 ML^{-1} TA solution, whose pH was previously adjusted to 5.1 using NaOH, for 1 hr at 100°C. The catalytic properties of the chirally modified materials were tested in the asymmetric hydrogenation of MAA to MHB. This reaction has been widely used as model reaction because of its simplicity. The initial catalytic test was similar to the method used by Keane and Webb.[107] H_2 (1 bar) was bubbled through the substrate/catalyst at 100°C. Different solvents such as THF, methanol, and *n*-butanol, were used. The catalyst/substrate ratio was varied too. The reactions were carried out for several hours, taking aliquots at different time intervals, and analysed by GC/HPLC. No conversion was observed under these conditions. Therefore, higher H_2 pressure (10 bar) was tried using autoclaves (Parr). Details are given in Section 3.4.3.

The results of the catalytic tests of the series Ni/Mg/Al and Ni/Zn/Al are presented in Tables 3.5.4.1.1 and 3.5.4.1.2, respectively.

Material	Activity(%)[a]	e.e. (%)
$Ni_{67}Al_{33}$	89	12
$Ni_{67}Al_{33}{}^{b}$	69	10
$Ni_{67}Al_{33}{}^{c}$	75	11
$Ni_{50}Mg_{17}Al_{33}$	77	0
$Ni_{50}Mg_{17}Al_{33}{}^{b}$	89	0
$Ni_{50}Mg_{17}Al_{33}{}^{c}$	62	0
$Ni_{35}Mg_{32}Al_{33}$	78	0
$Ni_{35}Mg_{32}Al_{33}{}^{b}$	57	0
$Ni_{35}Mg_{32}Al_{33}{}^{c}$	55	0
$Ni_{20}Mg_{47}Al_{33}$	43	0
$Ni_{20}Mg_{47}Al_{33}{}^{b}$	38	0
$Ni_{20}Mg_{47}Al_{33}{}^{c}$	35	0

Table 3.5.4.1.1: Catalytic properties of the catalysts obtained from HLCs precursors prepared by coprecipitation (Ni/Mg/Al series). [a]At 48 hrs of reaction. [b]Hydrothermally treated at 110°C for 24 hrs. [c]Hydrothermally treated at 110°C for 48 hrs.

Material	Activity(%)[a]	e.e. (%)
$Ni_{67}Al_{33}$	89	12
$Ni_{67}Al_{33}{}^{b}$	69	10
$Ni_{67}Al_{33}{}^{c}$	75	11
$Ni_{50}Zn_{17}Al_{33}$	68	0
$Ni_{50}Zn_{17}Al_{33}{}^{b}$	76	0
$Ni_{50}Zn_{17}Al_{33}{}^{c}$	75	0
$Ni_{35}Zn_{32}Al_{33}$	78	0
$Ni_{35}Zn_{32}Al_{33}{}^{b}$	57	0
$Ni_{35}Zn_{32}Al_{33}{}^{c}$	54	0
$Ni_{20}Zn_{47}Al_{33}$	43	0
$Ni_{20}Zn_{47}Al_{33}{}^{b}$	33	0
$Ni_{20}Zn_{47}Al_{33}{}^{c}$	44	0

Table 3.5.4.1.2: Catalytic properties of the catalysts obtained from HLCs precursors prepared by coprecipitation (Ni/Zn/Al series). [a]At 48 hrs of reaction. [b]Hydrothermally treated at 110°C for 24 hrs. [c]Hydrothermally treated at 110°C for 48 hrs.

The only useful catalyst in this series was the takovite-like material. Neither Mg nor Zn contributed to the enantiodifferentiation ability of the materials.

The results of the catalytic properties of the series Ni/Fe are shown in Table 3.5.4.1.3.

Material (initial formula)	Activity (%)	e.e. (R) (%)
$Ni_{67}Fe_{33}$	90	43
$Ni_{50}Mg_{17}Fe_{33}$	74	20
$Ni_{50}Zn_{17}Fe_{33}$	57	15

Table 3.5.4.1.3: Catalytic properties of the materials of the series Ni/Mg (or Zn)/Fe modified with D-TA.

From Table 3.5.4.1.3, the effect of Mg, Zn and Fe on the catalytic properties of TA-Ni can be seen. In general, all of the materials of the Ni/Fe series exhibited enantiodifferentiation ability. Moreover, incorporating Mg or Zn in the structure of Ni/Fe led to a diminution in activity and enantioselectivity. The combination of Zn with Fe as a support of TA-Ni results in a catalyst with the worst catalytic properties in the whole series. In addition, replacing L-TA for D-TA during chiral modification resulted in catalysts showing exactly the same values of activity and e.e., although towards MHB(S) (Table 3.5.4.1.4).

Material (initial formula)	Activity (%)	e.e. (S) (%)
$Ni_{67}Fe_{33}$	89	44
$Ni_{50}Mg_{17}Fe_{33}$	72	20
$Ni_{50}Zn_{17}Fe_{33}$	58	15

Table 3.5.4.1.4: Catalytic properties of the materials of the series Ni/Mg (or Zn)/Fe modified with L-TA.

The beneficial effect of Fe is not surprising at all as Fe has been used already in supports of TA-Ni (Ni-Fe-Al$_2$O$_3$ and Ni-Fe-SiO$_2$).[110] For those, the addition of about 10% Fe to Ni resulted in the most effective catalyst.

Results of the catalytic properties of the series Ni/Mg/Cr are shown in Table 3.5.4.1.5.

Material	Activity(%)	e.e.(%)
Ni$_{67}$Cr$_{33}$	99	36
Ni$_{50}$Mg$_{25}$Cr$_{25}$	87	0
Ni$_{35}$Mg$_{50}$Cr$_{25}$	67	0
Ni$_{25}$Mg$_{50}$Cr$_{25}$	52	0

Table 3.5.4.1.5: Catalytic properties of the materials of the series Ni/Mg/Cr.

The combination of Ni/Mg/Cr was not successful for the designing of a useful catalyst in the reaction of interest. However, the material with starting formulation Ni$_{67}$Cr$_{33}$ resulted in a material with good enantiodifferentiation ability.

Therefore, enantioselectivity on materials supported on a single oxide follows the trend Fe > Cr > Al. This shows that the nature of the cation constituting the support plays a central function in the catalytic properties of the active phase. Furthermore, if we do a simple comparison between Ni particles sizes of Ni/Al and Ni/Cr we will see that even though they are roughly of the same magnitude (27 and 28 nm, respectively), their enantioselective properties differ by a factor of ca. 3. These

findings defend the point that the nature of the cation constituting the support is very important in the design of an enantioselective catalyst and that enantioselectivity must not to be seen to merely depend upon the Ni particle size.

For comparison purposes, a TA-RaNi catalyst was prepared using the same method as Kukula et al.,[81] and tested under the same conditions used in our studies. The resulting catalyst showed a 100% activity and 20% e.e. in the reaction of interest. When NaBr was used during the chiral modification, e.e. was enhanced to 30%. The use of NaBr during modification is discussed in Section 3.5.4.2.1.

3.5.4.2 Catalysts Prepared from HLCs Precursors (Hydrolysis of Urea)

The catalytic properties of the materials prepared by hydrolysis of urea for both series, Ni/Mg/Al and Ni/Zn/Al, are shown in Tables 3.5.4.2.1 and 3.5.4.2.2, respectively. From them, it can be noticed that all of the materials exhibited enantiodifferentiation ability.

Ni/Mg ratio Al = 0.33	MHB$_{Conv}$ (%)	e.e. (R) (%)
∞	96.8	11.7
2.94	83.0	10.9
1.09	88.8	5.3
0.42	48.0	1.7

Table 3.5.4.2.1: Catalytic properties of the series of materials Ni/Mg/Al.

Ni/Zn ratio Al = 0.33	MHB$_{Conv}$ (%)	e.e. (R) (%)
2.94	58.0	17.3
1.09	50.5	18.6
0.42	51.4	19.4

Table 3.5.4.2.2: Catalytic properties of the series of materials Ni/Zn/Al.

From Table 3.5.4.2.1 it can be seen that in general both activity and enantioselectivity of the series Ni/Mg/Al decreases as Mg is incorporated into the materials. The variation in the tendency is presented by the material with Ni/Mg ratio equal to 1.09 which shows higher activity than the materials with Ni/Mg ratios equal to 2.94 and 0.42. Enantioselectivity fell from 11.7 to 1.7% as the amount of Mg increased in the catalysts.

Table 3.5.4.2.2 shows that as the amount of Zn increases in the materials the activity of the catalyst diminishes. However, enantioselectivity is enhanced with the increase in the amount of Zn. The sample containing the highest concentration of Zn shows the maximum e.e. value (19.4%). In general, the replacement of Zn by Mg in the materials leads to less active, but more enantioselective, catalysts.

3.5.4.2.1 Effect of the Addition of NaBr During Chiral Modification

It is argued in the literature that TA-Ni systems exhibit two types of active site: selective and nonselective.[60, 102, 103] Selective sites are associated with the chiral

molecule attached to the Ni surface, and these sites would produce the optically active product. The non-selective sites are attributed to residual Al (for RaNi-Al precursors) and to bare metal. In order to eliminate non-selective sites, the use of a co-modifier has been proposed and NaBr has proved to be the most effective salt.[104] This salt does not possess any enantiodifferentiation ability itself and it is believed that the non-enantioselective sites are blocked by the salt. The evidence is that enantioselectivity increased during catalysis when using it.[66] The materials of the last series were modified again using NaBr as a co-modifier and tested in the hydrogenation reaction under the same conditions. The catalytic properties of the materials are shown in Tables 3.5.4.2.1.1 and 3.5.4.2.1.2.

Ni/Mg ratio Al = 0.33	MHB_{Conv} (%)	e.e. (R) (%)
∞	66.4	18.9
2.94	83.6	9.2
1.09	83.3	2.9
0.42	40.2	2.4

Table 3.5.4.2.1.1: Catalytic properties of the materials Ni/Mg/Al using NaBr as a co-modifier.

Ni/Zn ratio Al = 0.33	MHB$_{Conv}$ (%)	e.e. (R) (%)
2.94	60.6	23.4
1.09	61.3	10.6
0.42	41.5	6.4

Table 3.5.4.2.1.2: Catalytic properties of the materials Ni/Zn/Al using NaBr as a co-modifier.

Using NaBr during the modification improved the enantioselectivity ability of the takovite-like material by 62%. However, its activity decreased by 31%. For the series Ni/Mg/Al, the activity remained almost the same, but enantioselectivity decreased. The exception was the material with Ni/Mg ratio equal to 0.42 which e.e. improved by ~30%. Two possible effects could be taking place during chiral modification with the addition of the salt. First of all, NaBr is indeed blocking non-enantioselective sites, which is mirrored in the increase of e.e. and the consequent decrease on activity for the catalysts obtained from Ni$_{67}$Al$_{33}$ and Ni$_{20}$Mg$_{47}$Al$_{33}$ precursors (Figures 3.5.4.2.1 and 3.5.4.2.1.1). At the same time NaBr could be competing with TA for space at the Ni metal surface and therefore the area available for the creation of enantioselective sites is reduced; this effect is observed in the decrease of e.e. presented for the materials prepared from Ni$_{50}$Mg$_{17}$Al$_{33}$ and Ni$_{35}$Mg$_{32}$Al$_{33}$ precursors (Figures 3.5.4.2.1 and 3.5.4.2.1.1).

Moreover, NaBr affected e.e. of the series Ni/Zn/Al. The material with Ni/Zn ratio equal to 2.94 was improved by 26%. For the rest of the series, NaBr had an unusual effect on e.e. For the material Ni/Zn = 1.09, activity increased but enantioselectivity decreased. The most enantioselective catalyst became the least enantioselective

e.g. the e.e. of Ni/Zn = 0.42 decreased by two thirds (Figures 3.5.4.2.1 and 3.5.4.2.1.1). The same theory as described above regarding the role of NaBr during modification could apply here as well.

3.5.5 Effects of pH of Modification on the Uptake of TA and on Ni Leaching

The crucial factor to attain high optical yields in the enantioselective hydrogenation of MAA is the modification process. As enantioselectivity is directly linked to the attachment of TA onto the Ni surface, it is imperative to delineate the surface environment in real systems to relate it to catalytic performance. But, apart from the work of Keane et al.,[107] there are no correlations between the amount of TA adsorbed onto Ni and the optical activity attained with the results obtained so far. Moreover, Ni leaching from supported systems has been studied previously.[104, 107] In those studies, it is concluded that Ni leaching leads to a disadvantageous performance of the solid during catalysis. Furthermore, in the same studies it has been found that Ni leaching increases with the severity of the modification conditions (usually high TA concentrations and temperature).

We have researched both TA uptake and Ni leaching on a takovite-like material, by varying pH during chiral modification. The reaction took place at 100°C and an initial TA concentration of 0.05 ML^{-1} was used. The results are presented in Figure 3.5.5.1, which shows that the number of TA molecules adsorbed on the catalyst decreases proportionally with increasing pH up to a pH of 9 and shows a slight increase from there to the value of 13.
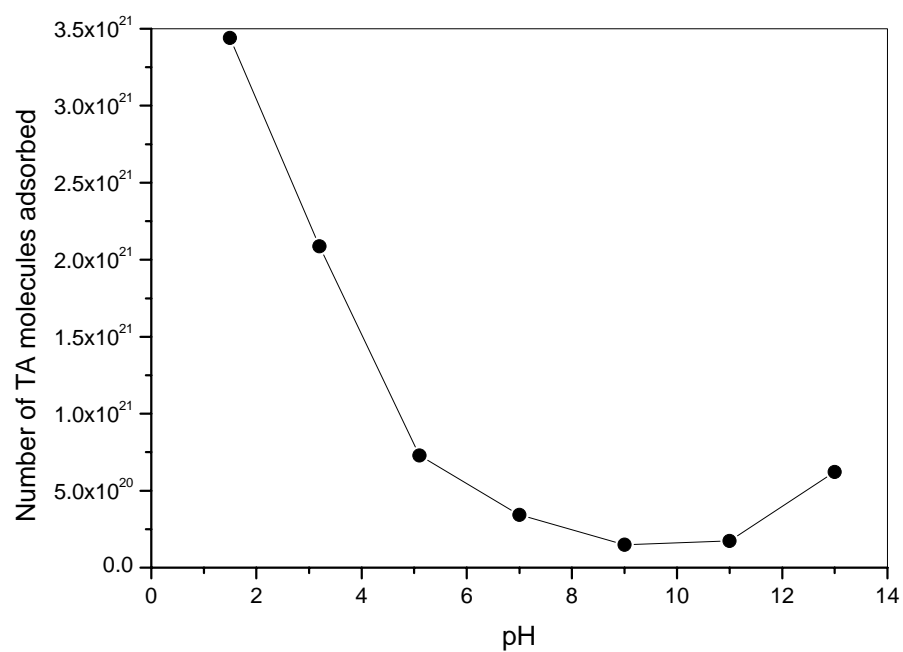
Figure 3.5.5.1: TA absorption with respect to pH of modification on a takovite-like material.

Figure 3.5.5.2 shows Ni leaching from the takovite-like material with respect to pH of modification.
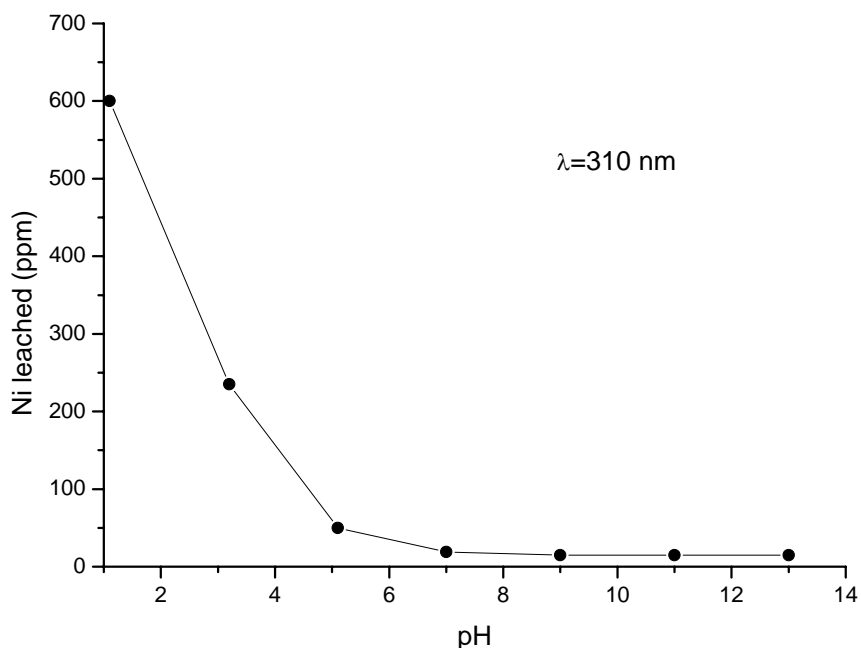
Figure 3.5.5.2: Ni leaching with respect to pH of modification on a takovite-like material.

From Figure 3.5.5.2, it can be seen that the most drastic effects are observed at acidic pHs. At neutral and basic pH, Ni leaching is controlled to a minimal value (~15 ppm). These results are in agreement with those obtained on Ni/SiO$_2$ materials reported by Keane et al.[107]

Therefore, from these last results it is clear that pH has a remarkable effect on TA uptake and Ni leaching. However, even though the surface features of the solid change as we vary TA concentration and pH during modification, enantioselectivity remained the same (See Tables 3.5.3.2.2 and 3.5.3.3.1).

3.5.5.1 Studies of Postmodifier Solutions Materials Prepared by Coprecipitation

Results of the analysis of the postmodifier solutions of the catalysts that presented enantiodifferentiation ability are shown in Table 3.5.5.1.1.

Material (initial formula)	TA$_{adsorbed}$ (molecules)	Ni$_{leached}$ (ppm)
Ni$_{67}$Fe$_{33}$	1.5×10^{22}	60
Ni$_{50}$Mg$_{17}$Fe$_{33}$	1.2×10^{22}	4
Ni$_{50}$Zn$_{17}$Fe$_{33}$	5.6×10^{21}	13
Ni$_{67}$Cr$_{33}$	2.1×10^{21}	33

Table 3.5.5.1.1: TA adsorbed and Ni leaching for materials of the series Ni/Mg (or Zn)/Fe and Ni/Cr.

From Table 3.5.5.1.1 it can be seen that the uptake of TA is higher for the material containing Ni/Fe = 2. This material also shows the highest Ni leaching compared to the rest of the series. For Ni/Mg = 2.94, TA uptake is higher than for Ni/Zn = 2.94, but Ni leaching of the latter is higher than that of the former.

Ni/Cr = 2 shows lower TA adsorption in comparison to the Ni/Fe series but more Ni was leached out from its surface in comparison to the materials containing Ni/Mg/Fe or Ni/Zn/Fe.

If we relate the surface environment of the materials to their catalytic properties, we will notice that the addition of Mg abated Ni leaching when introduced into the Ni/Fe material. Moreover, Ni/Fe and Ni/Mg/Fe adsorb TA in the same order of

magnitude. However, the e.e. found for the TA-Ni/Fe catalyst is bigger than that of TA-Ni/Mg/Fe (Table 3.5.4.1.4). It is possible that small Ni particles contributing to non-enantioselective sites could be kept on the material Ni/Mg/Fe as Ni leaching was decreased. With regard to the material containing Zn, TA adsorption was one order of magnitude lower than the rest of the materials in this series, which mirrored poorer results. However, even though TA adsorption of Ni/Cr is of the same order than the Ni/Zn/Fe, the Ni/Cr system shows better catalytic properties than the latter.

3.5.5.2 Studies of Postmodifier Solutions Materials Prepared by Urea

Results of TA adsorbed onto and Ni leached out from surface for both series Ni/Mg/Al and Ni/Zn/Al are shown in Tables 3.5.5.2.1 and 3.5.5.2.2, respectively. It can be noticed that for Ni/Mg/Al series, there is a direct correlation between the amount of Mg in the solid and the amount of molecules of TA adsorbed onto them. There is a factor of ca. four times greater the number of molecules adsorbed onto the material with Ni/Mg ratio equal to 0.42 in comparison to the rest of the series. With regard to the amount of Ni present in the solutions after modification, the material with Ni/Mg ratio equal to 0.42 presented less Ni leaching in comparison to the rest of the series, followed by the material with Ni/Mg ratio equal to 1.09. The material with Ni/Mg ratio equal to 2.94 presents a Ni leaching factor of five and ca. three times in comparison to Ni/Mg = 0.42 and Ni/Mg = 1.09, respectively. From these results we can conclude that for this series of materials the more Mg present in the structure, the more TA molecules were adsorbed onto the catalyst and the less Ni was leached out from their surfaces.

Ni/Mg ratio (Al = 0.33)	TA adsorbed (10^{21} molecules)	Ni leached (ppm)
2.94	2.32	150
1.09	2.48	38
0.42	9.57	30

Table 3.5.5.2.1: TA adsorbed onto and Ni leached out from the surface of the catalyst. Series Ni/Mg/Al prepared by hydrolysis of urea.

Ni/Zn ratio (Al = 0.33)	TA adsorbed (10^{21} molecules)	Ni leached (ppm)
2.94	5.38	112.4
1.09	3.09	231.6
0.42	3.49	206.4

Table 3.5.5.2.2: TA adsorbed onto and Ni leached out from the surface of the catalyst. Series Ni/Zn/Al prepared by hydrolysis of urea.

For the series Ni/Zn/Al, there is no direct relation between the amounts of TA adsorbed and Ni leached. However, the material with less zinc in its structure adsorbs more TA than the rest of the series. This material presents less Ni leaching (by a factor of ca. 2) in contrast to the rest of the materials in the series. For the materials with Ni/Zn ratio equal to 1.09 and 0.42, Ni leaching is considerably higher than that to their analogous materials of the Ni/Mg/Al series Tables 3.5.5.2.1 and 3.5.5.2.2)

Results of TA uptake and Ni leaching of both series of materials modified using NaBr as co-modifier are presented in Tables 3.5.5.2.3 and 3.5.5.2.4, respectively.

Ni/Mg ratio (Al = 0.33)	TA adsorbed (10^{21} molecules)	Ni leached (ppm)
2.94	3.54	60
1.09	3.15	30
0.42	4.68	20

Table 3.5.5.2.3: TA adsorbed onto and Ni leached from the surface of the catalyst. Series Ni/Mg/Al prepared by hydrolysis of urea modified using NaBr as a co-modifier.

Ni/Zn ratio (Al = 0.33)	TA adsorbed (10^{21} molecules)	Ni leached (ppm)
2.94	0.57	147.6
1.09	1.60	57.4
0.42	1.60	72.2

Table 3.5.5.2.4: TA adsorbed onto and Ni leached from the surface of the catalyst. Series Ni/Zn/Al prepared by hydrolysis of urea modified using NaBr as a co-modifier.

A similar trend is seen for the Ni/Mg/Al series when NaBr was added to the solutions during modification; that is, the material with a higher proportion of Mg in its structure adsorbed more TA and presented less Ni leaching (Table 3.5.5.2.3). The uptake of TA was higher for the materials with Ni/Mg ratio equal to 2.94 and 1.09. However, TA uptake was lower (by approximately a factor of two) for the material

with Ni/Mg ratio equal to 0.42. In general, Ni leaching was decreased when using NaBr. The most remarkable effect took place on Ni/Mg = 2.94 in which Ni leaching was diminished by a factor of 2.5.

From Table 3.5.5.2.3, the amount of TA adsorbed in the series Ni/Zn/Al is lower when NaBr was used as a co-modifier (by a factor of ca. 10 for the material with Ni/Zn ratio equal to 2.94 and by a factor of ca. 2 for the materials with Ni/Zn ratio equal to 1.09 and 0.42, respectively). Moreover, Ni leaching was diminished when using NaBr, the material with Ni/Zn ratio equal to 2.94 being the exception. This material presented a rise in Ni leaching.

In general for both series: the material showing the highest TA adsorption is the material which leaches the least Ni.

According to Bostelaar and Sachtler,[99] NaBr lowers the solubility of adsorbed species resulting in an increased stability of the surface complexed Ni. This is supported by Kukula et al.,[81] who speculated that the use of a salt would lower the possibility for Ni and its compounds to leach from the surface. From our results, the use of NaBr during the modification procedure lowered Ni leaching, except for the material with starting formula Ni/Zn = 2.94 (Tables 3.5.5.2.1-4) which showed a rise in Ni leaching. The enantiodifferentiation abilities of that and of the takovite-like material were improved as expected (Tables 3.5.4.2.2 and 3.5.4.2.1.2). Nevertheless, for the rest of the materials, e.e. was lowered when NaBr was used.

On the other hand, TA uptake had an interesting effect in enantioselectivity in each series. The materials with more TA were the less enantioselective from their respective series. The relation between the amount of TA adsorbed in a catalyst and

e.e. during hydrogenation has been explained in terms of surface coverage.[124, 125] For Ni-TA/SiO$_2$ systems, it is believed that there is an optimum surface coverage.[107, 108] The optimum amount of TA on the surface should assure a large enough distance between TA molecules to allow adsorbed MAA interact with only one modifier molecule, but small enough to minimize the number of bare metal sites that give rise to racemic product (all of this is based on the surface model arrangement in which a hydrogen bond is formed between the OH group of the hydroxy acid and the methoxy oxygen atom of MAA). According to the authors, if this optimum coverage value is not met, then NaBr would not have any effect on enantioselectivity.

It is possible that small Ni particles present in the solids were leached out from the surface during the corrosive process of modification. These small Ni particles could account for the non-enantioselective sites. When using NaBr, leaching of these small particles was lowered leading to more active but less enantioselective catalysts. Despite the use of NaBr, the material Ni/Zn = 2.94 leached more Ni (presumably small particles with non-enantioselective ability) and improved the e.e in the reaction.

Previously we mentioned the debate about the influence of Ni crystal size on enantioselectivity (Section 3.5.3.1). From our results we can see that even though we have used materials with roughly the same crystal size (considering the accuracy of the method of Scherrer to estimate particle sizes), though with different Ni loading, and under the same conditions of modification, the most important factor is the influence of the support, i.e. the nature of the cations. For example, if we take both catalyst Ni/Mg = 1.09 and Ni/Zn = 1.09 for comparison, we can see that even though

they possess roughly the same Ni particle size (~24), their Ni surface environment is different (Tables 3.5.5.2.1 and 3.5.5.2.2), and under the same conditions of chiral modification and catalytic test, the material containing Mg is more active than the material containing Zn, but the latter is more enantioselective than the former. Thus it would appear that Mg cations aid in the stabilisation of Ni in the support, including smaller particles with non-enantioselective ability. The high Ni leaching presented in the Ni/Zn/Al series is beneficial for e.e. due to the potential elimination of these non-enantioselective Ni particles. On the other hand, it is possible that varying Ni loading and ratio between cations in the support, leads to a variation in Ni particle size distribution. The narrower the distribution is, the more beneficial for e.e. Moreover, leaching of small Ni particles from Ni/Zn/Al catalysts could lead to a narrower particle size distribution.

Comparison between two catalysts of the same series shows the effect of cation on e.e. that is not related to Ni particle size. Ni/Zn = 2.94 and Ni/Zn = 0.42 have roughly the same Ni particle size (20.1 and 20.5 nm, respectively). However, the environment on their surfaces is different which is mirrored in their catalytic properties (Tables 3.5.4.2.2 and 3.5.5.2.2). The most enantioselective material was the one with the highest amount of Zn. It is possible that the traces of ZnO found in the starting material, would have a positive effect in enantioselectivity (these traces were more prominent as the amount of Zn was higher in the samples).

3.6 Conclusions

From the two methods of preparation of HLCs explored, hydrolysis of urea method leads to more crystalline compounds in contrast to coprecipitation method. Moreover, for materials containing the same combinations of cations (series Ni/Mg/Al and Ni/Zn/Al), only the catalysts prepared using the hydrolysis of urea method showed enantiodifferentiation ability. In general, from the two series prepared by hydrolysis of urea, the series of Ni/Mg/Al catalysts were more active than the Ni/Zn/Al series. The activity follows a direct relation to Ni loading. The Ni/Zn/Al series showed better enantioselectivity than its counterpart.

The more active catalysts were those which were modified without using NaBr (with the exception of the Takovite and Ni/Zn = 2.94 materials) and those which show more Ni leaching in the respective series. Therefore we conclude that it is possible that small Ni particles present in the materials, which contribute to non-enantioselective sites, were leached out during chiral modification. This effect made the Ni particle size distribution narrower and therefore e.e. was enhanced.

On the other hand, the nature of the cation present in the support plays an important role in the creation of enantioselective sites when combined with Ni in the solid solution. For example, the catalytic properties of Ni-Fe and Ni-Cr catalysts are negatively affected when another cation (Zn or Mg) are included into those materials.

In summary, the use of HLCs as precursors of supported Ni to design enantioselective catalysts is a viable option due to its flexibility in the choice of cations constituting the support and because it is possible to control Ni particle size through hydrothermal/thermal processes during materials preparation. This approach

allows us to obtain reproducible materials for a better comprehension of structural studies of the catalyst.

The successful design of a catalyst must embrace then the right choice of cations and their combinations. In addition, these studies affirm that enantioselectivity is a structure sensitive phenomenon in solid catalysts and that the nature of the cation(s) constituting the support plays an important role in the catalytic properties of the material. Izumi et al.[66] have stated that some cations are not advisable for the design of these catalysts. However, more structural studies must be done in order to understand the effect of different phases present in catalysts and their synergic effects with Ni.

CHAPTER 4. OMS AS SUPPORTS OF TA-Ni CATALYSTS

4.1 Definition of OMS

OMS is the general name given to silicas with structures consisting of systems of highly ordered pores in the mesoporous size range (2-50 nm according to IUPAC).[203] These materials show outstanding characteristics such as high surface areas (around 1000 m^2g^{-1}), tailored pore sizes and very narrow pore size distribution. Their pore sizes can be adjusted by varying the chain length of the surfactant used and/or using additional molecules which act like co-surfactants.[204-209]

4.2 Applications of OMS

Due to notable features such as tailoring pore sizes and high surface areas, OMS opened new possibilities in adsorption and catalysis.[210-224] In medicine, they have found application in drug delivery.[225] The scientific stimulus they arouse is mirrored in the vast amount of papers published and in the high number of new materials that the pioneering ones (M41S family) inspired.[226-232] In particular, in liquid phase systems for the synthesis of fine chemicals, the large pores of OMS facilitate mass transfer of large molecules.[233-238]

Due to their walls resembling amorphous silica, they do not possess catalytic activity on their own. Therefore, they are often modified using different methods to disperse active sites on their high surface areas which allow a high concentration of active sites per mass of material. Modification of the silica framework can be carried out either in direct synthesis[239-247] or by a post-treatment method.[248-252] Both methods

differ in their results. While the first method allows the homogeneous incorporation of the heteroatom, using the second one leads primarily to a coating of the walls of the solid.[253] The latter is possible due to the presence of silanol groups in the walls (2-3 $Si\text{-}OH/nm^2$)[254-256] which act like anchor sites. The incorporation of heteroatoms in OMS does not lead to the formation of defined sites, but to an ample range of diverse sites. It is the local environment of the site and the nature of the precursor material which plays a crucial role during catalysis.[224]

On the other hand, incorporating complexes in the inner surfaces of OMS is a common practice to develop catalysts for asymmetric reactions.[75, 257, 258] This technique, however, can face diffusion problems in the channels of OMS when big molecules are used.[257]

The most exploitative application of OMS is, perhaps, as supports of metal and metal oxide particles.[259-271] The easiest way to deposit a metal into a support is by incipient wetness and this technique has been successfully applied to OMS.[268-270, 272-274] In particular, Ni supported materials have been found to be useful catalysts in processes such as benzene hydrogenation[268] and methanation of carbon dioxide.[274]

4.3 Methods of Preparation of OMS

Their discovery was first reported in 1969,[275] but it was not until the 90's when they caught the attention of the scientific community, with the so-called Folded Sheet mesoporous Materials (FSM-n)[276] and Mobil Composition of Matter materials (MCM-n).[204, 277] Their synthesis embraces a co-operative interaction between

surfactant molecules and silicate species which leads to an organic/inorganic mesostructured composite. Further removal of the template leads to a hollow solid silica framework structurally similar to the phase present in solution. Essentially, parameters such as the kind of surfactant and source of silica, the type of interaction between these two, their stoichiometry, pH and temperature of the mother solution, have a substantial impact on the final structure of the desired material.[204, 276-288] Consequently, there are a number of different synthetic routes that can be used to obtain them. Very recently, a non-surfactant synthesis has been reported.[289]

Mobil Composition of Matter No. 41 (MCM-41), Mobil Composition of Matter No. 48 (MCM-48) and Mobil Composition of Matter No. 50 (MCM-50) are the best known materials. Their pore systems show hexagonal (Ia3-d), cubic (P6m) and lamellar structures, respectively (Figure 4.1.1).
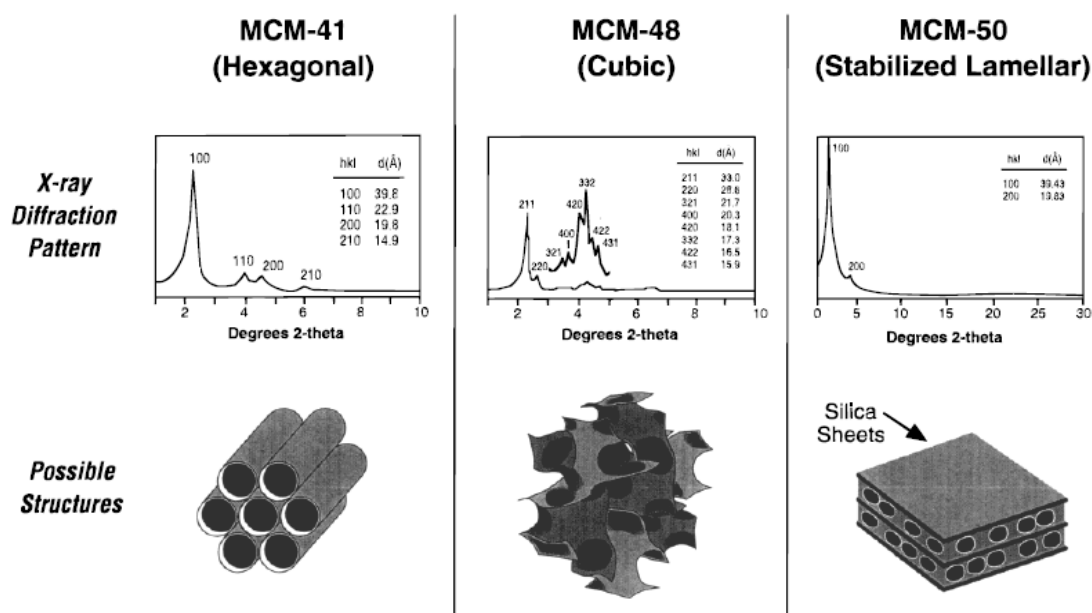
Figure 4.1.1: Powder X-ray diffraction patterns and proposed structures of MCM-41, MCM-48 and MCM-50 (Taken from[290]).

The synthesis of MCM-*n* materials has been explained in terms of a liquid-crystal approach where aggregates of surfactant molecules form a template around which silicate species condense.[204] Depending on the concentration of the surfactant in solution, the mechanism of formation can follow two pathways. At high surfactant concentrations, lyotropic mesophases with hexagonal, cubic and lamellar structures are formed prior to the addition of silicate species (the corresponding mesostructures of MCM-41, MCM-48 and MCM-50, respectively).[277] This pathway is supported by Attard et al.[279] in their True Liquid Crystal Templating mechanism.

In the second pathway, at very low surfactant concentration in solution, no micelle array is present and the addition of silicates leads to the formation of silicates-encasing surfactant micelles. Both pathways for the formation of MCM-41 are shown in Figure 4.1.2. However, even at extremely low surfactant concentration, MCM-41 can be prepared.[291]
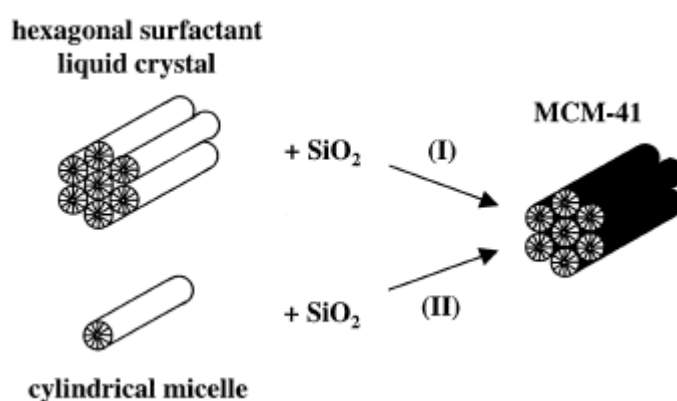
Figure 4.1.2: Proposed pathways for the formation of MCM-41. Taken from [204]

In either case, according to Stucky and co-workers,[281, 292-294] a co-operative formation mechanism allows the creation of the organic-inorganic composites based in electrostatic interactions between aggregates of surfactant molecules and silicates (Figure 4.1.3). Therefore, on the basis of this principle, the possibilities of synthesis of OMS are the following: using cationic surfactants and anionic inorganic silicate species,[204, 277, 283] anionic surfactants and cationic inorganic silicate species,[287, 288] combinations of surfactant and inorganic species mediated by a counter charge specie,[279, 281, 282] and a neutral approach where neutral or non-ionic surfactants are used.[279, 280, 282, 284-286]
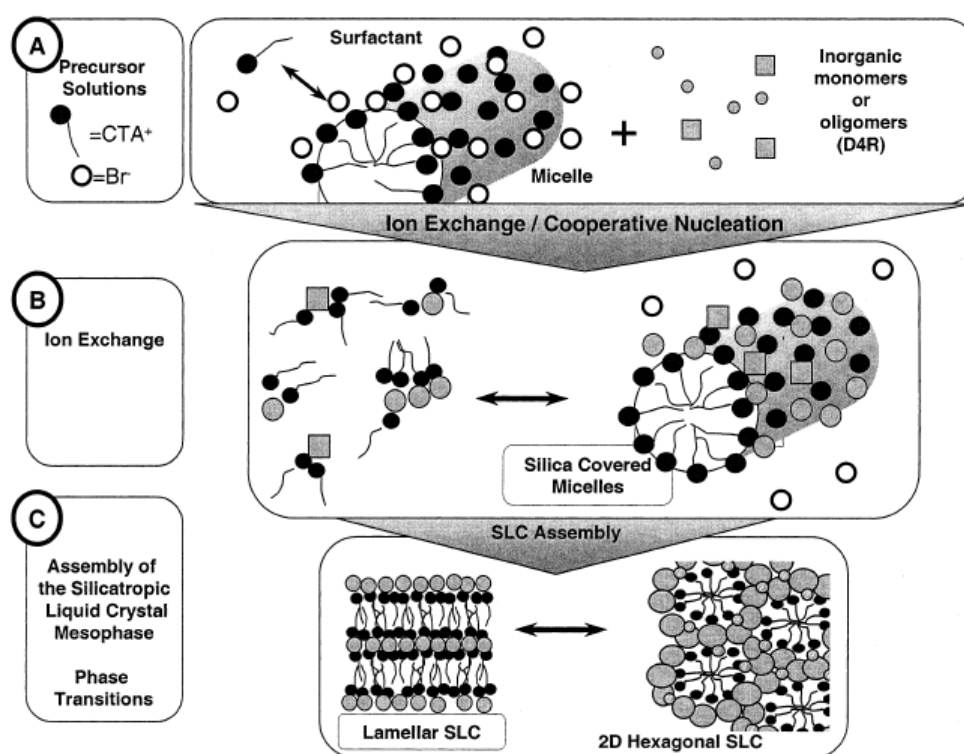
Figure 4.1.3: Pathways for the inorganic-surfactant co-operative formation mechanism. (Taken from[293]).

An alternative synthesis pathway, the so-called Folded Sheet Mechanism, was proposed for the synthesis of FSM-16.[295, 296] It is believed that in this mechanism, the organic-inorganic composite is formed by intercalation of the layers of kanemite with surfactant molecules. The transformation to the hexagonal mesophase takes place during hydrothermal treatments where the silanol groups condense.

It is possible to control the particle morphology of these materials. For example, hollow-tubular MCM-41,[297, 298] almost perfectly spherical MCM-41,[299] and spherical particles of MCM-48,[300] have been synthesised. In particular, spherical MCM-41 has found application as support material in enantioselective HPLC.[301]

On the other hand, a few years after M41S materials were disclosed, another family of OMS was developed in Santa Barbara University. Since then, the so called SBA-n materials have been the centre of much research in the last decades.[281, 285, 286] Of particular interest is the study of one member of this family: SBA-2.[281]

The three dimensional pore network of SBA-2 consists of spherical cages (rather than channels of uniform dimensions, in the case of MCM-41) arranged in a hexagonal close-packed configuration (hcp) array (with symmetry $P6_3/mmc$) and connected by channels.[302] It has been found in SBA-2 that the structure possesses disordered polytypic stacking sequences and also regions of a cubic close packed (ccp) phase.[303] In addition, the non-uniform channels connecting the neighbouring cages are much smaller than the diameter of the cage.[304-306] SBA-2 shows three particle morphologies: small solid spheres, plates, and larger hollow spheres.[304, 307]

4.4 Experimental

4.4.1 Preparation of Materials

4.4.1.1 Synthesis of MCM-41

MCM-41 was prepared according to the method of Cai et al.[291] 207 mL of aqueous NH_4OH (28-30%) were mixed up to 270 mL of deionised water. 2 g of CTAB were added to the solution under stirring, the solution was heated up to 40°C and then 5 mL of TEOS were added dropwise. The solution was kept at these conditions for 2 hrs. The product was filtered, washed with distilled water and dried at room temperature.

4.4.1.2 Synthesis of MCM-48

The synthesis of MCM-48 was carried out according to the method of Schumacher et al.[300, 308] 2.4 g of CTAB were dissolved in 100 mL of deionised water and 50 mL of ethanol. 12 mL of aqueous ammonium hydroxide were added to the solution. The solution was stirred and 3.65 mL of TEOS were added. The solution was further stirred for 5 hrs at room temperature. The solid was filtered, washed with distilled water and dried at room temperature.

4.4.1.3 Synthesis of SBA-2

Molecular sieve SBA-2 was synthesised following the procedure described by Huo et al.[294] The two-headed Gemini surfactant C16-3-1 (see synthesis below),

distilled water and tetramethylammonium hydroxide (25% in water), were mixed in the following molar ratios: 0.05 C16-3-1 : 0.5 TMAOH : 150 H_2O and stirred for 30 minutes at room temperature. Then, 1 mol of TEOS was added to the solution dropwise. The pH was adjusted to 11 by adding hydrochloric acid to the solution (37%). After 5 minutes the formation of a white precipitate was observed and the mixture was stirred for a further 4 hours. The precipitate was aged in an oven at 100°C for 1 hour. The solution was filtered and the precipitate was washed with deionised water. Finally, the solid was dried in an oven at 160°C for 4 hours.

4.4.1.4 Synthesis of Gemini Quaternary Ammonium Surfactant (C16-3-1)

The double headed gemini surfactant was synthesised by the equimolar reaction between (3-bromopropyl)trimethylammonium bromide (BPTMA) and dimethylhexadecylamine (DMHDA) in ethanol under stirring and reflux for 48 hours. After solvent extraction using a rotary evaporator, the remaining white solid was purified by dissolution using a minimum amount of ethanol followed by the slow addition of ethyl acetate until a white precipitate was observed. This white precipitate was recovered by filtration and dried at room temperature overnight.

4.4.1.5 Template Removal

For all of the OMS, the respective template was removed from the material by calcination at 550°C in flowing nitrogen and oxygen (1 and 7 hrs, respectively).

4.4.2 Characterisation of Materials

There is no single technique which tell us about the quality of OMS, that is the reason why XRD, nitrogen physisorption and electron microscopies are used together to fully characterise this kind of material.

4.4.2.1 Low Angle Powder XRD

Low angle powder XRD was used to characterise the solids using a Bruker D8 X-ray diffractometer using Cu-K$_{\alpha 1}$ radiation, λ = 1.54056 Å (40 kV and 30 mA), at steps of 0.020 degrees.

4.4.2.2 Nitrogen Physisorption

Nitrogen adsorption-desorption isotherms were determined at -196.6°C using an Autosorb-1C static volumetric instrument from Quanta Chrome. Prior to measurement the samples were degassed at 200°C in vacuum for prolonged times. Surface areas were determined using the Brunauer, Emmet and Teller model.[142] Pore size and pore size distribution were calculated from the desorption isotherm using the Barret, Joyner and Halenda (BJH) method.[144]

4.4.3 Incorporation of Ni into OMS

4.4.3.1 Incorporation of Ni from Solution

The OMS were impregnated by incipient wetness with an aqueous solution containing nickel citrate (Ni-Ci), which was prepared by reaction of nickel carbonate and citric acid (molar ratio 3 : 2), to give 10 wt.% Ni in the solid.[273] After impregnation, the catalyst was dried at 120°C for 17 hrs in an oven and calcined in flowing oxygen at 450°C for 4 hrs. The solid was reduced in 10% H_2 (in N_2) at 600°C for 6 hrs. A heating rate of 10°C min^{-1} was used in both thermal treatments.

4.4.3.2 Incorporation of Ni by Solid State Reaction

For this technique, both mesoporous silica and nickel precursor (Ni ACAC) were mixed together and ground using a mortar and pestle. The amount of Ni ACAC used was calculated to give 40 wt.% Ni in the solid. The mixture was then pressed to form a pellet. The pellet was reduced in flowing 10% H_2 (in N_2) at 500°C. This technique is an adaptation from the one used by Osawa et al.[111] on aluminas.

4.4.4 Chiral Modification of Ni Supported on OMS

The OMS supported Ni catalysts were dispersed in an aqueous TA solution under stirring and reflux for one hour. Details of the conditions of reaction are given throughout Section 4.5. After cooling down, the materials were washed with

deionised water (1 x 50 cm^3), methanol (2 x 50 cm^3), and the solvent used in the hydrogenation (1 x 50 cm^3), using a centrifuge.

4.4.5 Hydrogenation of MAA

The hydrogenation of MAA (2 mL) over the obtained catalyst (0.1 g) was carried out in a Parr batch reactor at 100°C under stirring for 48 hours. The initial hydrogen pressure was 10 bar and methanol was used as a solvent. Once hydrogenation was completed, the catalyst was recovered from the solution and the product of reaction was analyzed by means of HPLC. The column used was a ChiralPak AD with amylase tris-(3,5-dimethylphenylcarbonate) coated on silica-gel (250 x 4.6 mm). The mobile phase was 1% IPA in hexane. Detection of the species was carried out by means of UV at λ = 210 nm.

4.5 Results and Discussions

4.5.1 Low Angle Powder XRD

4.5.1.1 Pure Materials

Low angle XRD patterns of fresh and calcined materials are shown in Figures 4.5.1.1.1-3. All of the materials present reflections between 2 and 7° at 2θ Bragg degrees, which are characteristic of OMS. At low angle, the materials show basal reflection peaks of very high intensity and well resolved peaks of higher order which

indicates the long range order of the mesopores. As OMS are not crystalline at atomic level, reflections at higher angles cannot be seen.

For MCM-41, it has been reported that the use of surfactant with carbon chain of 12, 14 and 16 leads to a material with up to five well indexed reflections at low angle, that is, the *hk0* reflections of a hexagonal reticule (100, 110, 200, 210 and 300). In our case using CTAB led to a material showing 4 reflections at low angle (Figure 4.5.1.1.1).

On the other hand, the powder X-ray diffraction patterns of the MCM-48 material feature distinct Bragg peaks in the range $2\theta = 2\text{-}7°$, characteristic of this type of material (Figure 4.5.1.1.2). Figure 4.5.1.1.3 depicts the characteristic XRD pattern of SBA-2.

After calcination in flowing O_2, all of the materials were examined by XRD. Their X-ray diffraction patterns are shown in the corresponding figure for comparison.
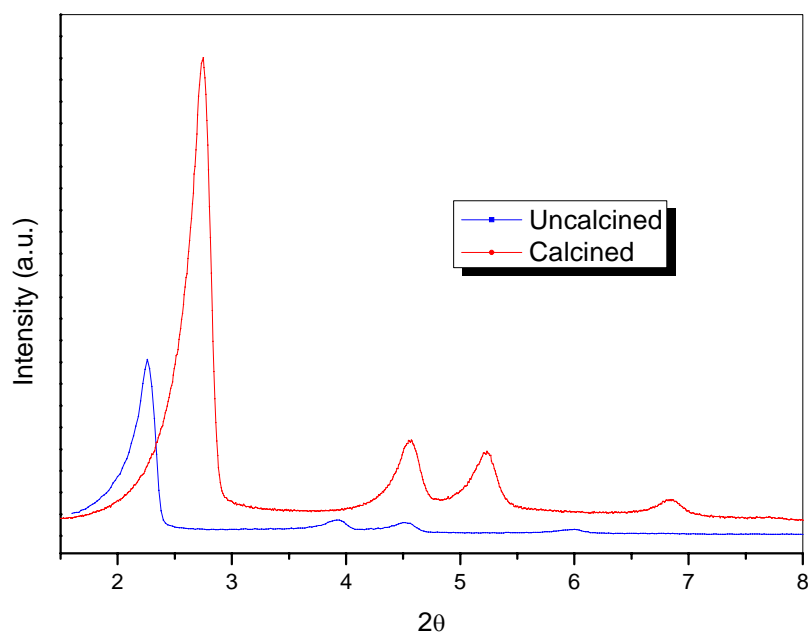
Figure 4.5.1.1.1: Low angle powder XRD patterns of MCM-41.
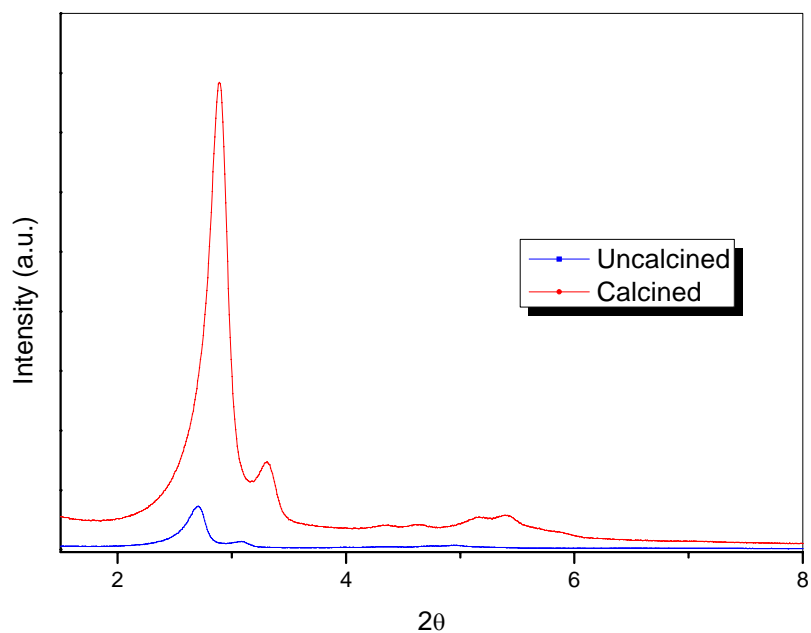
Figure 4.5.1.1.2: Low angle powder XRD patterns of MCM-48.
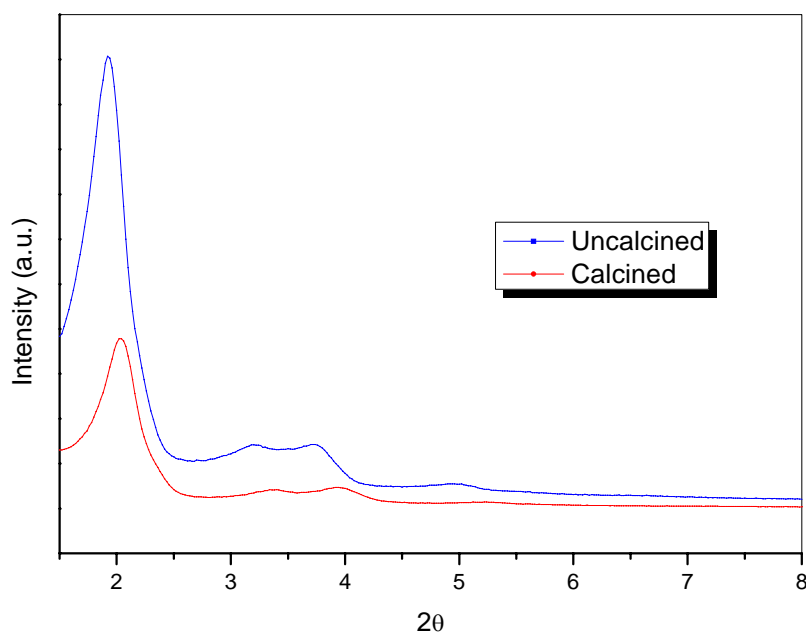
Figure 4.5.1.1.3: Low angle powder XRD patterns of SBA-2.

In general, removing the corresponding template leads to a change in intensity of the XRD patterns of the materials. In the case of MCM-41 and MCM-48, the peaks become more intense (Figures 4.5.1.1.1 and 4.5.1.1.2). On the contrary, the intensity of the XRD pattern of SBA-2 decreased after calcination (Figure 4.5.1.1.3). In general, the first peak shifts towards higher 2θ value after calcination. The values are given in table 4.5.1.1.1 These values correspond to the distance from the centre of one pore to the other. If we would rest the thickness of the wall to these values, the pore size could be estimated. The reduction in size of the d_{100} value indicates the shrinking of the structure because of the template elimination.

171

Material	distance* (nm)[a]	distance** (nm)[a]
MCM-41	4.01	3.32
MCM-48	3.92	3.44
SBA-2	4.63	4.34

Table 4.5.1.1.1: Distances between mesopores in the OMS, estimated using the first low angle XRD peak values. *Uncalcined. **Calcined. [a]The error in measuring the width at half height is 0.125°. Ni crystallite size calculation error is about ±5%.

4.5.1.2 Materials containing Ni incorporated from solution

After impregnation with Ni-Ci, the materials were calcined and scanned by XRD. The results are shown in Figures 4.5.1.2.1-3.
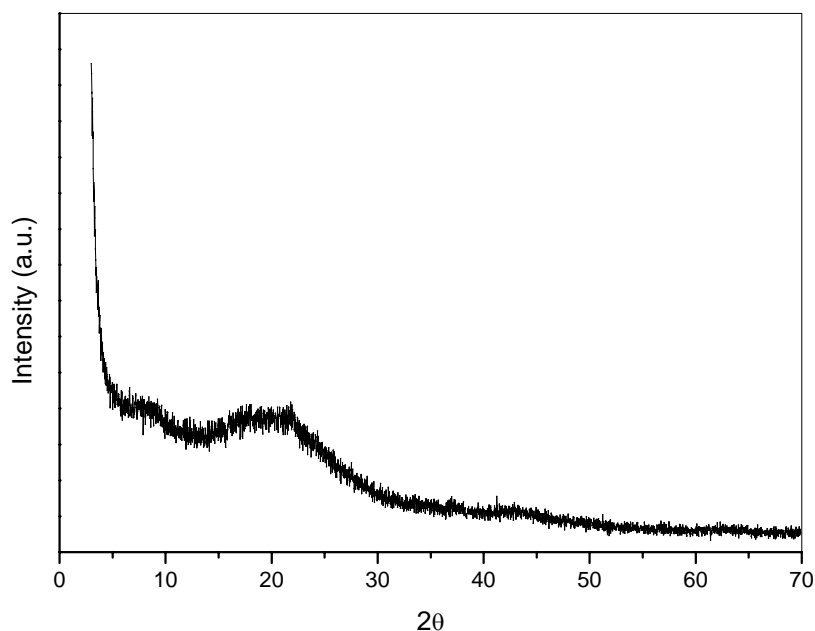
Figure 4.5.1.2.1: Powder XRD pattern of NiO/MCM-41.
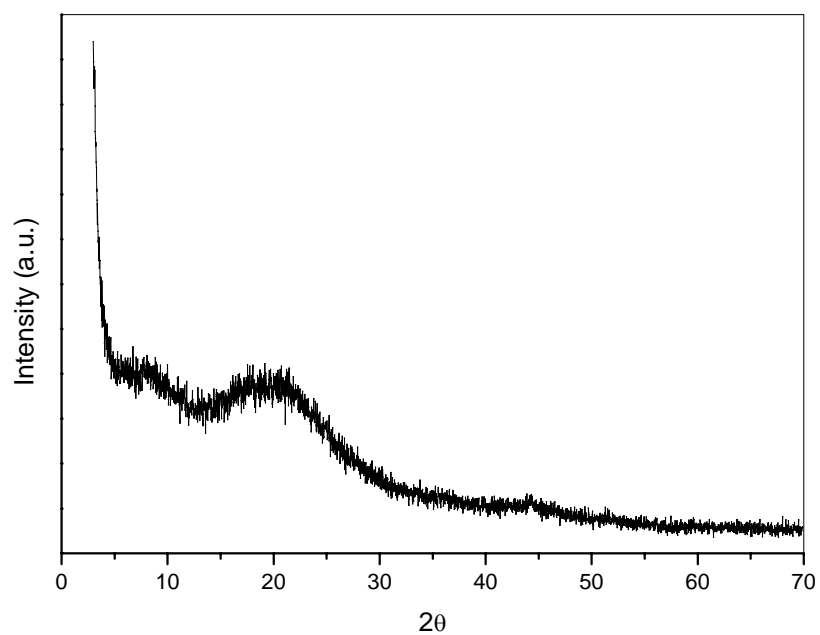
Figure 4.5.1.2.2: Powder XRD pattern of NiO/MCM-48.
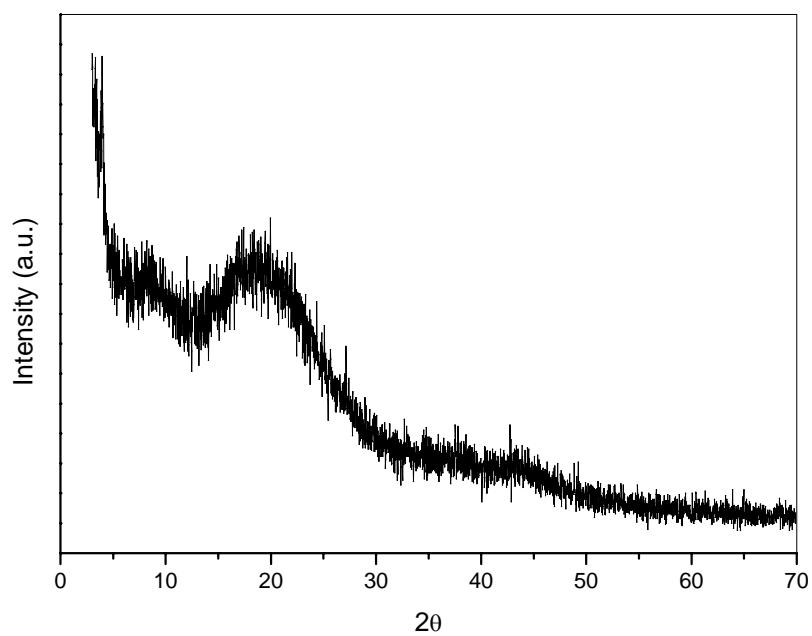
Figure 4.5.1.2.3: Powder XRD pattern of NiO/SBA-2.

The last three (Figures 4.5.1.2.1-3) do not display the characteristic XRD patterns of nickel oxide. This could indicate the formation of very small nickel oxide particles which are well dispersed in the OMS. Similar presumptions were made by Lensveld et al.[273]

After reduction in flowing 10% H_2 (in nitrogen), the materials were scanned again by powder XRD and the characteristic peaks of metallic nickel were observed (Figures 4.5.1.2.4-6). It is not possible to tell from the patterns if the mesostructure was retained after reduction. It is possible that the structure collapsed.
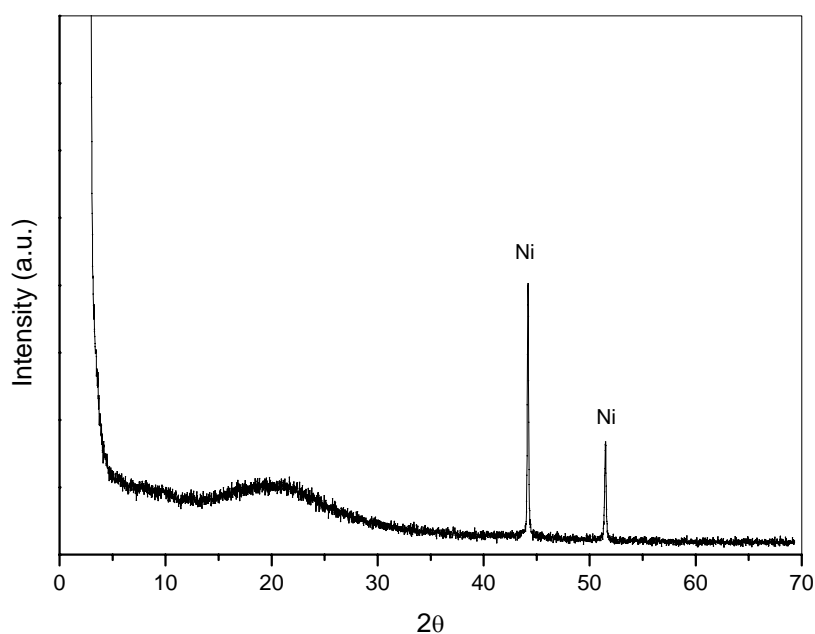
Figure 4.5.1.2.4: Powder XRD pattern of Ni/MCM-41 after reduction in flowing H_2 (diluted in N_2).

174
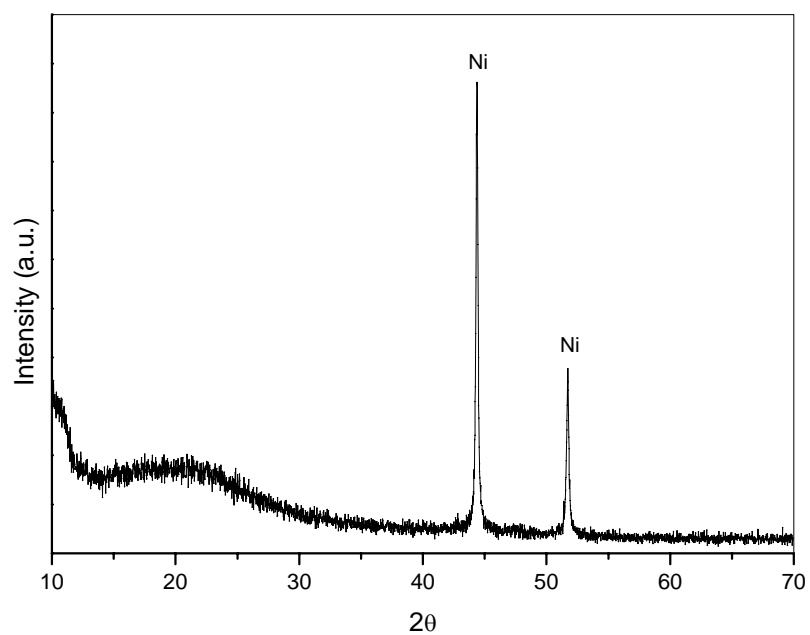
Figure 4.5.1.2.5: Powder XRD pattern of Ni/MCM-48 after reduction in flowing H_2 (diluted in N_2).
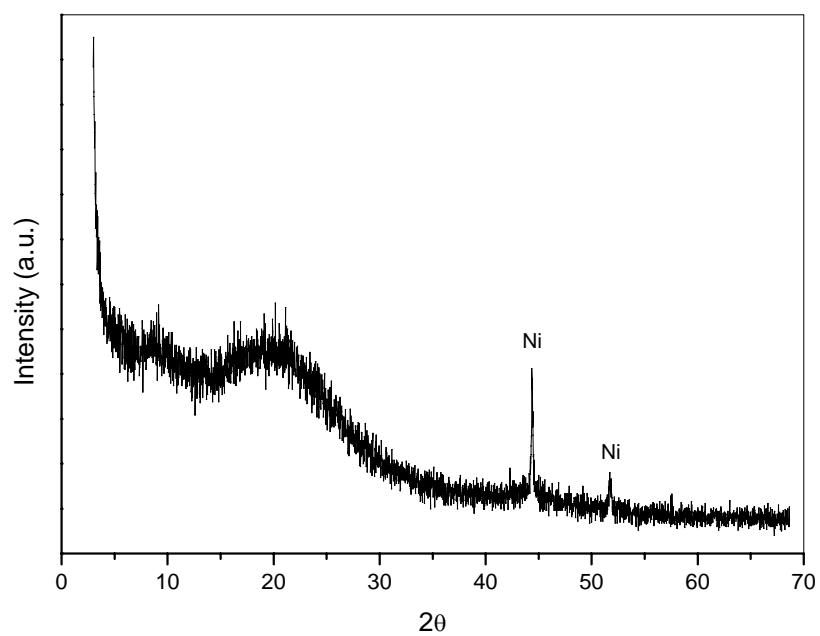
Figure 4.5.1.2.6: Powder XRD pattern of Ni/SBA-2after reduction in flowing H_2 (diluted in N_2).

The Ni metallic particle sizes were determined from the FHMW of the metal Ni peaks using the Scherrer equation. The results are shown in Table 4.5.1.2.1

Material	Ni crystallite size (nm)[a]
Ni/MCM-41	58
Ni/MCM-48	82
Ni/SBA-2	23

Table 4.5.1.2.1: Ni crystallite size of materials prepared using Ni-Ci as precursor of Ni. [a]The error in measuring the width at half height is 0.125°. Ni crystallite size calculation error is about ±5%.

As was previously mentioned, there are two main ways to incorporate elements/compounds in the mesoporous of OMS: by direct or postsynthetic methods. The direct incorporation of Ni leads to very low Ni loadings (< 1.5 wt.%).[309] Moreover, in order to incorporate higher loads of Ni into MCM-41, some other techniques have been used, such as ion exchange with $NiCl_2$.[310] However, incipient wetness impregnation has been proven to give the highest metal loading and dispersion of nickel oxide when Ni-Ci has been used as the precursor of Ni.[273] Therefore, Ni-Ci was used in the present studies.

Incorporation of metals into carrier materials by incipient wetness impregnation is a very common technique to design metal supported catalysts. In this method, the metal precursor is dissolved in a suitable solvent. Then, the metal-containing solution is added to the support and drawn into the pores by capillarity. Finally, the solid is

dried and calcined to eliminate the remaining organic compounds from the surface of the carrier.

During reduction, Ni particles sintered, and they grew outside of the mesopores. Their sizes could be related to the particle sizes/morphology of the solids.

Even though it was not possible to develop Ni metal inside the mesopores by this method, it seems that the external surface of OMS, more specifically their morphology, played an important role during catalysis. This will be further discussed in section 4.5.4.

4.5.1.3 Materials Containing Ni Incorporated by Solid State Reaction

Another technique for supporting Ni onto OMS was explored. That involved the use of Ni ACAC as a source of Ni. The reaction took place in the solid state.

The powder XRD pattern of SBA-2 after mixing with Ni ACAC is presented in Figure 4.5.1.3.1 The XRD pattern of the mechanical mixture shows the organic phase at high angles. From the X-ray diffraction pattern can also be appreciated the d_{100} peak of SBA-2 at lower angle.

The X-ray diffraction pattern of the mechanical mixture after reduction is presented in Figure 4.5.1.3.2. From it, the characteristic peaks of metallic Ni can be observed.

The same sample was scanned again after the catalytic hydrogenation reaction. The X-ray diffractogram is presented in Figure 4.5.1.3.3. The comparison of Figures 4.5.1.3.2 and 4.5.1.3.3 threw that the intensity of metallic Ni peaks decreased after reaction. The change in size of Ni particles could take place due to some loss of Ni

during chiral modification. Nevertheless, the evidence is that TA-Ni stays in the support after reaction.
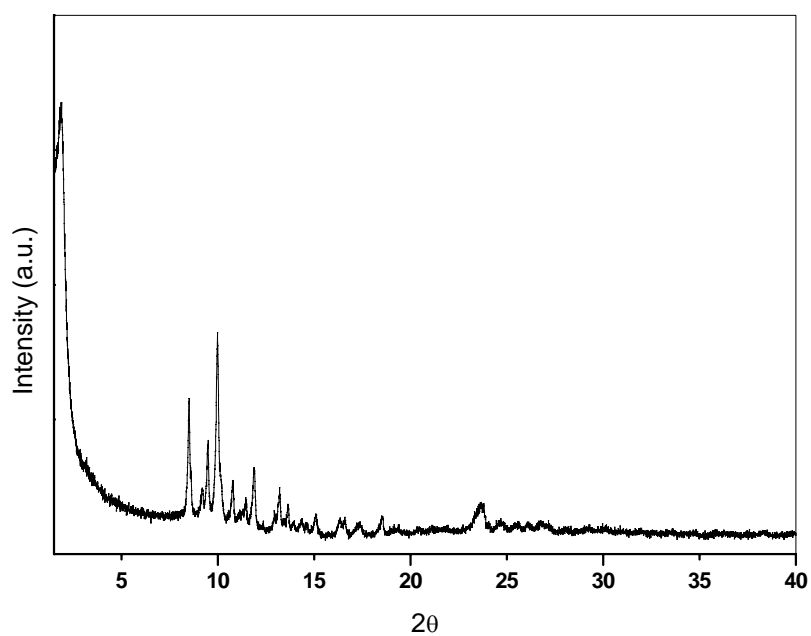
Figure 4.5.1.3.1: Powder XRD pattern of a mechanical mixture of SBA-2 and Ni ACAC.
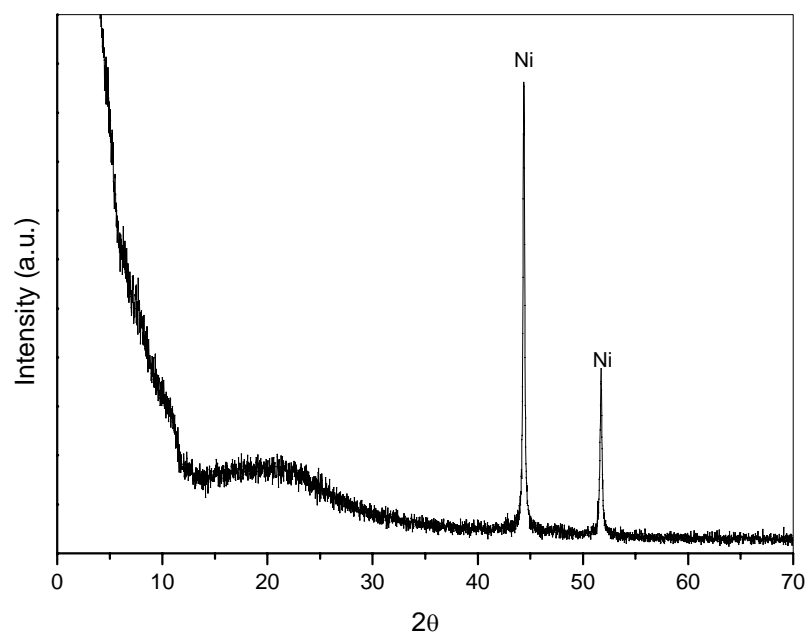
Figure 4.5.1.3.2: Powder XRD pattern of Ni particles developed on SBA-2 after reduction. Ni crystallite size = 24 nm.
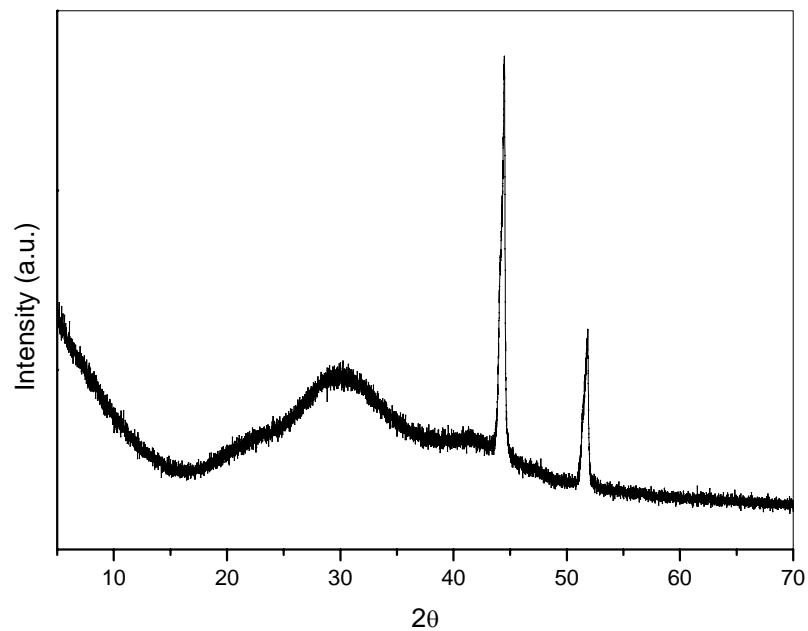
Figure 4.5.1.3.3: Powder XRD pattern of Ni/SBA-2 after catalytic hydrogenation reaction. Ni crystallite size = 23 nm.

4.5.2 N_2 Physisorption

Adsorption of molecules has been widely used for depicting surface areas and pore size distribution in solid catalysts. Therefore, the adsorption of gases such as N_2 has been a useful tool to characterise the texture of OMS. This technique can also be applied to study the interaction between molecules and the internal surface of OMS. Therefore, the use of this method is quite important for a better understanding of both diffusion and catalysis.

Nitrogen adsorption/desorption isotherms of the synthesised materials are shown in Figures 4.5.2.1 and 4.5.2.2. Both isotherms are of type IV according to IUPAC.[203]

MCM-41 shows a sharp increase of nitrogen uptake at $p/p^0 \approx 0.4$. This step is characteristic of type IV isotherms and it is caused by capillary condensation of nitrogen inside the mesopores. Below this pressure, the formation of an adsorbed monolayer of N_2 takes place. The further increase in N_2 pressure leads to the formation of a multilayer till capillarity occurs. This way, an increment in the volume of adsorbed N_2 is observed. Once the pores are filled, the adsorption carries on on the external surface of the solids.

Qualitatively speaking, a well defined step in the adsorption isotherm mirrors a narrow and uniform pore size distribution while its height is related to the pore volume. The poorly defined step in the MCM-41 isotherm (Figure 4.5.2.1) is indicative of a certain disorder in the mesostructure and a broad pore size distribution. Moreover, the isotherm of this material shows a hysteresis loop which supports the non-uniformity in size of the channels and structural defects.[311] On the contrary, SBA-2 shows a sharp step indicating a narrower pore size distribution and uniform

pores (Figure 4.5.2.2). SBA-2 shows the capillary inflection at a lower relative pressure (~0.3).

The volume of N_2 used for filling the mesopores of MCM-41 is ca. 640 cm^3g^{-1} while the volume of N_2 used for filling the mesopores of SBA-2 is 350 cm^3g^{-1}. This clearly indicates that the MCM-41 inner surface area is higher than that of SBA-2.

Table 4.5.2.1 summarises the physical properties of OMS. Surface area was estimated using the BET method[142] in the range of p/p^0 = 0.05 to 0.3 (always trying to get the highest coefficient of the plot). The average diameter of the pores and pore volume were estimated from the adsorption isotherm using the BJH method.[144]
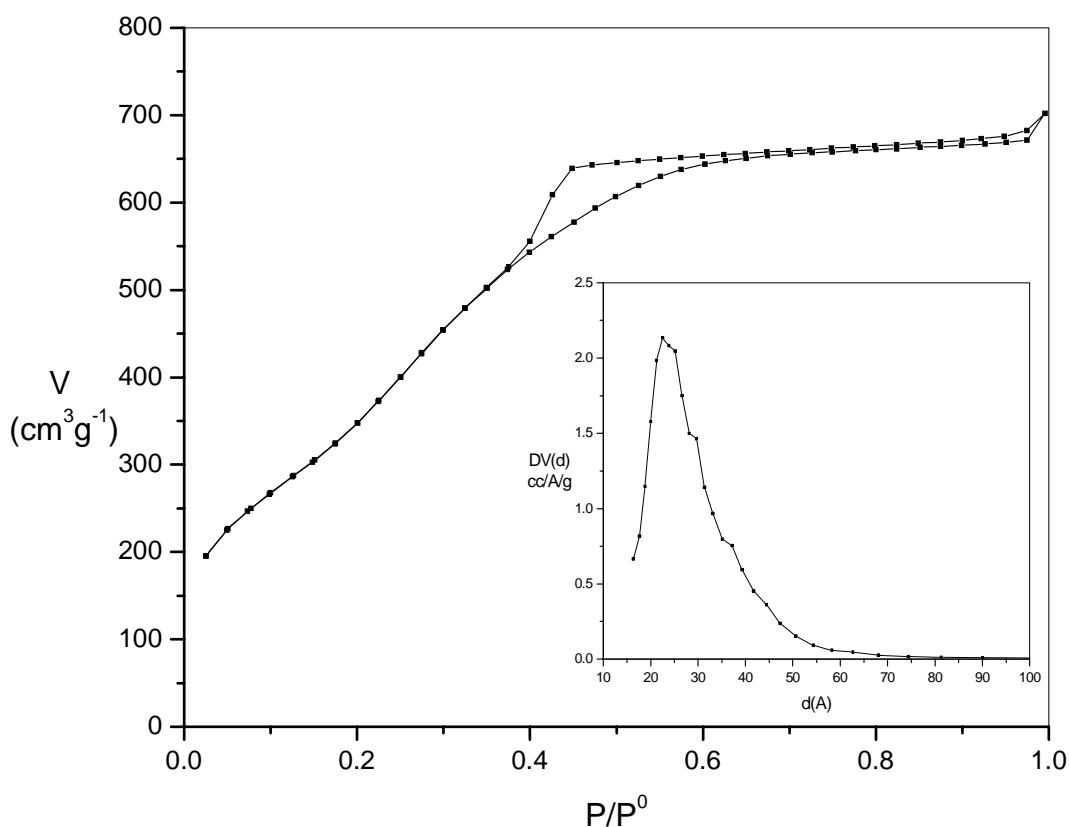
Figure 4.5.2.1: Adsorption/desorption isotherm of MCM-41.
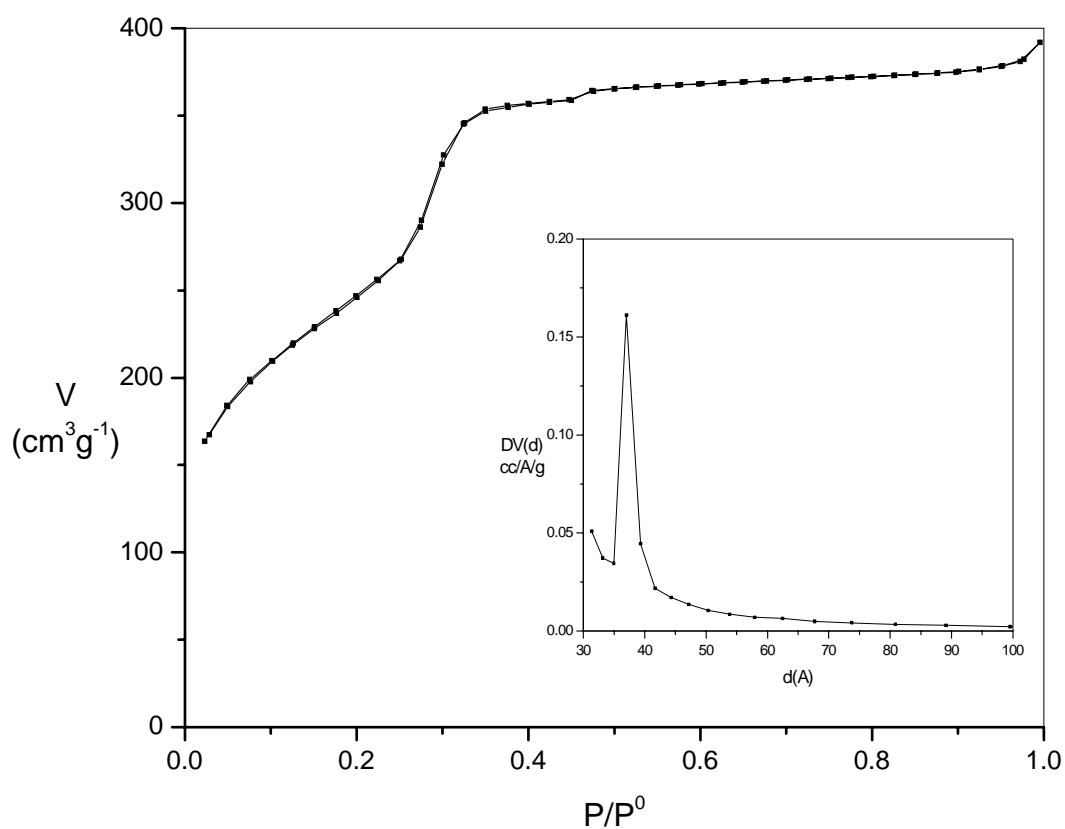
Figure 4.5.2.2: Adsorption/desorption isotherm of SBA-2.

Material	S_{BET} (m^2g^{-1})	Pore Diameter* (nm)	Pore Volume* (cm^3g^{-1})
MCM-41	1680	3.3	1.039
SBA-2	896	3.7	0.585

Table 4.5.2.1: Physical properties of OMS. *Calculated from the adsorption branch.

From Table 4.5.2.1 it can be seen that the MCM-41 surface area is higher than that of SBA-2. In fact, reports of surface areas for MCM-41 are around 1200 m^2g^{-1}.

Therefore, we have obtained a MCM-41 type material with a very high surface area. This may be related to a material containing very small particles.

MCM-41 shows a broad pore size distribution (~1.5-6 nm), whose maximum value is centred at 3.3 nm. In contrast, the pore size distribution in SBA-2 is narrower than that of MCM-41 (~3.5-4.2 nm) with the maximum centred at 3.7 nm. On the other hand, MCM-41 pore volume is ca. 20 times higher than that of SBA-2. This can be explained by particle size. MCM-41 particles might be bigger than SBA-2 particles. The textural properties of the materials seem to have an influence on the hydrogenation reaction when they were used as catalytic supports of active phases of TA-Ni. This will be discussed in Section 4.5.4.

4.5.3 Chiral Modification

4.5.3.1 Effects of Variables of Modification on e.e.

As mentioned in Section 3.5.3., variables of reaction during chiral modification of Ni supported have an effect on e.e. during catalysis (i.e. TA concentration and pH). These variables have been researched on TA-Ni supported on OMS.

Tables 4.5.3.1.1 and 4.5.3.1.2 show the effect of TA concentration and pH on e.e. during catalytic test, respectively. The material used was TA-Ni/MCM-41 in which Ni was incorporated by incipient wetness. For the studies of the effect of TA concentration, chiral modification was carried out at 100°C for 1 hr, using water as a solvent. The pH of the solution was adjusted to 5.1 in advance. On the other hand, in the case of the variation of pH studies, the initial TA concentration was 0.05 ML^{-1}.

Hydrogenation reactions (2 mL of MAA over 0.1 g of catalyst) were carried out at 100°C using an initial hydrogen pressure of 10 bar.

[TA]/ML^{-1}	%e.e.(R)
0.01	0
0.02	20
0.05	30
0.1	0
0.2	0
0.3	0
0.5	0

Table 4.5.3.1.1: Effect of TA concentration on e.e. over TA-Ni/MCM-41. Ni was incorporated by incipient wetness impregnation onto MCM-41 using Ni-Ci as precursor of Ni.

It was found that the optimum concentration of TA was 0.05 ML^{-1} (Table 4.5.3.1.1). At concentrations above this value, no enantioselectivity was observed. This TA concentration is therefore the optimal to modify OMS under the conditions of reaction studied.

The adjustment of the pH of the solution containing the modifier proved to be important in the catalytic performance of the solid. The only pH value which had an influence on e.e. was 5.1. Adjusting the pH to higher values did not lead to enantiodifferentiation (Table 4.5.3.1.2).

pH	%e.e.(R)
3.2	0
5.1	30
7	0
9	0
13	0

Table 4.5.3.1.2: Effect of pH on e.e. over a TA-Ni/MCM-41.

Using L-TA gave exactly the same results of e.e. but the product had reversed sign (MHB(S)).

4.5.4 Catalysis

4.5.4.1 TA-Ni Supported on OMS (Ni Obtained from Ni-Ci Precursor)

The catalytic properties of the solids are shown in Table 4.5.4.1.1

Catalyst	Activity (%)	e.e. (%)
TA-Ni/MCM-41	12	30
TA-Ni/SBA-2	9	6
TA-Ni/MCM-48	95	0

Table 4.5.4.1.1: Catalytic properties of TA-Ni supported on OMS catalysts. Ni was incorporated by incipient wetness impregnation onto OMS using Ni-Ci as precursor of Ni. Modification conditions used: [TA] = 0.05 ML^{-1}, T = 100°C, t = 1 hr. Hydrogenation reaction used: catalysts = 0.1 g, MAA = 2 mL, CH$_3$OH = 18 mL, P(H$_2$) = 10 bar. T = 100°C, t = 48 hrs.

From Table 4.5.4.1.1 it can be seen that all of the materials were active to the reaction studied. Moreover, TA-Ni/MCM-41 and TA-Ni/SBA-2 were also selective. The highest e.e. obtained is when MCM-41 is used as the support, with an e.e of 30%. However, its catalytic activity is just 12%. The TA-Ni/SBA-2 supported catalyst exhibited very low activity and enantioselectivity (9 and 6%, respectively). TA-Ni/MCM-48 showed the highest activity of this series of materials but it did not discriminate between the enantiomers.

4.5.4.2 TA-Ni Supported on OMS (Ni Obtained from Ni ACAC Precursor)

The activity of the catalysts is directly linked to metallic Ni. Therefore, in order to augment the metal loading, and hence the activity of the catalyst that showed enantiodifferentiation ability, another technique of metal deposition was examined. This technique consisted of the deposition of Ni into OMS by solid state reaction and Ni ACAC was used as the precursor of Ni.

Results of the catalytic evaluation of the solids are shown in Table 4.5.4.2.1. Activity was enhanced for both TA-Ni/MCM-41 and TA-Ni/SBA-2. This is a direct

effect of the higher metal loading present in the catalyst. However, in the case of MCM-41, no enantiodifferentiation took place. On the contrary, SBA-2 enantioselectivity was improved by a factor of two in comparison to the wet deposition technique (12%, Table 4.5.4.1.1). The higher amount of Ni incorporated in SBA-2 by solid state reaction could improve the density of active sites of the same nature which enhanced both activity and enantioselectivity in the hydrogenation. On the other hand, TA-Ni/MCM-48 showed the same values of activity and enantioselectivity in both techniques of Ni incorporation (liquid and solid state reactions).

Catalyst	Activity (%)	e.e. (%)
TA-Ni/MCM-41	88	0
TA-Ni/SBA-2	90	12
TA-Ni/MCM-48	96	0

Table 4.5.4.2.1: Catalytic properties shown by TA-Ni/OMS catalysts. Ni was deposited onto OMS by solid state reaction using Ni ACAC as precursor of Ni. Modification conditions applied: [TA] = 0.05 ML^{-1}, T = 100°C, t = 1 hr. Hydrogenation reaction used: catalysts = 0.1 g, MAA = 2 mL, CH_3OH = 18 mL, P(H_2) = 10 bar. T = 100°C, t = 48 hrs.

Nitta et al.[98] have tried to relate e.e. to pore size distribution and they found that for a series of catalysts supported on silicas with similar pore size distributions, e.e. showed variation. On the contrary, some other materials showed the same e.e. even though they had different pore size distributions. Moreover, in their communication, they took a negative view of the presence of mesopores in the range of 10-30 nm in the catalysts as they would have an adverse effect on e.e. We have found that for materials showing roughly the same pore size (around 3-4 nm), the most important

variable in e.e. is the morphology of the particle. Even though we do not have evidence about the size and shape of them, we have found that Ni particle sizes are much bigger than the pore sizes; therefore it is assumed that Ni is deposited on the external surface of OMS. Therefore, the pores could not have a direct function in the enantioselective properties of the solid.

4.5.1.3 Studies of Postmodifier Solutions

Studies of the postmodifier solutions showed that the TA molecules adsorbed in SBA-2 by using both techniques (wet and solid state approaches) is within the same range (3 $\times 10^{21}$ and 4 $\times 10^{21}$, respectively) which indicates that this is the right number of molecules to develop a suitable surface in order that enantiodifferentiation occurs for this particular system.

For both techniques, no e.e. was observed at TA concentrations below or above 0.05 mol dm^3. At lower TA concentrations, the surface of Ni bare metal is big and therefore the result of the hydrogenation is the racemic mixture. On the other hand, at higher TA concentrations, molecules could be so strained and close each other and therefore, space for MAA to reach the active sites could not be available.

Therefore, the modification of Ni-SBA-2 with 0.05 TA solutions led to the optimum concentration of TA to develop effective enantioselective sites on the Ni surface available.

4.6 Conclusions

A series of OMS of types MCM-41, MCM-48 and SBA-2 was successfully synthesised. Their physical characterisation shows that they possess high surface areas and long range ordered pore system.

Ni was successfully incorporated in OMS by incipient wetness impregnation using Ni-Ci as the precursor of Ni. The further calcination of the materials, led to well dispersed NiO particles inside the mesopores; reduction made those nanoparticles migrate from the pores to the external surface, and sinter.

The supported Ni particles obtained, were chirally modified with TA. The catalytic properties of the solids were tested in the asymmetric hydrogenation of MAA.

From the catalytic test results, the effect of the support on e.e. could be seen. With the exception of MCM-48, the other two materials displayed enantiodifferentiation ability. MCM-41 showed the best enantiodifferentiation ability. On the other hand, despite its most favourable mass transfer, MCM-48 did not discriminate between the two enantiomers.

In order to improve the activity of the catalysts, another technique to impregnate Ni onto OMS was explored. The solid state reaction between Ni ACAC and OMS proved to be useful to augment Ni loading in the solids and, as a consequence, the density of active sites was enhanced, and consequently, the catalytic properties of the solid TA-Ni/SBA-2.

It is clear then, that the nature of the support played an important role in the development of the chiral catalyst, in particular, its morphology.

CHAPTER 5. CONCLUSIONS AND FURTHER WORK DIRECTION

5.1 HLCS

A series of supported nickel materials were prepared from thermal treatment of Ni^{2+}/Mg^{2+}(or Zn^{2+})/Al^{3+}(or Fe^{3+} or Cr^{3+}) hydrotalcite-like compound (HLC) precursors, with variable cation ratios, and chirally modified with L-(+)-tartaric acid (TA) under controlled temperature and pH conditions. The catalytic properties of the materials obtained were tested in the hydrogenation of methyl acetoacetate (MAA) to 3-methyl hydroxybutyrate (MHB).

From the methods of HLCs preparation explored, the series of materials containing Ni/Mg (or Zn)/Al prepared by coprecipitation required an aging step in order to improve crystallinity in the materials. On the contrary, the hydrolysis of urea method led to materials with good crystallinity without any further rectifying process being required. For the Ni/Zn/Al series, the rectifying process of the solutions obtained by coprecipitation led to HLC and ZnO phases. By using the hydrolysis of urea method in the same series of materials, only small traces of ZnO were formed and only when the amount of Zn incorporated in the solid approached the maximum of the range studied.

Materials obtained by the hydrolysis of urea method promoted the reaction enantioselectively, whereas materials obtained by coprecipitation did not. For the materials prepared by urea hydrolysis, materials of the series Ni/Zn/Al were more enantioselective than materials of the series Ni/Mg/Al. In order to understand this divergence, the structure of the materials as well as their surface environment must be taken into account.

For example, after reduction, Ni metal and spinel phases were developed in the materials. The Ni/Zn/Al series displayed a major amount of spinel phases compared to its Ni/Mg/Al counterpart.

On the other hand, analysis of the postmodifying solutions showed that in general, materials containing Zn were more susceptible to Ni leaching but showed greater TA adsorption in comparison to the materials containing Mg.

Our preliminary studies showed that materials containing Ni particles of sizes around 10 nm and below did not possess enantiodifferentiation ability. By controlled thermal treatments, routes were developed to materials containing Ni particles of around 20 nm in size, which showed differentiation ability.

Therefore, it is clear that Ni particle size plays an important role in e.e., but for materials with similar Ni particle size, the influence of the other metal cations present in the support and the phase in which they are contained are of high importance. For example, the presence of spinels in the Ni/Zn/Al material allowed the elimination of small Ni particles acting as non-enantioselective sites during modification, leading to an improvement in e.e. Therefore, Ni leaching had a positive effect on the catalytic properties in these materials. This was corroborated when NaBr was used as a comodifier as the amount of Ni leaching decreased. The claimed beneficial effect of the addition of NaBr during modification enhanced the enantiodifferentiation ability of just the TA-Ni/Al catalyst.

An important highlight of these studies is that, even though the pH during modification controls the TA adsorption and Ni leaching (acidic pH leads to a great extent of TA uptake while basic pH controls Ni leaching to a lesser extent), neither pH nor TA concentration, in the range studied, had any significant effect on the

enantiodifferentiation ability of the catalysts. Therefore, it is valid to state that the nature of the cation constituting the support is a key factor in the design of TA-Ni supported catalysts. This theory is supported by studies carried out on materials containing other cations. For example, Ni/Cr showed good catalytic properties, but the combination of Ni/Mg/Cr did not lead to a useful enantioselective catalyst.

For the series of materials Ni/Mg (or Zn)/Fe, the combination Ni/Fe led to the most active and most enantioselective catalyst of the series. Incorporating Mg or Zn to the structure negatively altered the catalytic properties of the solid.

The hydrolysis of urea synthesis method proved not to be suitable for precipitating materials containing Ni/Mg (or Zn)/Fe (or Cr). Therefore, we cannot compare materials prepared by two different methods of synthesis.

Enantioselectivity on materials supported on a single oxide follows the trend Fe > Cr > Al. As Ni/Al and Ni/Cr have the same Ni particle size (~28 nm) and their enantioselective properties differ by a factor of ca. 3, this clearly shows that the nature of the cation constituting the support is very important in the design of an enantioselective catalyst and that enantioselectivity must not to be seen to merely depend upon the Ni particle size.

Therefore, the use of HLCs as precursors of enantioselective catalysts is a viable option due to the benefit in using cations of different nature and controlled Ni particle size.

Further research on related materials containing other cations such as Mn^{3+}, In^{3+} or Ga^{3+} and/or the use of different precursors of metals (i.e. chlorides) during synthesis should be done.

5.2 OMS

A series of OMS of types MCM-41, MCM-48 and SBA-2 were successfully synthesised. Their physical characterisation shows that they possess a long range ordered pore system and very high surface areas.

Ni was incorporated into their structure by using two techniques: incipient wetness impregnation and solid state reaction. By the wet impregnation, NiO could be incorporated inside the mesopores. In order to obtain metallic Ni, the materials had to be reduced and this thermal process made the Ni particles grow outside of the mesopores. Even though Ni is not deposited in the mesopores, it seems that the pore systems of each individual material played an important role during catalysis.

Therefore it can be concluded that the architecture of the pore systems have an effect in e.e. when they are used as supports of TA-Ni catalysts. MCM-41 showed good catalytic properties whereas MCM-48 showed excellent activity with a racemic mixture product. The most active and selective catalyst was obtained using SBA-2.

As the mesostructures collapsed after the different thermal processes carried out on the materials, it is evident that the external surface is having an important function as a support for TA-Ni. Therefore, the morphology of the OMS is another factor to take into account for the design of TA-Ni/OMS catalysts.

In general, for all of the catalysts studied in here, further research should be done, and apart from the materials optimisation, the study of the variables of the hydrogenation reaction, i.e. the use of different reactors and reaction media, additives, pressures, etc., must be considered as they might have beneficial effects on e.e.

BIBLIOGRAPHY

1.   M.W. Roberts, *Catal. Lett.,* 67 (2000) 1.
2.   P.M.D. Collins, *Platinum Metals Rev.,* 30 (1986) 141.
3.   J. Wisniak, *Educ. quím.,* 21 (2010) 60.
4.   B.B. Corson, *J. Chem. Ed.,* (1947) 99.
5.   W.S. Knowles, *Acc. Chem. Res.,* 16 (1983) 106.
6.   W.S. Knowles, *J. Chem. Ed.,* 63 (1986) 222.
7.   R. Selke, and H. Pracejus, *J. Mol. Catal.,* 37 (1986) 213.
8.   W. Vocke, R. Hanel, and F.U. Flother, *Chem. Technol.,* 39 (1987) 123.
9.   I. Ojima, N. Clos, and C. Bastos, *Tetrahedron,* 45 (1989) 6901.
10.   S. Akutagawa, *Appl. Catal., A,* 128 (1995) 171.
11.   R. Imwinkelried, *Chimia,* 51 (1997) 300.
12.   H.U. Blaser, H.P. Buser, K. Coers, R. Hanreich, H.P. Jalett, E. Jelsch, B. Pugin, H.D. Schneider, F. Spindler, and A. Wegmann, *Chimia,* 53 (1999) 275.
13.   R. Noyori, M. Tokunaga, and M. Kitamura, *Bull. Chem. Soc. Jpn.,* 68 (1995) 36.
14.   H.U. Blaser, and M. Studer, *Chirality,* 11 (1999) 459.
15.   T. Aratani, *Pure Appl. Chem.,* 57 (1985) 1839.
16.   J.W. Scott, *Topics in Stereochem.,* 19 (1989) 209.
17.   D.L. Hughes, G.B. Smith, J. Liu, G.C. Dezeny, C.H. Senanayake, R.D. Larsen, T.R. Verhoeven, and P.J. Reider, *J. Org. Chem.,* 62 (1997) 2222.
18.   H. Cotton, T. Elebring, M. Larsson, L. Li, H. Sorensen, and S. von Unge, *Tetrahedron: Asymmetry,* 11 (2000) 3819.
19.   H.U. Blaser, F. Spindler, and A. Studer, *Appl. Catal., A,* 221 (2001) 119.
20.   B. Sharpless, W. Knowles, and R. Noyori, *Chem. Br.,* 37 (2001) 24.
21.   D. Lipkin, and T.D. Stewart, *J. Am. Chem. Soc.,* 61 (1939) 3295.
22.   T.D. Stewart, and D. Lipkin, *J. Am. Chem. Soc.,* 61 (1939) 3297.
23.   M. Nakazaki, *J. Chem. Soc. Jpn. Pure Chem. Sect.,* 75 (1954) 831.
24.   S. Akabori, Y. Izumi, Y. Fuji, and S. Sakurai, *Nippon Nagaku Zasshi,* 77 (1956) 1956.
25.   S. Akabori, S. Sakurai, Y. Izumi, and Y. Fujii, *Nature,* 178 (1956) 323.
26.   S. Akabori, Y. Izumi, and Y. Fuji, *Nippon Nagaku Zasshi,* 78 (1957) 886.
27.   A.A. Balandin, E.I. Klabunovskii, and Petrov, II, *Dokl. Akad. Nauk. SSSR,* 127 (1959) 557.
28.   Y. Izumi, M. Imaida, H. Fukawa, and S. Akabori, *Bull. Chem. Soc. Jpn.,* 36 (1963) 155.
29.   Y. Izumi, M. Imaida, H. Fukawa, and S. Akabori, *Bull. Chem. Soc. Jpn.,* 36 (1963) 21.
30.   S. Tatsumi, M. Imaida, Y. Fukuda, Y. Izumi, and S. Akabori, *Bull. Chem. Soc. Jpn.,* 37 (1964) 846.
31.   Y. Izumi, S. Tatsumi, M. Imaida, Y. Fukuda, and S. Akabori, *Bull. Chem. Soc. Jpn.,* 38 (1965) 1206.
32.   Y. Izumi, S. Tatsumi, and M. Imaida, *Bull. Chem. Soc. Jpn.,* 39 (1966) 2223.
33.   Y. Izumi, S. Tatsumi, and M. Imaida, *Bull. Chem. Soc. Jpn.,* 39 (1966) 1087.
34.   Y. Izumi, S. Tatsumi, M. Imaida, Y. Fukuda, and S. Akabori, *Bull. Chem. Soc. Jpn.,* 39 (1966) 361.

35. H. Pracejus, *Fortsch. Chem. Forsch.,* 8 (1967) 493.
36. Y. Izumi, Matsunag.K, S. Tatsumi, and M. Imaida, *Bull. Chem. Soc. Jpn.,* 41 (1968) 2515.
37. Y. Izumi, T. Tanabe, S. Yajima, and M. Imaida, *Bull. Chem. Soc. Jpn.,* 41 (1968) 941.
38. S. Tatsumi, *Bull. Chem. Soc. Jpn.,* 41 (1968) 408.
39. R.L. Beamer, R.H. Belding, and C.S. Fickling, *J. Pharm. Sci.,* 58 (1969) 1419.
40. Y. Izumi, M. Imaida, T. Harada, T. Tanabe, S. Yajima, and T. Ninomiya, *Bull. Chem. Soc. Jpn.,* 42 (1969) 241.
41. Y. Izumi, S. Tatsumi, and M. Imaida, *Bull. Chem. Soc. Jpn.,* 42 (1969) 2373.
42. K. Harada, and T. Yoshida, *Naturwiss,* 57 (1970) 306.
43. K. Harada, and T. Yoshida, *Naturwiss,* 57 (1970) 131.
44. Y. Izumi, and T. Ninomiya, *Bull. Chem. Soc. Jpn.,* 43 (1970) 579.
45. Y. Izumi, H. Takizawa, K. Nakagawa, R. Imamura, M. Imaida, T. Ninomiya, and S. Yajima, *Bull. Chem. Soc. Jpn.,* 43 (1970) 1792.
46. Y. Izumi, S. Tatsumi, M. Imaida, and K. Okubo, *Bull. Chem. Soc. Jpn.,* 43 (1970) 566.
47. T. Tanabe, T. Ninomiya, and Y. Izumi, *Bull. Chem. Soc. Jpn.,* 43 (1970) 2276.
48. T. Harada, M. Imaida, and Y. Izumi, *Bull. Chem. Soc. Jpn.,* 44 (1971) 1419.
49. F. Higashi, T. Ninomiya, and Y. Izumi, *Bull. Chem. Soc. Jpn.,* 44 (1971) 1333.
50. H. Hirai, and T. Furuta, *J. Polym. Sci., Part B: Polym. Lett.,* 9 (1971) 459.
51. Y. Izumi, *Angew. Chem. Int. Ed.,* 10 (1971) 871.
52. Y. Izumi, T. Harada, T. Tanabe, and K. Okuda, *Bull. Chem. Soc. Jpn.,* 44 (1971) 1418.
53. Y. Izumi, and K. Ohkubo, *Bull. Chem. Soc. Jpn.,* 44 (1971) 1330.
54. Y. Izumi, S. Yajima, K. Okubo, and Babievsk.Kk, *Bull. Chem. Soc. Jpn.,* 44 (1971) 1416.
55. T. Tanabe, and Y. Izumi, *Bull. Chem. Soc. Jpn.,* 46 (1973) 1550.
56. T. Tanabe, K. Okuda, and Y. Izumi, *Bull. Chem. Soc. Jpn.,* 46 (1973) 514.
57. H. Ozaki, A. Tai, and Y. Izumi, *Chem. Lett.,* (1974) 935.
58. E.S. Neupokoeva, E.I. Karpeiskaya, L.F. Godunova, and E.I. Klabunovskii, *Bull. Acad. Sci. USSR Div. Chem. Sci.,* 24 (1975) 2241.
59. T. Harada, S. Onaka, A. Tai, and Y. Izumi, *Chem. Lett.,* (1977) 1131.
60. T. Harada, and Y. Izumi, *Chem. Lett.,* (1978) 1195.
61. H. Ozaki, A. Tai, S. Kobatake, H. Watanabe, and Y. Izumi, *Bull. Chem. Soc. Jpn.,* 51 (1978) 3559.
62. T. Harada, M. Yamamoto, K. Itoh, S. Matsukiyo, S. Murakami, H. Ozaki, A. Tai, and Y. Izumi, *Abstr. Pap. Am. Chem. Soc.,* (1979) 131.
63. Y. Orito, S. Imai, and S. Niwa, *Nippon Kagaku Kaishi,* (1979) 1118.
64. Y. Orito, S. Imai, S. Niwa, and Nguyengiahung, *J. Synth. Org. Chem Jpn.,* 37 (1979) 173.
65. Y. Orito, S. Imai, and S. Niwa, *Nippon Kagaku Kaishi,* (1980) 670.
66. T. Harada, M. Yamamoto, S. Onaka, M. Imaida, H. Ozaki, A. Tai, and Y. Izumi, *Bull. Chem. Soc. Jpn.,* 54 (1981) 2323.
67. Y. Izumi, *Adv. Catal.,* 32 (1983) 215.
68. A. Miyashita, A. Yasuda, H. Takaya, K. Toriumi, T. Ito, T. Souchi, and R. Noyori, *J. Am. Chem. Soc.,* 102 (1980) 7932.
69. H. Kumobayashi, *Recl. Trava. Chim. Pays- Bas,* 115 (1996) 201.

70. R. Noyori, and S. Hashiguchi, *Acc. Chem. Res.,* 30 (1997) 97.
71. R. Noyori, M. Yamakawa, and S. Hashiguchi, *J. Org. Chem.,* 66 (2001) 7931.
72. R. Noyori, *Adv. Synth. Catal.,* 345 (2003) 15.
73. M.D. Jones, R. Raja, J.M. Thomas, B.F.G. Johnson, D.W. Lewis, J. Rouzaud, and K.D.M. Harris, *Angew. Chem. Int. Ed.,* 42 (2003) 4326.
74. R. Raja, J.M. Thomas, M.D. Jones, B.F.G. Johnson, and D.E.W. Vaughan, *J. Am. Chem. Soc.,* 125 (2003) 14982.
75. A. Ghosh, and R. Kumar, *J. Catal.,* 228 (2004) 386.
76. P. McMorn, and G.J. Hutchings, *Chem. Soc. Rev.,* 33 (2004) 108.
77. A. Tai, T. Kikukawa, T. Sugimura, Y. Inoue, T. Osawa, and S. Fujii, *J. Chem. Soc., Chem. Commun.,* (1991) 795.
78. A. Tai, T. Kikukawa, T. Sugimura, Y. Inoue, S. Abe, T. Osawa, and T. Harada, *Stud. Surf. Sci. Catal.,* 75 (1993) 2443.
79. A. Tai, T. Kikukawa, T. Sugimura, Y. Inoue, S. Abe, T. Osawa, and T. Harada, *Bull. Chem. Soc. Jpn.,* 67 (1994) 2473.
80. T. Sugimura, *Catal. Surv. Jpn.,* 3 (1999) 37.
81. P. Kukula, and L. Cerveny, *Appl. Catal., A,* 210 (2001) 237.
82. P. Kukula, and L. Cerveny, *J. Mol. Catal. A: Chem.,* 185 (2002) 195.
83. P. Kukula, and L. Cerveny, *Appl. Catal., A,* 223 (2002) 43.
84. T. Sugimura, S. Nakagawa, and A. Tai, *Bull. Chem. Soc. Jpn.,* 75 (2002) 355.
85. P. Kukula, and L. Cerveny, *Res. Chem. Intermed.,* 29 (2003) 91.
86. H.N. Chen, R. Li, H.L. Wang, L.A. Yin, F.S. Wang, and J.T. Ma, *Chem. Lett.,* 35 (2006) 910.
87. T. Osawa, K. Yoshino, K. Takimoto, O. Takayasu, and T. Harada, *Catal. Lett.,* 112 (2006) 167.
88. H.N. Chen, R. Li, H.L. Wang, J.W. Liu, F.S. Wang, and J.T. Ma, *J. Mol. Catal. A: Chem.,* 269 (2007) 125.
89. C.F. Wang, Y.F. Zheng, S.L. Cai, J.T. Ma, and R. Li, *React. Kinet. Catal. Lett.,* 95 (2008) 129.
90. S.L. Cai, K. Ma, H.N. Chen, Y.F. Zheng, J. Jiang, and R. Li, *Catal. Lett.,* 128 (2009) 227.
91. Y. Orito, S. Niwa, and S. Imai, *J. Synth. Org. Chem Jpn.,* 35 (1977) 753.
92. J.A. Groenewegen, and W.M.H. Sachtler, *J. Catal.,* 38 (1975) 501.
93. Y. Nitta, F. Sekine, T. Imanaka, and S. Teranishi, *Bull. Chem. Soc. Jpn.,* 54 (1981) 980.
94. Y. Nitta, F. Sekine, J. Sasaki, T. Imanaka, and S. Teranishi, *Chem. Lett.,* (1981) 541.
95. Y. Nitta, F. Sekine, T. Imanaka, and S. Teranishi, *J. Catal.,* 74 (1982) 382.
96. H.M. Woerde, L.J. Bostelaar, A. Hoek, and W.M.H. Sachtler, *J. Catal.,* 76 (1982) 316.
97. Y. Nitta, F. Sekine, J. Sasaki, T. Imanaka, and S. Teranishi, *J. Catal.,* 79 (1983) 211.
98. Y. Nitta, O. Yamanishi, F. Sekine, T. Imanaka, and S. Teranishi, *J. Catal.,* 79 (1983) 475.
99. L.J. Bostelaar, and W.M.H. Sachtler, *J. Mol. Catal.,* 27 (1984) 387.
100. L.J. Bostelaar, and W.M.H. Sachtler, *J. Mol. Catal.,* 27 (1984) 377.
101. Y. Nitta, T. Utsumi, T. Imanaka, and S. Teranishi, *Chem. Lett.,* (1984) 1339.
102. Y. Nitta, T. Utsumi, T. Imanaka, and S. Teranishi, *J. Catal.,* 101 (1986) 376.

103. D.R. Richards, H.H. Kung, and W.M.H. Sachtler, *Journal of Molecular Catalysis,* 36 (1986) 329.
104. L. Fu, H.H. Kung, and W.M.H. Sachtler, *J. Mol. Catal.,* 42 (1987) 29.
105. Y. Nitta, and T. Imanaka, *Bull. Chem. Soc. Jpn.,* 61 (1988) 295.
106. M.A. Keane, and G. Webb, *J. Chem. Soc., Chem. Commun.,* (1991) 1619.
107. M.A. Keane, and G. Webb, *J. Catal.,* 136 (1992) 1.
108. M.A. Keane, *Can. J. Chem.,* 72 (1994) 372.
109. M.A. Keane, *Langmuir,* 13 (1997) 41.
110. Y. Nitta, M. Kawabe, and T. Imanaka, *Appl. Catal.,* 30 (1987) 141.
111. T. Osawa, S. Mita, A. Iwai, O. Takayasu, H. Hashiba, S. Hashimoto, T. Harada, and I. Matsuura, *J. Mol. Catal. A: Chem.,* 157 (2000) 207.
112. M.A. Keane, *Zeolites,* 13 (1993) 14.
113. M.A. Keane, *Zeolites,* 13 (1993) 22.
114. M.A. Keane, *Zeolites,* 13 (1993) 330.
115. E. Leclercq, A. Rives, E. Payen, and R. Hubaut, *Appl. Catal., A,* 168 (1998) 279.
116. A. Tai, T. Harada, Y. Hiraki, and S. Murakami, *Bull. Chem. Soc. Jpn.,* 56 (1983) 1414.
117. A. Hoek, and W.M.H. Sachtler, *J. Catal.,* 58 (1979) 276.
118. S.J. Thomson, and G. Webb, *J. Chem. Soc., Chem. Commun.,* (1976) 526.
119. T. Osawa, T. Harada, and O. Takayasu, *Top. Catal.,* 13 (2000) 155.
120. M.O. Lorenzo, S. Haq, T. Bertrams, P. Murray, R. Raval, and C.J. Baddeley, *J. Phys. Chem. B,* 103 (1999) 10661.
121. M.O. Lorenzo, C.J. Baddeley, C. Muryn, and R. Raval, *Nature,* 404 (2000) 376.
122. R. Raval, *Cattech,* 5 (2001) 12.
123. V. Humblot, S. Haq, C. Muryn, W.A. Hofer, and R. Raval, *J. Am. Chem. Soc.,* 124 (2002) 503.
124. T.E. Jones, and C.J. Baddeley, *Surf. Sci.,* 519 (2002) 237.
125. T.E. Jones, and C.J. Baddeley, *Surf. Sci.,* 513 (2002) 453.
126. M.O. Lorenzo, V. Humblot, P. Murray, C.J. Baddeley, S. Haq, and R. Raval, *J. Catal.,* 205 (2002) 123.
127. R. Raval, *J. Phys.: Condens. Matter,* 14 (2002) 4119.
128. R. Raval, *Nature,* 425 (2003) 463.
129. R. Raval, *Curr. Opin. Solid State Mater. Sci.,* 7 (2003) 67.
130. W.A. Hofer, V. Humblot, and R. Raval, *Surf. Sci.,* 554 (2004) 141.
131. V. Humblot, S.M. Barlow, and R. Raval, *Prog. Surf. Sci.,* 76 (2004) 1.
132. V. Humblot, S. Haq, C. Muryn, and R. Raval, *J. Catal.,* 228 (2004) 130.
133. V. Humblot, and R. Raval, *Appl. Surf. Sci.,* 241 (2004) 150.
134. T.E. Jones, and C.J. Baddeley, *J. Mol. Catal. A: Chem.,* 216 (2004) 223.
135. S.M. Barlow, and R. Raval, *Curr. Opin. Colloid Interface Sci.,* 13 (2008) 65.
136. R. Raval, *Chem. Soc. Rev.,* 38 (2009) 707.
137. V.K. Pecharsky, and P.Y. Zavalij, *Fundamentals of Powder Diffraction and Structural Characterization of Materials,* (2003) 105 Kluwer Academic Publishers.
138. A.R. West, *Basic Solid State Chemistry,* 2nd ed., (1999) 127 John wiley & Sons.

139. P.W. Atkins, *Physical Chemistry,* Fifth ed., (1994) 728 Oxford University Press.
140. K. Horn, J. Dinardo, W. Eberhardt, H.J. Freund, and E.W. Plummer, *Surf. Sci.,* 118 (1982) 465.
141. E.F. Rissmann, and J.M. Parry, *Catal. Lett.,* 16 (1992) 159.
142. S. Brunauer, P.H. Emmett, and E. Teller, *J. Am. Chem. Soc.,* 60 (1938) 309.
143. G.W. Castellan, *Physical Chemistry,* 2nd ed., (1971) 436 Addison Wesley.
144. E.P. Barrett, L.G. Joyner, and P.P. Halenda, *J. Am. Chem. Soc.,* 73 (1951) 373.
145. R. Allmann, *Acta Crystallogr., Sect. B: Struct. Cryst. Crystal Chem.,* B 24 (1968) 972.
146. H.F.W. Taylor, *Mineral. Mag.,* 37 (1969) 338.
147. F. Cavani, O. Clause, F. Trifiro, and A. Vaccari, *Advances in Catalyst Design,* (1991) 186.
148. R. Allmann, *Chimia,* 24 (1970) 99.
149. W.T. Reichle, *Solid State Ionics,* 22 (1986) 135.
150. U. Costantino, M. Casciola, L. Massinelli, M. Nocchetti, and R. Vivani, *Solid State Ionics,* 97 (1997) 203.
151. U. Costantino, F. Marmottini, M. Nocchetti, and R. Vivani, *Eur. J. Org. Chem.,* (1998) 1439.
152. D.R. Hines, S.A. Solin, U. Costantino, and M. Nocchetti, *Solid State Commun.,* 108 (1998) 971.
153. U. Costantino, N. Coletti, M. Nocchetti, G.G. Aloisi, and F. Elisei, *Langmuir,* 15 (1999) 4454.
154. U. Costantino, N. Coletti, M. Nocchetti, G.G. Aloisi, F. Elisei, and L. Latterini, *Langmuir,* 16 (2000) 10351.
155. S. Murcia-Mascaros, R.M. Navarro, L. Gomez-Sainero, U. Costantino, M. Nocchetti, and J.L.G. Fierro, *J. Catal.,* 198 (2001) 338.
156. G.G. Aloisi, U. Costantino, F. Elisei, L. Latterini, C. Natali, and M. Nocchetti, *J. Mater. Chem.,* 12 (2002) 3316.
157. A. Caneschi, D. Gatteschi, C. Sangregorio, M.G.F. Vaz, U. Costantino, M. Nocchetti, and R. Vivani, *Inorg. Chim. Acta,* 338 (2002) 127.
158. L. Latterini, F. Elisei, G.G. Aloisi, U. Costantino, and M. Nocchetti, *Phys. Chem. Chem. Phys.,* 4 (2002) 2792.
159. U. Costantino, M. Curini, F. Montanari, M. Nocchetti, and O. Rosati, *J. Mol. Catal. A: Chem.,* 195 (2003) 245.
160. M. Turco, G. Bagnasco, U. Costantino, F. Marmottini, T. Montanari, G. Ramis, and G. Busca, *J. Catal.,* 228 (2004) 43.
161. M. Turco, G. Bagnasco, U. Costantino, F. Marmottini, T. Montanari, G. Ramis, and G. Busca, *J. Catal.,* 228 (2004) 56.
162. P.P. Yang, J.F. Yu, Z.L. Wang, T. Wu, and T.H. Wu, *React. Kinet. Catal. Lett.,* 83 (2004) 275.
163. P.P. Yang, J.F. Yu, T.H. Wu, G.Z. Liu, T.S. Chang, D.K. Lee, and D.H. Cho, *Chin. Chem. Lett.,* 15 (2004) 90.
164. U. Costantino, A. Gallipoli, M. Nocchetti, G. Camino, F. Bellucci, and A. Frache, *Polym. Degrad. Stab.,* 90 (2005) 586.
165. G.M. Lombardo, G.C. Pappalardo, F. Punzo, F. Costantino, U. Costantino, and M. Sisani, *Eur. J. Org. Chem.,* (2005) 5026.

166. L. Tammaro, M. Tortora, V. Vittoria, U. Costantino, and F. Marmottini, *J. Polym. Sci., Part A: Polym. Chem.,* 43 (2005) 2281.
167. U. Costantino, F. Marmottini, M. Sisani, T. Montanari, G. Ramis, G. Busca, M. Turco, and G. Bagnasco, *Solid State Ionics,* 176 (2005) 2917.
168. G. Busca, U. Costantino, F. Marmottini, T. Montanari, P. Patrono, F. Pinzari, and G. Ramis, *Appl. Catal., A,* 310 (2006) 70.
169. A. Aguzzi, V. Ambrogi, U. Costantino, and F. Marmottini, *J. Phys. Chem. Solids,* 68 (2007) 808.
170. U. Costantino, F. Montanari, M. Nocchetti, F. Canepa, and A. Frache, *J. Mater. Chem.,* 17 (2007) 1079.
171. L. Latterini, M. Nocchetti, G.G. Aloisi, U. Costantino, and F. Elisei, *Inorg. Chim. Acta,* 360 (2007) 728.
172. M. Turco, G. Bagnasco, C. Cammarano, P. Senese, U. Costantino, and M. Sisani, *Appl. Catal. B,* 77 (2007) 46.
173. M.A.L. Vargas, G. Busca, U. Costantino, F. Marmottini, T. Montanari, P. Patrono, F. Pinzari, and G. Ramis, *J. Mol. Catal. A: Chem.,* 266 (2007) 188.
174. U. Costantino, M. Curini, F. Montanari, M. Nocchetti, and O. Rosati, *Micropor. Mesopor. Mater.,* 107 (2008) 16.
175. U. Costantino, V. Ambrogi, M. Nocchetti, and L. Perioli, *Micropor. Mesopor. Mater.,* 107 (2008) 149.
176. L. Perioli, M. Nocchetti, V. Ambrogi, L. Latterini, C. Rossi, and U. Costantino, *Micropor. Mesopor. Mater.,* 107 (2008) 180.
177. U. Costantino, M. Nocchetti, M. Sisani, and R. Vivani, *Z. Kristallogr.,* 224 (2009) 273.
178. C. Resini, T. Montanari, L. Barattini, G. Ramis, G. Busca, S. Presto, P. Riani, R. Marazza, M. Sisani, F. Marmottini, and U. Costantino, *Appl. Catal., A,* 355 (2009) 83.
179. H.Y. Zeng, X. Deng, Y.J. Wang, and K.B. Liao, *AIChE J.,* 55 (2009) 1229.
180. W.H.R. Shaw, and J.J. Bordeaux, *J. Am. Chem. Soc.,* 77 (1955) 4729.
181. T. Bujdoso, A. Patzko, Z. Galbacs, and I. Dekany, *Appl. Clay Sci.,* 44 (2009) 75.
182. X. Cheng, X.R. Huang, X.Z. Wang, B.Q. Zhao, A.Y. Chen, and D.Z. Sun, *J. Hazard. Mater.,* 169 (2009) 958.
183. Y. Du, N. Rees, and D. O'Hare, *Dalton Trans.,* (2009) 8197.
184. M. Islam, and R. Patel, *J. Hazard. Mater.,* 169 (2009) 524.
185. J. Shibata, N. Murayama, D. Sakamoto, and M. Okada, *Kagaku Kogaku Ronbunshu,* 35 (2009) 60.
186. P.A. Terry, *J. Environ. Eng. Sci.,* 26 (2009) 691.
187. M. Silion, D. Hritcu, and M.I. Popa, *Optoelectron. Adv. Mater. Rapid Commun.,* 3 (2009) 817.
188. M. Silion, D. Hritcu, and M.I. Popa, *J. Optoelectron. Adv. Mater.,* 11 (2009) 528.
189. Q. Zhenlan, Y. Heng, Z. Bin, and H. Wanguo, *Colloids Surf., A,* 348 (2009) 164.
190. W.T. Reichle, S.Y. Kang, and D.S. Everhardt, *J. Catal.,* 101 (1986) 352.
191. D. Tichit, M.H. Lhouty, A. Guida, B.H. Chiche, F. Figueras, A. Auroux, D. Bartalini, and E. Garrone, *J. Catal.,* 151 (1995) 50.
192. W.T. Reichle, *J. Catal.,* 94 (1985) 547.

193. M.J. Climent, A. Corma, S. Iborra, and A. Velty, *J. Catal.,* 221 (2004) 474.
194. N. Zelinsky, and W. Kommarewsky, *Ber. Dtsch. Chem. Ges.,* 57 (1924) 667.
195. F.J. Brocker, and K. Kaempfer, *Chem. Ing. Tech.,* 47 (1975) 513.
196. T.G. Fawcett, J. Faber, S. Kabbekodu, F. McClune, and D. Rafaja, *PDF-4+, the material identification database, Microstructure Analysis in Materials Science, Freiberg,* (2005) 1.
197. S. Miyata, *Clays Clay Miner.,* 31 (1983) 305.
198. G.W. Brindley, and S. Kikkawa, *Clays Clay Miner.,* 28 (1980) 87.
199. S. Miyata, *Clays Clay Miner.,* 28 (1980) 50.
200. T. Osawa, S. Mita, A. Iwai, O. Takayasu, T. Harada, and I. Matsuura, *Preparation of Catalysts VII,* 118 (1998) 313.
201. D. Tichit, F. Medina, B. Coq, and R. Dutartre, *Appl. Catal., A,* 159 (1997) 241.
202. A. Bennett, Christie, S., Keane, M. A., Peacock, R.D., and Webb, G., *Catal. Today.,* 10 (1991).
203. K.S.W. Sing, D.H. Everett, R.A.W. Haul, L. Moscou, R.A. Pierotti, J. Rouquerol, and T. Siemieniewska, *Pure Appl. Chem.,* 57 (1985) 603.
204. J.S. Beck, J.C. Vartuli, W.J. Roth, M.E. Leonowicz, C.T. Kresge, K.D. Schmitt, C.T.W. Chu, D.H. Olson, E.W. Sheppard, S.B. McCullen, J.B. Higgins, and J.L. Schlenker, *J. Am. Chem. Soc.,* 114 (1992) 10834.
205. N. Ulagappan, and C.N.R. Rao, *Chem. Commun.,* (1996) 2759.
206. S. Namba, A. Mochizuki, and M. Kito, *Chem. Lett.,* (1998) 569.
207. S. Namba, and A. Mochizuki, *Res. Chem. Intermed.,* 24 (1998) 561.
208. M. Linden, P. Agren, S. Karlsson, P. Bussain, and H. Amenitsch, *Langmuir,* 16 (2000) 5831.
209. A. Lind, J. Andersson, S. Karlsson, P. Agren, P. Bussian, H. Amenitsch, and M. Linden, *Langmuir,* 18 (2002) 1380.
210. A. Corma, *Chem. Rev.,* 97 (1997) 2373.
211. M. Linden, S. Schacht, F. Schuth, A. Steel, and K.K. Unger, *J. Porous. Mater.,* 5 (1998) 177.
212. U. Ciesla, and F. Schuth, *Micropor. Mesopor. Mater.,* 27 (1999) 131.
213. J.M. Thomas, *Angew. Chem. Int. Ed.,* 38 (1999) 3589.
214. A. Tuel, *Micropor. Mesopor. Mater.,* 27 (1999) 151.
215. J.Y. Ying, C.P. Mehnert, and M.S. Wong, *Angew. Chem. Int. Ed.,* 38 (1999) 56.
216. R. Anwander, *Chem. Mater.,* 13 (2001) 4419.
217. P. Selvam, S.K. Bhatia, and C.G. Sonwane, *Ind. Eng. Chem. Res.,* 40 (2001) 3237.
218. D.E. De Vos, M. Dams, B.F. Sels, and P.A. Jacobs, *Chem. Rev.,* 102 (2002) 3615.
219. X. He, and D. Antonelli, *Angew. Chem. Int. Ed.,* 41 (2002) 214.
220. Y. Liu, and T.J. Pinnavaia, *J. Mater. Chem.,* 12 (2002) 3179.
221. G.J.D. Soler-illia, C. Sanchez, B. Lebeau, and J. Patarin, *Chem. Rev.,* 102 (2002) 4093.
222. A.P. Wight, and M.E. Davis, *Chem. Rev.,* 102 (2002) 3589.
223. D.T. On, D. Desplantier-Giscard, C. Danumah, and S. Kaliaguine, *Appl. Catal., A,* 253 (2003) 543.
224. A. Taguchi, and F. Schuth, *Micropor. Mesopor. Mater.,* 77 (2005) 1.

225. M. Vallet-Regi, A. Ramila, R.P. del Real, and J. Perez-Pariente, *Chem. Mater.,* 13 (2001) 308.
226. Q.S. Huo, D.I. Margolese, U. Ciesla, D.G. Demuth, P.Y. Feng, T.E. Gier, P. Sieger, A. Firouzi, B.F. Chmelka, F. Schuth, and G.D. Stucky, *Chem. Mater.,* 6 (1994) 1176.
227. Q.S. Huo, D.I. Margolese, U. Ciesla, P.Y. Feng, T.E. Gier, P. Sieger, R. Leon, P.M. Petroff, F. Schuth, and G.D. Stucky, *Nature,* 368 (1994) 317.
228. D.M. Antonelli, A. Nakahira, and J.Y. Ying, *Inorg. Chem.,* 35 (1996) 3126.
229. D.M. Antonelli, and J.Y. Ying, *Chem. Mater.,* 8 (1996) 874.
230. D.M. Antonelli, and J.Y. Ying, *Angew. Chem., Int. Ed. Engl.,* 35 (1996) 426.
231. R. Ryoo, S.H. Joo, and S. Jun, *J. Phys. Chem. B,* 103 (1999) 7743.
232. S.H. Joo, S.J. Choi, I. Oh, J. Kwak, Z. Liu, O. Terasaki, and R. Ryoo, *Nature,* 412 (2001) 169.
233. E. Armengol, M.L. Cano, A. Corma, H. Garcia, and M.T. Navarro, *J. Chem. Soc., Chem. Commun.,* (1995) 519.
234. M.J. Climent, A. Corma, S. Iborra, M.C. Navarro, and J. Primo, *J. Catal.,* 161 (1996) 783.
235. M.J. Climent, A. Corma, R. Guil-Lopez, S. Iborra, and J. Primo, *J. Catal.,* 175 (1998) 70.
236. A. Corma, S. Iborra, S. Miquel, and J. Primo, *J. Catal.,* 173 (1998) 315.
237. M. Iwamoto, Y. Tanaka, N. Sawamura, and S. Namba, *J. Am. Chem. Soc.,* 125 (2003) 13032.
238. T. Kugita, S.K. Jana, T. Owada, N. Hashimoto, M. Onaka, and S. Namba, *Appl. Catal., A,* 245 (2003) 353.
239. A. Corma, M.T. Navarro, and J.P. Pariente, *J. Chem. Soc., Chem. Commun.,* (1994) 147.
240. R.B. Borade, and A. Clearfield, *Catal. Lett.,* 31 (1995) 267.
241. Z.H. Luan, C.F. Cheng, H.Y. He, and J. Klinowski, *J. Phys. Chem.,* 99 (1995) 10590.
242. M.D. Alba, Z.H. Luan, and J. Klinowski, *J. Phys. Chem.,* 100 (1996) 2178.
243. M.L. Occelli, S. Biz, A. Auroux, and G.J. Ray, *Micropor. Mesopor. Mater.,* 26 (1998) 193.
244. B. Chakraborty, and B. Viswanathan, *Catal. Today,* 49 (1999) 253.
245. Y.H. Yue, A. Gedeon, J.L. Bonardet, N. Melosh, J.B. D'Espinose, and J. Fraissard, *Chem. Commun.,* (1999) 1967.
246. J. El Haskouri, S. Cabrera, M. Gutierrez, A. Beltran-Porter, D. Beltran-Porter, M.D. Marcos, and P. Amoros, *Chem. Commun.,* (2001) 309.
247. M.A. Markowitz, S. Jayasundera, J.B. Miller, J. Klaehn, M.C. Burleigh, M.S. Spector, S.L. Golledge, D.G. Castner, and B.P. Gaber, *Dalton Trans.,* (2003) 3398.
248. B.J. Aronson, C.F. Blanford, and A. Stein, *Chem. Mater.,* 9 (1997) 2842.
249. R. Ryoo, S. Jun, J.M. Kim, and M.J. Kim, *Chem. Commun.,* (1997) 2225.
250. R.D. Oldroyd, G. Sankar, J.M. Thomas, and D. Ozkaya, *J. Phys. Chem. B,* 102 (1998) 1849.
251. Z.H. Luan, E.M. Maes, P.A.W. van der Heide, D.Y. Zhao, R.S. Czernuszewicz, and L. Kevan, *Chem. Mater.,* 11 (1999) 3680.
252. M. Widenmeyer, S. Grasser, K. Kohler, and R. Anwander, *Micropor. Mesopor. Mater.,* 44 (2001) 327.

253. R. Mokaya, and W. Jones, *J. Mater. Chem.,* 9 (1999) 555.
254. H. Landmesser, H. Kosslick, W. Storek, and R. Fricke, *Solid State Ionics,* 101 (1997) 271.
255. X.S. Zhao, G.Q. Lu, A.K. Whittaker, G.J. Millar, and H.Y. Zhu, *J. Phys. Chem. B,* 101 (1997) 6525.
256. M. Widenmeyer, and R. Anwander, *Chem. Mater.,* 14 (2002) 1827.
257. J.L. Zhang, Y.L. Liu, and C.M. Che, *Chem. Commun.,* (2002) 2906.
258. P. Xue, and T. Wu, *Chin. J. Catal.,* 27 (2006) 489.
259. R. Burch, N. Cruise, D. Gleeson, and S.C. Tsang, *Chem. Commun.,* (1996) 951.
260. A. Corma, A. Martinez, and V. MartinezSoria, *J. Catal.,* 169 (1997) 480.
261. C.P. Mehnert, and J.Y. Ying, *Chem. Commun.,* (1997) 2215.
262. C.P. Mehnert, D.W. Weaver, and J.Y. Ying, *J. Am. Chem. Soc.,* 120 (1998) 12289.
263. M. Okumura, S. Tsubota, M. Iwamoto, and M. Haruta, *Chem. Lett.,* (1998) 315.
264. V.R. Choudhary, S.K. Jana, and B.P. Kiran, *J. Catal.,* 192 (2000) 257.
265. A. Wingen, N. Anastasievic, A. Hollnagel, D. Werner, and F. Schuth, *J. Catal.,* 193 (2000) 248.
266. R. Raja, T. Khimyak, J.M. Thomas, S. Hermans, and B.F.G. Johnson, *Angew. Chem. Int. Ed.,* 40 (2001) 4638.
267. S.N. Coman, V.I. Parvulescu, M. De Bruyn, D.E. De Vos, and P.A. Jacobs, *J. Catal.,* 206 (2002) 218.
268. A. Lewandowska, S. Monteverdi, M. Bettahar, and M. Ziolek, *J. Mol. Catal. A: Chem.,* 188 (2002) 85.
269. J. Panpranot, J.G. Goodwin, and A. Sayari, *Catal. Today,* 77 (2002) 269.
270. J. Panpranot, J.G. Goodwin, and A. Sayari, *J. Catal.,* 211 (2002) 530.
271. M. Jacquin, D.J. Jones, J. Roziere, S. Albertazzi, A. Vaccari, M. Lenarda, L. Storaro, and R. Ganzerla, *Appl. Catal., A,* 251 (2003) 131.
272. A.Y. Khodakov, A. Griboval-Constant, R. Bechara, and V.L. Zholobenko, *J. Catal.,* 206 (2002) 230.
273. D.J. Lensveld, J.G. Mesu, A.J. van Dillen, and K.P. de Jong, *Micropor. Mesopor. Mater.,* 44 (2001) 401.
274. G.A. Du, S. Lim, Y.H. Yang, C. Wang, L. Pfefferle, and G.L. Haller, *J. Catal.,* 249 (2007) 370.
275. F. Di Renzo, H. Cambon, and R. Dutartre, *Micropor. Mater.,* 10 (1997) 283.
276. T. Yanagisawa, T. Shimizu, K. Kuroda, and C. Kato, *Bull. Chem. Soc. Jpn.,* 63 (1990) 988.
277. C.T. Kresge, M.E. Leonowicz, W.J. Roth, J.C. Vartuli, and J.S. Beck, *Nature,* 359 (1992) 710.
278. J.C. Vartuli, C.T. Kresge, M.E. Leonowicz, A.S. Chu, S.B. McCullen, I.D. Johnsen, and E.W. Sheppard, *Chem. Mater.,* 6 (1994) 2070.
279. G.S. Attard, J.C. Glyde, and C.G. Goltner, *Nature,* 378 (1995) 366.
280. S.A. Bagshaw, E. Prouzet, and T.J. Pinnavaia, *Science,* 269 (1995) 1242.
281. Q.S. Huo, R. Leon, P.M. Petroff, and G.D. Stucky, *Science,* 268 (1995) 1324.
282. P.T. Tanev, and T.J. Pinnavaia, *Science,* 267 (1995) 865.
283. S. Inagaki, A. Koiwai, N. Suzuki, Y. Fukushima, and K. Kuroda, *Bull. Chem. Soc. Jpn.,* 69 (1996) 1449.

284. E. Prouzet, and T.J. Pinnavaia, *Angew. Chem. Int. Ed.,* 36 (1997) 516.
285. D.Y. Zhao, J.L. Feng, Q.S. Huo, N. Melosh, G.H. Fredrickson, B.F. Chmelka, and G.D. Stucky, *Science,* 279 (1998) 548.
286. D.Y. Zhao, Q.S. Huo, J.L. Feng, B.F. Chmelka, and G.D. Stucky, *J. Am. Chem. Soc.,* 120 (1998) 6024.
287. S. Che, A.E. Garcia-Bennett, T. Yokoi, K. Sakamoto, H. Kunieda, O. Terasaki, and T. Tatsumi, *Nature Mater.,* 2 (2003) 801.
288. A.E. Garcia-Bennett, O. Terasaki, S. Che, and T. Tatsumi, *Chem. Mater.,* 16 (2004) 813.
289. R. Atluri, N. Hedin, and A.E. Garcia-Bennett, *J. Am. Chem. Soc.,* 131 (2009) 3189.
290. T.J. Barton, L.M. Bull, W.G. Klemperer, D.A. Loy, B. McEnaney, M. Misono, P.A. Monson, G. Pez, G.W. Scherer, J.C. Vartuli, and O.M. Yaghi, *Chem. Mater.,* 11 (1999) 2633.
291. Q. Cai, W.Y. Lin, F.S. Xiao, W.Q. Pang, X.H. Chen, and B.S. Zou, *Micropor. Mesopor. Mater.,* 32 (1999) 1.
292. A. Monnier, F. Schuth, Q. Huo, D. Kumar, D. Margolese, R.S. Maxwell, G.D. Stucky, M. Krishnamurty, P. Petroff, A. Firouzi, M. Janicke, and B.F. Chmelka, *Science,* 261 (1993) 1299.
293. A. Firouzi, D. Kumar, L.M. Bull, T. Besier, P. Sieger, Q. Huo, S.A. Walker, J.A. Zasadzinski, C. Glinka, J. Nicol, D. Margolese, G.D. Stucky, and B.F. Chmelka, *Science* 267 (1995) 1138.
294. Q.S. Huo, D.I. Margolese, and G.D. Stucky, *Chem. Mater.,* 8 (1996) 1147.
295. Y. Fukushima, S. Inagaki, and K. Kuroda, *Abstr. Pap. Am. Chem. Soc.,* 209 (1995) 33.
296. Y. Fukushima, S. Inagaki, and K. Kuroda, *Nippon Kagaku Kaishi,* (1995) 327.
297. H.P. Lin, S. Cheng, and C.Y. Mou, *Chem. Mater.,* 10 (1998) 581.
298. H.P. Lin, and C.Y. Mou, *Science,* 273 (1996) 765.
299. M. Grun, K.K. Unger, A. Matsumoto, and K. Tsutsumi, *Micropor. Mesopor. Mater.,* 27 (1999) 207.
300. K. Schumacher, M. Grun, and K.K. Unger, *Micropor. Mesopor. Mater.,* 27 (1999) 201.
301. C. Thoelen, J. Paul, I.F.J. Vankelecom, and P.A. Jacobs, *Tetrahedron: Asymmetry,* 11 (2000) 4819.
302. H.M. Hunter, and P.A. Wright, *Micropor. Mesopor. Mater.,* 43 (2001) 361.
303. W.Z. Zhou, H.M.A. Hunter, P.A. Wright, Q.F. Ge, and J.M. Thomas, *J. Phys. Chem. B,* 102 (1998) 6933.
304. A.E. Garcia-Bennett, S. Willliamson, P.A. Wright, and I.J. Shannon, *J. Mater. Chem.,* 12 (2002) 3533.
305. M. Perez-Mendoza, J. Gonzalez, P.A. Wright, and N.A. Seaton, *Langmuir,* 20 (2004) 7653.
306. M. Perez-Mendoza, J. Gonzalez, P.A. Wright, and N.A. Seaton, *Langmuir,* 20 (2004) 9856.
307. H.M.A. Hunter, A.E. Garcia-Bennett, I.J. Shannon, W.Z. Zhou, and P.A. Wright, *J. Mater. Chem.,* 12 (2002) 20.
308. K. Schumacher, P.I. Ravikovitch, A. Du Chesne, A.V. Neimark, and K.K. Unger, *Langmuir,* 16 (2000) 4648.

309. U. Junges, S. Disser, G. Schmid, and F. Schuth, *Stud. Surf. Sci. Catal.,* 117 (1998) 391.
310. M. Hartmann, A. Poppl, and L. Kevan, *J. Phys. Chem.,* 100 (1996) 9906.
311. H.-P. Lin, S.-T. Wong, C.-Y. Mou, and C.-Y. Tang, *J. Phys. Chem. B,* 104 (2000) 8967.